Trap-induced resonances in controlled atomic collisions for quantum information processing

by

René Stock

Vordiplom, Physics, University of Würzburg, Germany, 1996
Masters of Science, Physics, University of New Mexico, 2001

DISSERTATION

Submitted in Partial Fulfillment of the
Requirements for the Degree of

Doctor of Philosophy
Physics

The University of New Mexico

Albuquerque, New Mexico

May, 2005

Dedication

In memory of my grandmother, Margarethe Müller.

Acknowledgments

I have had many excellent physics teachers since I first started out in physics. I thank all of them for providing inspiration and support. However, no other teacher has helped shape me into a scientist as much as my advisor Professor Ivan Deutsch. He first introduced me to the wonderful fields of quantum optics and quantum information, and even managed to convince me to get involved in scattering theory and atomic physics. It is impossible to express in words my thanks for all his guidance and his continuing confidence in me. Furthermore, I would like to thank the members of my dissertation committee, Professor Paul Alsing, Professor Debi Evans, and Professor Carl Caves for their support, the many discussions, and all their comments and suggestions. The members of the theoretical atomic physics group at NIST, Gaithersburg, Dr. Carl Williams, Dr. Paul Julienne, Dr. Eita Tiesinga, and Dr. Sanjiv Shresta have taught me much about atomic collisional physics. In particular, I would like to thank Dr. Eric Bolda for his help in shaping this work and for all the long telephone discussions. Thanks to Professor Poul Jessen's experimental group at the University of Arizona for always keeping this work down to earth.

This process would not have been as enjoyable without all the people in the quantum information group at UNM. Thanks to John, Gavin, Trace, Dave, Iris and especially Drew for many helpful discussions. Very special thanks also to Joe, Kiran, Andrew, Bryan and Steve, who never grew tired of joining for lunch.

I would like to specially thank my parents. Without their encouragement, help, and support, I would not be the person I am today. Many heartfelt thanks also to my brother Patrick. I hope I can provide as much support during his Ph.D. as he did for me. And last but most importantly, I would like to thank my wife Shohini, for all her love and her never-ending support. Without her many 'pep' talks I would have never been able to make it this far. I would climb rooftops again anytime for my other half.

Trap-induced resonances in controlled atomic collisions for quantum information processing

by

René Stock

ABSTRACT OF DISSERTATION

Submitted in Partial Fulfillment of the
Requirements for the Degree of

Doctor of Philosophy
Physics

The University of New Mexico

Albuquerque, New Mexico

May, 2005

Trap-induced resonances in controlled atomic collisions for quantum information processing

by

René Stock

Vordiplom, Physics, University of Würzburg, Germany, 1996
Masters of Science, Physics, University of New Mexico, 2001

Doctor of Philosophy, Physics, University of New Mexico, 2005

Abstract

Controlled collisions of ultracold atoms in optical lattices provide new avenues for quantum control and quantum information processing. The ability to precisely vary lattice parameters and the rich internal structure of trapped atoms allow for novel state manipulation. In this research, we investigate and develop new methods for analyzing and designing coherent controlled collisions of ultracold atoms in separated traps.

In order to describe controlled atomic collisions, we develop a detailed scattering model, based on a fully generalized multichannel Fermi pseudopotential, which captures the complete scattering properties and bound states of the true atomic interaction. We derive a proper generalized version of Fermi's pseudopotential for all higher partial waves based on a δ-shell potential in the limit as the shell radius approaches zero, thereby taking into account the higher multipoles not captured by

a δ-function at the origin. This pseudopotential corrects long-standing problems in previous generalizations and opens up new possibilities for studying interacting cold atomic gases with high accuracy. We show that this energy-dependent δ-shell potential not only captures the scattering behavior of realistic potentials correctly, but also reproduces the bound-state spectrum when the scattering length is extended to negative energies.

Our generalized pseudopotential can be applied to study interacting trapped atoms in harmonic traps. Using the δ-shell approach, we derive analytical equations for the energy eigenvalues and the eigensolutions. The resulting higher partial wave solutions are investigated and discussed in detail. By analyzing a spherical step-well test potential, we evaluate and discuss the breakdown of the pseudopotential approximation in the regime of strong confinement by the trapping potential.

Of particular interest is the investigation of controlled collisions of atoms in separated but close traps. We show that for certain trap separations, resonances between molecular bound states and trap eigenstates appear. As the separation between the traps is increased, the energy of the molecular bound state closest to dissociation increases. Avoided crossings occur in the eigenspectrum when the energy of this molecular bound state becomes resonant with eigenstates of the trapping potential. These newly predicted "trap-induced resonances" represent the main result of this work. They are not accounted for in a perturbation theory approach and can be easily observed in very tight traps, which are typical, for example, in optical lattices. The properties of these trap-induced resonances are analyzed and discussed in detail for isotropic and anisotropic separated traps.

These newly predicted trap-induced resonances could feasibly be experimentally observed under realistic circumstances. A particularly promising candidate species is ^{133}Cs. A detailed multichannel scattering calculation, based on realistic interaction potentials of ^{133}Cs including higher partial waves and second order spin-orbit

coupling, shows an extremely weakly bound state near dissociation. We apply a multichannel formulation of our generalized pseudopotential to calculate the energy spectrum for interacting ^{133}Cs atoms as a function of trap separation. The energy gap in the spectrum provides a signature by which the trap-induced resonance could be experimentally observed, and we discuss how this could be done in detail. Furthermore, we evaluate the possible implementation of two-qubit logic gates under realistic conditions in ^{133}Cs using this resonant interaction, and address some of the limitations to the fidelity of such gates.

Contents

List of Figures

List of Tables

Chapter 1

Introduction

The central goal of this dissertation is the development of a detailed scattering model for the description of interacting trapped atoms with particular focus on spatially separated trapped atoms for quantum information processing. Our description of the interaction between atoms is based on a correctly generalized energy-dependent pseudopotential, which captures the complete higher partial-wave scattering and bound-state spectrum of the true interaction. We apply this model to trapped atoms with an emphasis on ultra-cold collisions of separated atoms in optical lattices. We show that this setting provides new possibilities for controlling collisions via trap-induced resonances (TIR). These newly predicted resonances between a weakly bound state of the molecular interaction and trap eigenstates result in a strong coupling of atoms in separated traps, thus providing new avenues for robust encoding of quantum information and for controlling the two-qubit interaction for entangling neutral atoms for quantum computing. We evaluate the feasibility of observing these resonances in a particular promising species, ^{133}Cs, via a detailed multichannel calculation of the relevant scattering properties.

The description of atomic interactions by scattering models and more concretely

by pseudopotentials, has existed for close to 70 years starting with Fermi's original pseudopotential. The application of these scattering models to trapped atoms has become important due to the huge advances in cooling and trapping of atoms over the past decade. More recently, trapped neutral atoms have been proposed for quantum information processing. Here, the interactions between atoms are essential to design a necessary ingredient for quantum computing, two-qubit entangling gates.

In this introduction, we will attempt to review some of current research in this field. We will identify crucial unresolved problems and open questions, which we address in this thesis. Although our primary goal was to address specific questions regarding entangling atoms for QIP, the general models we developed during the course of this research are widely applicable to variety of contexts. We present a short overview of the dissertation at the end of this chapter.

1.1 Coherent control of atoms and quantum information processing

The ability to arbitrarily manipulate the quantum state of a many-body ensemble represents the ultimate control of a physical system. This task has steadily advanced in atomic-molecular-optical systems starting with developments in coherent radio frequency, microwave, and laser spectroscopy, and with the tremendous progress in cooling and trapping technology. This has led to the creation of Bose-Einstein condensates (BEC) and Fermi degenerate gases, and the explorations of new forms of matter and mesoscopic quantum states previously accessible only in condensed matter systems [1]. The addition of engineered traps, such as optical lattices [2] and other optical [3, 4] and magnetic [5] microtraps provides a new knob with which to control the quantum state. A dramatic example of many-body control in lattices was

demonstrated through the observation of a superfluid to Mott insulator quantum phase transition [6], the collapse and revival of the mean field coherence [7], and recently the observation of a 1D Tonks gas of impenetrable bosonic atoms [8].

The standard approach to modeling and designing coherent states of matter has its foundations in condensed matter theory, where one considers solutions to the entire many-body Hamiltonian. An alternative viewpoint arises from a fundamental theorem of quantum information theory [9]. Given a well defined Hilbert space that is a tensor product of many subsystems ("bodies"), any unitary operator on the large space can be constructed from a tensor product of well defined operators acting solely on one subsystem or pairs of subsystems [9]. This theorem about "universal quantum logic gates" implies that an *arbitrary* state of a many-body system can be reached entirely through operations on single bodies and pairwise interactions. Moreover, one requires only a *single* two-body interaction (e.g. CPHASE or CNOT gate) that entangles the "particles" to contribute to a universal set of quantum logic gates. Thus the control of the two-body interaction is the crucial step in many-body coherent control problems including all quantum information processing protocols.

In this thesis, we attack the problem of many-body control from a quantum information perspective. Rather than modeling the entire many-body Hamiltonian, we will focus on the detailed description of the two-body interaction that can be used to implement a universal two-body unitary and ultimately to control the complete many-body system.

1.1.1 Optical traps and optical lattices

The quantum control of neutral atoms is closely linked to the particular trapping and cooling arrangements used. Neutral atoms generally interact very weakly with the environment and hence represent one of most coherent physical systems. While this

feature is of importance e.g. for the success of neutral atom clocks, this also represent one of the biggest challenges for neutral atom trapping and control. Whereas ions can be easily trapped using Coulomb interactions, neutral atom traps are more difficult to achieve and are generally based on weak interaction of their electric or magnetic dipole moments with AC and/or DC electromagnetic fields.

In this dissertation, we will focus in particular on atoms trapped in optical lattices. The idea of optical lattices grew originally out of Doppler cooling experiments where two red detuned, counter propagating laser beams are used to exert an effective frictional force on the atoms. Very early, it was realized that the atoms are not only cooled in this arrangement, but also trapped in a periodic potential created by the counter propagating laser beams. This realization is also closely linked to the surprising fact that the inclusion of the complicated internal structure of the atom leads to more efficient cooling of atoms beyond the Doppler limit (Sisyphus cooling). A more detailed history of laser cooling and trapping can be found in Ref. [10].

In order to understand the optical lattice system, consider two counter propagating linear polarized laser beams detuned by Δ from the $S_{1/2}$ to $P_{3/2}$ transition of an alkali atom (e.g. Rb or Cs). Depending on the angle between the linear polarizations of these two beams (1-D lin-angle-lin lattice), the resulting light field can be decomposed into σ_+ and σ_- standing waves whose nodes are separated by θ_l/k_l, where k_l is the wave number of the applied light field. The corresponding light shift potential results from the dipole interaction between the atom and the laser field $\mathbf{E}_l = E_0\mathbf{e}_l$ [10],

$$\hat{U} = -\frac{1}{4}\mathbf{E}_l^* \cdot \hat{\boldsymbol{\alpha}} \cdot \mathbf{E}_l \,, \tag{1.1}$$

where $\hat{\alpha}$ is the atomic polarizability tensor. For a multilevel atom, the polarizability tensor depends on the internal states of the atom and can be broken down into its irreducible components: a scalar, a vector, and a rank-2 tensor term. For a two level atom (e.g. an alkali atom with a single valence electron with spin-1/2) the

polarizability tensor consists of only the scalar term, which is independent of the atomic state, and a vector term, which is state dependent. This leads to an effective Zeeman interaction [2, 10],

$$\hat{U} = U_0(z) - \hat{\mu} \cdot \mathbf{B}_{fict}(z) \tag{1.2}$$

with $\mu = -\mu_B \sigma$. Here, μ_B is the Bohr magneton and σ is the vector consisting of the Pauli matrices. $U_0 = \frac{2}{3} U_1 |\mathbf{e}_l(z)|^2$ where $\mathbf{e}_l(z)$ is the local laser polarization [10]. The single beam light shift U_1 determines the depth of the optical lattice and is proportional to E_0^2/Δ. For large detuning Δ, one can still achieve deep optical lattices while keeping the spontaneous emission rate $\gamma \propto 1/\Delta^2$ low.

In the case of the lin-angle-lin geometry, the state-dependent light-shift potential for a two level system with spin up ($\uparrow$) and spin down ($\downarrow$) is

$$\hat{U}_{\uparrow\downarrow}(z) = \frac{4}{3} U_1 \cos\theta_l \cos(2k_l z) \mp \frac{2}{3} U_1 \sin\theta_l \sin(2k_l z)\,. \tag{1.3}$$

If we include the hyperfine structure of realistic multilevel alkali atoms with total angular momentum vector $\hat{\mathbf{f}}$ and quantum number f, the form of the light shift potential remains the same if the optical trap laser is detuned sufficiently far from resonance. In that case, the excited state hyperfine splitting is not resolved and the trap laser only couples to the electron spin, not the nuclear spin. Then the atom effectively looks like a spin 1/2 system. The atomic magnetic moment in Eq. (1.2) follows from the Lande projection theorem and is given by

$$\hat{\mu} = -g\,\mu_B \frac{\hat{\mathbf{f}}}{f}\,, \tag{1.4}$$

where γ is the gyromagnetic ratio, and the g-factor is -1 $(+1)$ for the lower (upper) hyperfine manifold. The 1D lin-angle-lin lattice potential for an atom in the magnetic hyperfine sublevel denoted by m_f is then

$$\hat{U}_{f,m_f}(z) = \frac{4}{3} U_1 \cos\theta_l \cos(2k_l z) - \frac{2}{3} U_1 \sin\theta_l \sin(2k_l z) \frac{g\,m_f}{f}\,. \tag{1.5}$$

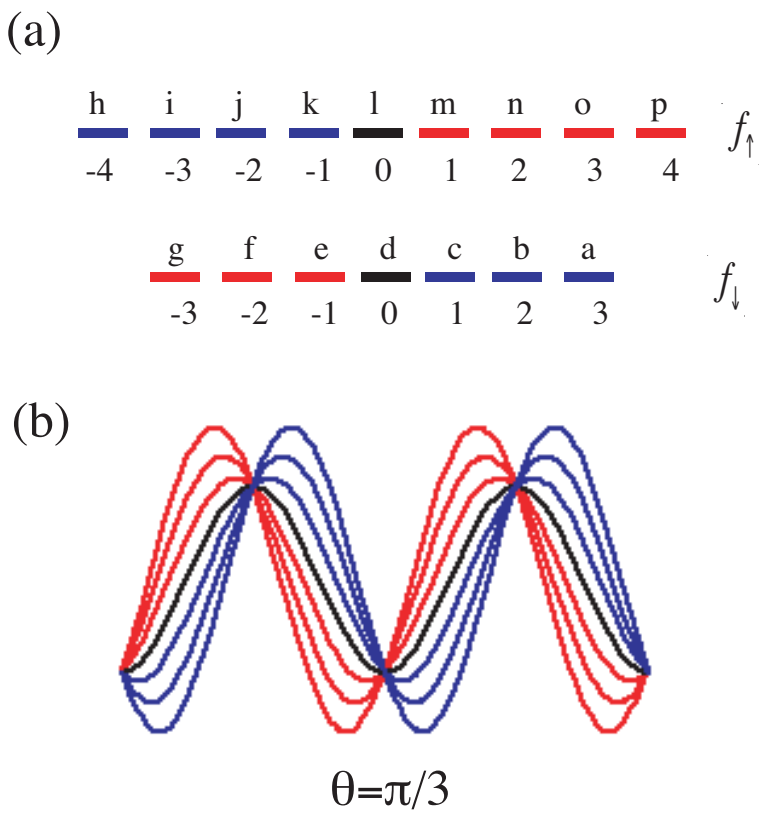

Figure 1.1: (a) Atomic hyperfine levels for Cs with hyperfine ground states $f = 3$ and $f = 4$. The blue levels are primarily trapped in the σ_+ standing wave, the red levels are primarily trapped in the σ_- standing wave. (b) Corresponding state-dependent optical lattice potential for $\theta = \pi/3$.

Here m_f is the quantum number of the projection of $\mathbf{f}$ along the quantization axis.

This state-dependent trapping potential is the foundation for designing quantum-computing protocols. Figure 1.1(a) shows the different magnet hyperfine sublevels that are primarily trapped by the σ_+ (blue levels) vs. the σ_- (red colored levels). The signs of the $\sigma_\pm$ trapped magnetic sublevels are switched for the excited hyperfine manifold due to the opposite sign of the g-factor. If we consider two atoms in different states, which experience different light shifts, we can simply control the separation between atoms by rotating the polarization angle between the linear polarizations of

the lattice beams as illustrated in Fig. 1.2. Since the interaction between atoms is of fairly short range, this translates into a precise way for controlling the interatomic interaction. As an alternative to optical lattices, several other trap arrangements, which are based on other optical [3, 4] and/or magnetic [5] microtraps, have been conceived.

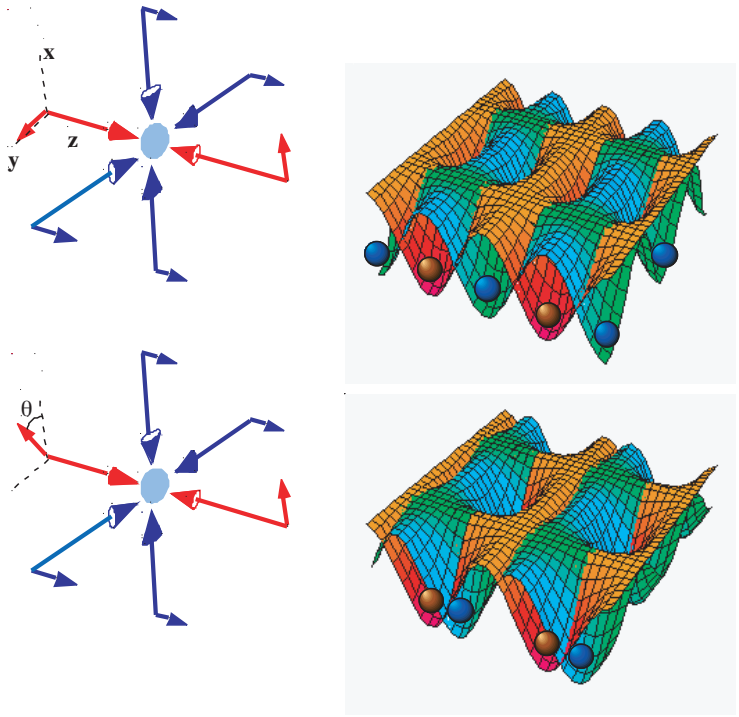

Figure 1.2: Schematic of a 3D optical lattice. (a) Two pairs of linearly polarized beams provide transverse confinement, and the beams along z in the lin-angle-lin configuration provide longitudinal confinement in σ_+ and σ_- standing waves. (b) Potential surfaces for the atom in different magnetic sublevels, described in the text, shown here as in gray and white, are moved along the z-axis through a rotation of the angle θ between polarization vectors for controlled collisions.

1.1.2 Interacting atoms under strong confinement

Atoms in traps have become an important tool for atomic physics, condensed matter physics, and more recently quantum information physics. For many of these systems, interactions between atoms play a crucial role. The interaction strength and sign determines for example the stability of the Bose condensate, and is responsible for the creation of molecules. Many body collisions close to a scattering resonance have led to the implosion ("Bosenova") of a BEC [11]. In addition, the tunability of the atomic interaction via molecular Feshbach resonances has widely expanded the controllability of such atomic systems [12]. Feshbach resonances describe in general the coupling of an energetically accessible state (open channel) to a bound state of an energetically inaccessible state (closed channel) [13–15] (see Fig. 1.3). At

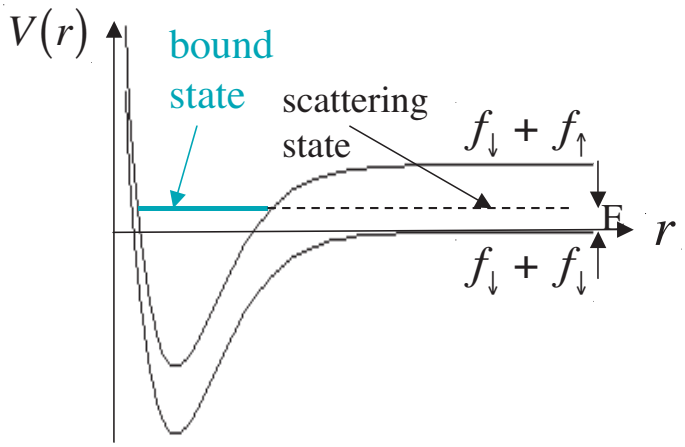

Figure 1.3: Schematic of a Feshbach resonance. Here, an energetically accessible scattering state (open channel) couples to a molecular bound state of an asymptotically energetically inaccessible state (closed channel) for a higher hyperfine manifold.

the Feshbach resonance, the scattering length a diverges and changes signs. For energies slightly below the resonance, $a \to -\infty$ and the interaction is attractive; for energies slightly above, $a \to +\infty$ and the interaction is repulsive. The location of the Feshbach resonant bound state is in general sensitive to magnetic fields. The

interaction is therefore tunable by changes in the applied magnetic field.

The above examples illustrate the importance of the interaction for atoms in traps. The reverse is true as well. Strong confinement can have a large effect on the interaction between atoms, even to the degree that an interacting Bosonic system can effectively behave as gas of Fermions and obey Fermi statistics [16, 17]. Important examples of such systems are interacting atoms under strong 1D or 2D confinement. Quasi 1D systems, where the atomic gas is strongly confinement in two directions, have been studied in great detail by several authors [18–21]. These systems are of particular interest due to the prediction of a Tonks-Girardeu gas [16–18], which has recently been observed experimentally in an optical lattice system of tightly confined 1D tubes [8]. Olshanii [18] derived an effective 1D coupling strength that is related to 3D scattering length a and the confinement in the transverse direction $\rho_\perp$ via

$$g_{1\mathrm{D}} = \frac{2\hbar^2 a}{\mu\rho_\perp^2}\frac{1}{1 - C\frac{a}{\rho_\perp}}\,, \tag{1.6}$$

where the constant $C \approx 1.4603$. For $a = \rho_\perp/C$, a resonance in the coupling strength occurs, which leads to a 1D chain of impenetrable bosons [18]. Due to the strong repulsive interactions and the 1D confinement, the exchange of atoms is not possible and it has been shown that the elementary excitations in this system obey Fermi statistics [16, 17]. Recently, the origin of the resonance in Eq. (1.6) has been attributed to a Feshbach like, confinement-induced resonance where the resonance is caused by a bound state of a closed channel of the transverse mode [20]. This resonance is of particular importance since it allows the control of the effective 1D interaction strength and exploration of different regimes of the BEC vs. the Tonks-gas by simply varying the confinement of atoms in the transverse direction. In this thesis, we will show another example where the confinement represents an important knob with which to control the interaction between atoms.

Quasi 2D systems where the gas is only strongly confined in one direction have been the focus of much research as well [22–24]. Here, the strong confinement of

the atomic system provides a clean condensed matter system to study fractional anyon statistics and the fractional quantum hall effect [25] or the Kosterlitz-Thouless transition for interacting bosons in 2D [26].

An example of a 3D many-body system is a BEC loaded into a shallow 3D optical lattice. It has been shown that this system undergoes a quantum phase transition if the lattice depth is increased gradually [27]. During this process, the ratio of the atomic interaction strength to the tunneling rate determines the different regimes for a superfluid and the Mott insulator state similar to experimental realization of the Tonks-Girardeau gas described earlier. In the Mott insulator state the Poissonian number fluctuation of atoms per site is suppressed and only an integer number of atoms is found at each site. The experimental realization by Greiner *et al.* [6] represents one of the most important steps towards a neutral atom quantum computer, since the Mott insulator state with exactly one atom per site presents the perfect way of initializing the many-body state that is necessary for quantum computing. Due to the breakthrough experiments by Greiner *et al.* this quantum phase transition has attracted considerable interest over the past few years.

The multitude of the systems discussed here, underlines the importance of confinement induced effects on the interaction between atoms and its description. The modeling of the interactions in trapped environments constitutes an interesting and important problem, and has rightfully become the main topic of the first few chapters of this thesis.

1.2 Quantum computation in optical lattices

Confinement induced effects on the interaction between atoms as discussed in the previous section represent a very new and exciting field. Its importance in applications where interactions play a central role, cannot be underestimated as we will show

later in this thesis. We are particularly interested in ways that confinement induced effects will impact the design of two-qubit gates for quantum information processing and possibly extend existing protocols. In the following section, we briefly describe the general requirements for quantum computation and discuss protocols for implementations in optical lattices. We further discuss the experimental progress towards neutral atom quantum computation that has taken place over the last few years.

1.2.1 Protocols for neutral atom quantum computing

The basic design of a QIP protocol in the standard quantum circuit model involves a choice of qubit encoding, initialization method, single- and two-qubit gates, and read-out method. For neutral atoms that only interact weakly at very short distances, the implementation of two-qubit entangling gates through basic interatomic interactions poses the biggest challenge. In the following, we will focus on the different proposals for entangling atoms that have been developed by several groups. As an example of a unitary two-qubit gate, we consider the controlled-phase (CPhase) gate [9] which maps the two-qubit logical basis states $|11\rangle \rightarrow -|11\rangle$, and leaves the others unchanged according to

$$CPHASE = \begin{pmatrix} 1 & 0 & 0 & 0 \\ 0 & 1 & 0 & 0 \\ 0 & 0 & 1 & 0 \\ 0 & 0 & 0 & -1 \end{pmatrix}. \tag{1.7}$$

The controlled-phase gate can be easily implemented via a simple unitary operation

$$U = \begin{pmatrix} e^{-i\frac{E_{00}}{\hbar}t_{\mathrm{int}}} & 0 & 0 & 0 \\ 0 & e^{-i\frac{E_{01}}{\hbar}t_{\mathrm{int}}} & 0 & 0 \\ 0 & 0 & e^{-i\frac{E_{10}}{\hbar}t_{\mathrm{int}}} & 0 \\ 0 & 0 & 0 & e^{-i\frac{E_{11}}{\hbar}t_{\mathrm{int}}} \end{pmatrix} \tag{1.8}$$

that is obtained if the different logical two qubit states are shifted by the interaction by different energies E_{00}, E_{01}, E_{10}, and E_{11}. Here, the energy shifts must be non-separable, $\Delta E = E_{00} + E_{01} - (E_{10} + E_{11}) \neq 0$. The interaction time $t_{\rm int}$ is then determined by

$$t_{\rm int} = \frac{\pi\hbar}{\Delta E}\,. \tag{1.9}$$

The unitary can then be simply transformed into a CPhase gate by single body unitaries [9].

The challenge is to design this nonseparable energy or phase shift by a given two-body interaction. A natural candidate for the entangling gate interaction is the ground state collisional interaction, as proposed in one of the first neutral atom QIP protocols by Jaksch *et al.* [28]. Here, the logical basis is encoded into the internal state of the atoms by choosing suitable hyperfine states in Fig. 1.1. To implement a high-fidelity quantum logic gate, the collisions must be state dependent and at the same time scattering into states outside the computational basis must be suppressed. For two-body collisions, these couplings are due to spin-changing collisions caused by the Heisenberg spin-exchange interaction, which preserves only the total magnetic quantum number $m_{\rm total} = m_{f_1} + m_{f_2}$, but not m_{f_1} and m_{f_2} of the individual atoms. By encoding qubits in the stretched states $|1\rangle = |f_+, m_f = f_+\rangle$ and $|0\rangle = |f_-, m_f = f_-\rangle$ (see Fig. 1.1), Jaksch *et al.* designed an interaction that preserves the individual m_f since neither m_{f_1} or m_{f_2} can increase. Examining the state-dependent optical lattice potential for these states, it can be seen that these states move in opposite directions in a lattice as discussed in the previous section. Rotating the lattice polarization angle from $\theta = 0$ to $\theta = \pi$ will then cause an atom in the state $|1\rangle$ and moving to the right to collide with an atom in the state $|0\rangle$ which is moving to the left. In this protocol, the state-dependent interaction is provided naturally by the encoding since the two qubits interact only if the state is $|10\rangle$ and not otherwise.

Several other protocols for two-qubit entangling gates that are based on the

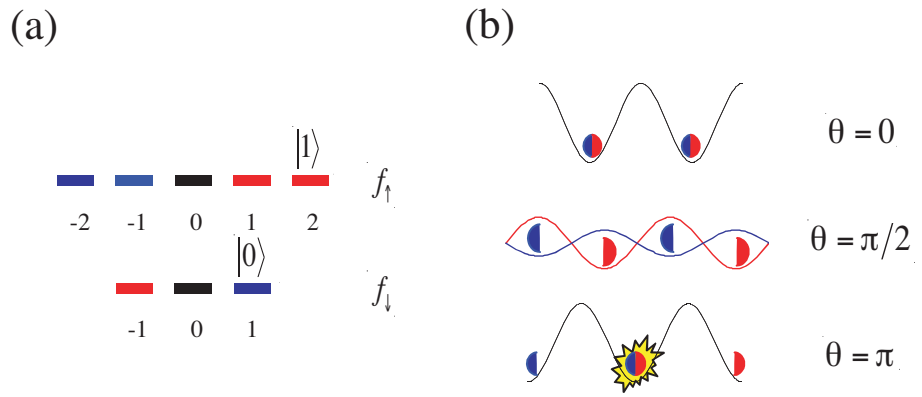

Figure 1.4: Schematic of a collisional gate as proposed by Jaksch *et al.* [28]. Here, the logical states are encoded in the stretched stated as seen in the sketch of the hyperfine manifold on the left.

ground state collisional interaction have been proposed. For example, Charron *et al.* [29] and Eckert *et al.* [30] considered encoding qubits in the ground and first excited center-of-mass vibrational states of trapped atoms in a double-well potential. In these protocols, the state-dependent coupling between qubits is facilitated by lowering the potential barrier between adjacent sites and correspondingly increasing the overlap of the two excited state atomic wave packets. This leads to an increased collisional interaction for both atoms in the first excited state of the center of mass motion compared to the other logical basis combinations. An alternative interaction has been considered by Brennen *et al.* [31–33]. This proposal is based on the electric dipole-dipole interactions created by an additional off-resonant laser field that mixes the ground-state manifold with excited electronic states. This interaction has a longer-range behavior corresponding to $-C_3/r^3$ compared to ground state collisions that are due to the shorter-range van der Waals interaction $-C_6/r^6$. In this protocol, the atoms remain separated so that the individual atomic quantum numbers are preserved. This process that includes the dressing of the ground state by longer-range excited state potential can also be described in the framework of the atomic scattering theory and optical Feshbach resonances [34]. Even longer-range

interactions that are due to the permanent dipoles of atoms in high-lying Rydberg states provide yet another strategy to implement quantum logic with neutrals [35].

1.2.2 Experimental Progress

Efforts to implement neutral atom QIP in the laboratory represent a natural but challenging extension of existing tools to prepare, control, and measure the quantum state of trapped neutrals. A number of experiments have demonstrated several of the key components that go into QIP, and very recently some of these have been combined for the first time to demonstrate control and entanglement in a neutral-atom many-body system. In this section, we briefly review progress in three main areas: initialization of the qubit register, implementation of single- and two-qubit gates, and methods to address individual qubits.

Optical lattices typically confine atoms tightly on the scale of an optical wavelength, and lend themselves readily to the use of Raman sideband cooling. In a first demonstration, Hamann et al. initialized 98% of a 10^6-atom ensemble in a single spin- and vibrational-ground state of a sparsely filled 2D lattice [36], and subsequent work has achieved a somewhat lesser degree of state preparation in nearly filled 3D lattices [37,38]. These laser cooling-based approaches work well in any tightly confining trap geometry, but when used in a lattice, will produce a random pattern of vacant and occupied sites. Sparse, random filling may suffice for ensemble-based investigations of quantum logic, but falls short of the requirements of full-scale lattice-based QIP.

Better filling and initialization can be achieved by loading a 3D lattice from a high-density Bose-Einstein condensate and driving the atom/lattice through a superfluid to Mott insulator phase transition as described in Section 1.1.2. The group of Bloch and Hänsch at MPQ in Münich used this approach as a starting point for a

series of proof of principle experiments to establish the viability of the Jaksch *et al.* collisional protocol [28]. As the first step, Greiner *et al.* successfully demonstrated the transition to an insulator phase consisting of individual ^{87}Rb atoms localized in the ground state of separate potential wells [6]. Mandel *et al.* then explored spin-dependent coherent transport in the context of interferometry [39]. This was done by preparing atoms in the logical-$|0\rangle$ state, transferring them to an equal superposition of the states $|0\rangle$ and $|1\rangle$ with a microwave $\pi/2$ pulse, and splitting them into two wave packets by rotating the laser polarization vectors as described above. The which way information was then erased with a final pulse $\pi/2$ and the atoms released from the lattice, allowing the separated wave packets of each atom to overlap and interfere as in a two-slit experiment. As an alternative to this measurement of the spatial interference pattern, experiments were performed where the atoms were bought back to their initial site. For these measurements, after a final pulse with relative phase α compared to the initial pulse, the population in the $|1\rangle$ state was measured and Ramsey interference fringes recorded as a function of α. Inhomogeneously acquired phase shifts across the ensemble were partially cancelled using additional π-pulses in a spin-echo procedure. In this fashion, the experiment achieved fringe visibilities of 60% for transport across three lattice sites, limited by remaining quantum phase-errors induced by magnetic field noise, vibrational heating and residual inhomogeneities. Finally, Mandel *et al.* performed a many-body version of this experiment in a nearly filled lattice [40], where the majority of atoms underwent collisional interactions with their neighbors according to the Jaksch et al. protocol. For appropriate collision-induced phase shifts, this leads to the formation of chains of entangled atoms, which cannot be disentangled again by local operations such as the final $\pi/2$ pulse. For maximally entangled atoms this results in the complete disappearance of the interference fringes. In the experiment, a periodic disappearance and reappearance of interferometer fringe visibility was clearly observed as a function of interaction time and corresponding degree of entanglement. Technical limitations,

in particular the inability to perform single qubit measurements, have so far made it difficult to obtain quantitative estimates for the size and degree of entanglement of these cluster states, or to extract the fidelity of the underlying CPhase gate.

While the experiments just described allow a detailed investigation and optimization of two-qubit gate protocols via ensemble measurements, the next step towards universal QIP involves the necessary ability to manipulate and read out the state of individual atomic qubits. In principle, this can be accomplished by performing single-qubit rotations and readout with focused laser beams rather than microwave fields. However, the necessary optical resolving power will be nearly impossible to achieve in current lattices whose sites are separated by roughly 0.5 μm. Possible solutions are longer wavelength lattices with a site spacing of 5 μm, which are formed by a long wavelength CO_2 laser [41]. Other experimentally demonstrated alternatives where atoms remain tightly localized are conventional lattices that are pattern loaded so that atoms occupy only every nth well [42]. Alternative trapping geometries, such as mentioned earlier, provide different possibilities and are investigated by several groups [3–5].

The experiments by the Münich group have demonstrated the feasibility of coherent spin transport and entanglement via controlled collisions, but also served to highlight some of the fundamental limitations of the particular protocol employed. To implement high-fidelity collisional gates, one must achieve a spin-dependent phase shift, while at the same time restrict the interaction to a single collisional channel so as to prevent scattering outside the computational basis. Jaksch *et al.* accomplished this with their stretched-state encoding, but at the cost of being maximally sensitive to magnetic field- and trap noise. In the experiments, this resulted in the random phase acquired by the different qubit states and was one of the main limiting factors. While problems during the initialization stage such as the limited fidelity of the Mott insulator state can be corrected a priori by filtering schemes as proposed by Rabl

et al. [43] or additional cooling techniques, the correction of these limiting phase fluctuations can only be accomplished by using different, more robust encodings and correspondingly altered entangling gate protocols. This dissertation will explore alternative protocols to circumvent these limitations. In particular, we will explore the collisional interaction between atoms in separated traps since in this case the restrictions for the encoding that was used in the original Jaksch *et al.* proposal can be relaxed and inelastic collisions can be suppressed by the state-dependent trapping potentials in the separated trap case.

1.3 Overview of thesis

The central topic of this dissertation is the study of ultracold collisions of trapped atoms with particular emphasis on collisions between atoms in separated traps. The motivation for this research is given mainly by applications in quantum information processing, but also has impact on more general aspects of confinement induced effects on the atomic interaction. With respect to QIP, we would like to analyze and expand existing proposals for quantum computing with neutral atoms that relax some of the requirements of the original proposal as discussed in Section 1.2.1. In particular, we choose to approach the problem of interacting atoms in separated traps from a scattering theory perspective, since this allows a very nice and complete treatment of the collisional and other short-range interactions.

Chapter 2 is dedicated to a complete and thorough discussion of our scattering model, based on a correctly generalized pseudopotential approach. After a short review of scattering theory and the basic interaction that dominates atomic collisions at low energies, we will lay out some of the existing formulations of the pseudopotential approach and discuss problems that have been pointed out in the literature. We will then develop a generalized pseudopotential formalism that corrects and clar-

ifies the previous approaches and represents one of the major cornerstones in this dissertation.

In Chapter 3 we will discuss some of the fundamental issues when one tries to describe the interactions between trapped atoms by a pseudopotential. We will then apply our generalized pseudopotential derived in Chapter 2 to atoms in isotropic harmonic trap. We derive a general analytic eigenvalue equation for these interacting atoms including all higher partial-wave solutions.

In Chapter 4 we present the main result of this thesis when we analyze collisions in separated traps. We show that in this setting, trap-induced shape resonances (TIR) between trap eigenstates and weakly bound states of the molecular interaction can occur. This effect is similar to the Feshbach-like, confinement induced resonances of 1D systems that have been of such fundamental importance for the observation of the Tonks-Girardeau gas as discussed in Section 1.1.2. These newly predicted resonances result in a strong coupling of atoms in separated traps, thus providing new avenues for robust encoding of quantum information and for controlling the two-qubit interaction for entangling neutral atoms for quantum computing. In the remainder of this chapter we discuss some of the important properties of trap-induced resonances as well as the more general case of TIR in separated anisotropic traps.

In Chapter 5 we evaluate the feasibility of observing these resonances in ^{133}Cs. Cesium represents a particularly promising species due to its anomalously large scattering lengths and the resulting strong interatomic interactions [44, 45]. To this end we extend our scattering model discussed in Chapter 2 to its multichannel formulation. The necessary ^{133}Cs multichannel scattering parameters are then calculated using codes developed in the Atomic Physics Division at the National Institute of Standards and Technology, modified and applied to the case of separated atoms and trap-induced resonances with the help of the developed scattering model.

We conclude in Chapter 6 with a short summary of the thesis and highlight the main achievements of this research. We also provide an outlook to future work, and how it can be efficiently approached.

A large fraction of the research presented in this thesis can be found in published form as listed in Table 1.1 for each chapter.

Chapter 1	P. S. Jessen, I. H. Deutsch, and R. Stock. Quantum information processing with trapped neutral atoms. Quant. Inf. Proc., **3**, 1527 (2004).
Chapter 2 and Chapter 3	R. Stock, A. Silberfarb, I. H. Deutsch, and E. L. Bolda. Generalized pseudopotentials for higher partial wave scattering. Phys. Rev. Lett., **93**, 023202 (2005).
Chapter 4	R. Stock, I. H. Deutsch, and E. L. Bolda. Quantum state control via trap-induced shape resonance in ultracold atomic collisions. Phys. Rev. Lett., **91**, 183201 (2003).
Chapter 5	R. Stock and I. H. Deutsch. Trap-induced resonances in controlled collisions of Cesium atoms. In preparation.

Table 1.1: List of chapters in this dissertation and corresponding published articles.

Chapter 2

Scattering models based on generalized zero-range pseudopotentials

2.1 Introduction

Over the past few years atomic many-body systems have attracted considerable interest due to the tremendous progress in laser cooling and trapping of atomic gases, the creation of atomic Bose-Einstein condensates (BEC) [1], and more recently due to the experimental observation of quantum phase transitions in interacting many-body systems [6]. The first step in studying the complex physics of such many-body systems is modeling the fundamental two-body interactions. It is therefore natural that this huge progress in experimental cold atomic physics has gone hand in hand with a more detailed understanding of atomic interactions at low temperatures. As a result, atomic scattering theory and the study of collisions of neutral atoms at low temperatures have been the focus of much attention over the past decade (see

for example reviews of atomic collision physics by Burnett *et al.* [1], Julienne [46], and Weiner *et al.* [47]). For example, atomic collisions are essential for thermalization during evaporative cooling and for determining the properties of a BEC [1]. Furthermore, the collisional interaction plays an important role in quantum phase transitions as in the case of the superfluid to Mott-insulator transition [27]. It is also of interest for entangling atoms for quantum information processing, where the exact control and the proper modeling of the collisional interaction is crucial for the fidelity of the entangling gate.

An accurate way of modeling atomic interactions is the pseudopotential approach, which originates from scattering theory and is the focus of this chapter. In the following, we first present a basic review of cold atomic collision physics and a short introduction to formal scattering theory, followed by a review of the Fermi pseudopotential and its generalization to higher partial waves by Huang and Yang and observed problems with this generalization. We then present our new derivation of a generalized higher partial-wave pseudopotential based on a δ-shell potential, which corrects the long standing fundamental problem in Huang's pseudopotential and captures the critical features of both the scattering and bound-state spectrum of the realistic interaction potential. This derivation is followed by a detailed discussion of the energy-dependent pseudopotential approximation and its relation to the scattering and bound-state spectrum.

2.2 Background

2.2.1 Born-Oppenheimer potentials for diatomic molecules

The description of the atomic interaction has its origin in two very different physical fields. On one side, we have the spectroscopic description of diatomic molecules in

molecular physics, which focuses mainly on the bound-state spectrum. On the other side we have atomic scattering theory that describes the interaction between unbound atoms. Before we focus on the scattering description of the atomic interaction, we will discuss the diatomic Hamiltonian and the interaction from a molecular perspective. A nice review of the physics of diatomic molecules can be found in Ref. [48]. One of the most important approximations in the description of a diatomic system is the Born-Oppenheimer or adiabatic approximation, which we outline here. Consider two atoms that form a diatomic molecule, consisting of two nuclei A and B, separated by $\mathbf{r}$, and N electrons located at $\mathbf{r}_{el_1}$, $\mathbf{r}_{el_2}$, ...$\mathbf{r}_{el_N}$ with respect to the center of mass of A and B. Inserting the complete Hamiltonian operator including interactions into the Schrödinger equation and expanding the total molecular wave function Ψ in terms of products of the nuclear motion wave functions $F_\alpha(\mathbf{r})/r$ and electron wave function ψ_α,

$$\Psi\left(\mathbf{r};\, \mathbf{r}_{el_1},\, \mathbf{r}_{el_2},\, ...\mathbf{r}_{el_N}\right) = \sum_\alpha \frac{F_\alpha(\mathbf{r})}{r} \psi_\alpha(\mathbf{r}_{el_1},\, \mathbf{r}_{el_2},\, ...\mathbf{r}_{el_N})\,, \tag{2.1}$$

we arrive at a set of coupled equations [49]

$$\sum_\alpha \langle\psi_{\alpha'}| - \frac{\hbar^2}{2\mu}\frac{1}{r^2}\frac{\partial}{\partial r}\left(r^2\frac{\partial}{\partial r}\right) + \frac{\hat{\mathbf{L}}_r^2}{2\mu r^2}\,|\psi_\alpha\rangle\,\frac{F_\alpha(\mathbf{r})}{r} + \left[E_{\alpha'}(\mathbf{r}) - E\right]\frac{F_{\alpha'}(\mathbf{r})}{r} = 0. \tag{2.2}$$

Here, μ is the reduced mass of atoms A and B, $\mathbf{L}_r$ is the nuclear orbital angular momentum operator and $E_{\alpha'}$ are the energy eigenvalues of the molecule in the electronic state $|\psi_{\alpha'}\rangle$. In the Born-Oppenheimer approximation, one uses the fact that the nuclear motion is much slower than the electronic motion. In this case, the electronic wave function is independent of the nuclear coordinates $\mathbf{r}$ and approximately commutes with the radial kinetic energy operator. The set of equations (2.2) decouple and we get an equation for the nuclear motion when the electronic system is in the state α,

$$\left[-\frac{\hbar^2}{2\mu}\frac{1}{r^2}\frac{\partial}{\partial r}\left(r^2\frac{\partial}{\partial r}\right) + \frac{\langle\psi_\alpha|\,\hat{\mathbf{L}}_r^2\,|\psi_\alpha\rangle}{2\mu r^2} + E_\alpha(\mathbf{r}) - E\right].\frac{F_\alpha(\mathbf{r})}{r} = 0. \tag{2.3}$$

For alkali atoms with a single valence electron, the Born-Oppenheimer (BO) potentials at short range in the Hund's case (a) result in two different interaction potentials, the singlet ${}^1\Sigma_g^+$ (V_S) and triplet ${}^3\Sigma_u^+$ potential (V_T), depending on the total coupled spin of the valence electrons $\vec{s}_i$ of the two atoms,

$$\hat{V}_{BO} = \frac{1}{4}\hat{V}_S(r) + \frac{3}{4}\hat{V}_T(r) + \left[\hat{V}_T(r) - \hat{V}_S(r)\right] \vec{s}_1 \cdot \vec{s}_2 \,. \tag{2.4}$$

Figure 2.1 shows an example of the BO potentials for sodium. For very small r,

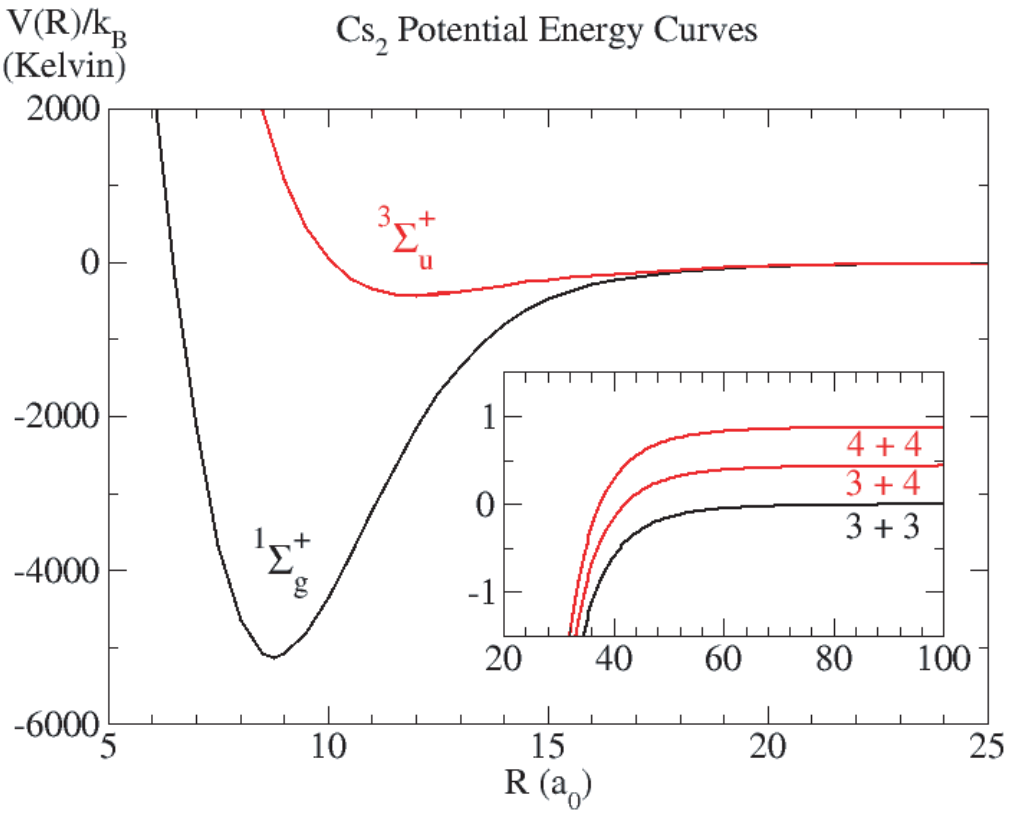

Figure 2.1: Adiabatic Born-Oppenheimer potential energy curves for the Cs_2 molecule. The inset shows the asymptotic connection to the three two-atom hyperfine levels. Figure courtesy of Paul S. Julienne.

the interaction is dominated by the Coulomb repulsion between the two nuclei and the exchange interaction between the electronic distributions. At longer range, the

interaction is attractive and determined by the van der Waals interaction. The van der Waals interaction results from the dipole induced in each atom by the other and behaves as $-C_6/r^6$ [48, 49]. The characteristic length scale for a $-C_n/r^n$ interaction is [50]

$$\beta_n = \frac{1}{2}\left(\frac{2\mu C_n}{\hbar^2}\right)^{\frac{1}{n-2}} . \tag{2.5}$$

Despite the relatively simple one-electron character of the alkali atoms, the Born-Oppenheimer potentials can be still quite difficult to work with in the description of the atomic interaction, so that an even "simpler" model for the interaction is required. For cold atoms, the deBroglie wavelength λ_{dB} is usually much longer than the characteristic length scale of the Born-Oppenheimer potential β_n so that the interaction effectively looks like a δ-function interaction. This is the basis for the widely used Fermi pseudopotential and its generalizations, which we will discuss in a later section.

2.2.2 A brief review of scattering theory

In the last section, we briefly reviewed the interaction between two atoms from a molecular viewpoint. Before we continue with a scattering theory description of the interaction, it is helpful to review some of the formal aspects of scattering theory.

The S-matrix

When trying to describe the quantum mechanical scattering process of one particle that interacts with a (fixed) scatterer (which is identical to the two-body problem in the relative coordinate frame), we start with a free particle wave packet long before the scattering event and far away from the scatterer. The state then evolves according to the time-dependent Schrödinger equation (T. D. S. E.) until the final

wave packet emerges. This leads to the concept of "in" and "out" states in scattering theory. The "in" state ψ_{in} is the free particle state that matches the actual evolving state ψ at $t = -\infty$. It can therefore be defined by

$$\lim_{t\to-\infty}\left[\hat{U}(t)\,|\psi\rangle - \hat{U}_0(t)\,|\psi\rangle_{\text{in}}\right] = 0\,, \tag{2.6}$$

where the operator $\hat{U}_0(t)$ describes the free evolution of the state ψ_{in} according to the free Hamiltonian H_0 and $\hat{U}(t)$ describes the actual evolution of the state ψ including the interaction V. The out state ψ_{out} can be defined analogously for $t \to +\infty$. The "in" and "out" states in quantum mechanics are equivalent to the asymptotic trajectories to a given particle orbit in classical scattering theory.

The Moller operators $\hat{\Omega}_{\pm}$ are defined to be

$$\hat{\Omega}_{\pm} \equiv \lim_{t\to\mp\infty} \hat{U}^{\dagger}(t)\hat{U}_0(t) \tag{2.7}$$

with

$$\psi = \hat{\Omega}_{+}\psi_{\text{in}} = \hat{\Omega}_{-}\psi_{\text{out}}\,. \tag{2.8}$$

The isometric Moller operators describe the transformation of ψ_{in} at $t = -\infty$ to the actual state ψ at $t = 0$ to the "out" state ψ_{out} at $t = +\infty$ as follows:

$$\psi_{\text{in}} \xrightarrow{\hat{\Omega}_{+}} \psi \xrightarrow{\hat{\Omega}_{-}^{\dagger}} \psi_{\text{out}}\,. \tag{2.9}$$

We can then define the scattering operator or S-matrix as the operator that connects the free particle "in" states and "out" states via

$$\hat{S} = \hat{\Omega}_{-}^{\dagger}\hat{\Omega}_{+}\,. \tag{2.10}$$

The unitary transformation via the S-matrix is given by

$$\psi_{\text{in}} \xrightarrow{\hat{S}} \psi_{\text{out}}\,. \tag{2.11}$$

The S-matrix is one of the most important concepts of scattering theory. Although we have limited ourselves in this discussion to a single input state and a single output

state (single channel problem), the concept of the S-matrix can be readily generalized to the multichannel problem with several possible "in" states [51]. The S-matrix then connects all "in" states to all "out" states of the scattering problem. If the S-matrix is known for a particular problem, all other important scattering parameters can easily be derived. For example in the multichannel case, the S-matrix can be used to calculate the scattering amplitudes $f(\mathbf{p}', \xi' \longleftarrow \mathbf{p}, \xi)$ for transitions from a state $|\mathbf{p}, \xi\rangle$ to $|\mathbf{p}', \xi'\rangle$ via

$$\langle \mathbf{p}', \xi' | \, S \, | \mathbf{p}, \xi \rangle = \delta^{(3)}(\mathbf{p}' - \mathbf{p}) + \frac{i}{2\pi\mu} \delta(E_{p'} - E_p) f(\mathbf{p}', \xi' \longleftarrow \mathbf{p}, \xi) \, . \tag{2.12}$$

The quantity p describes the momentum of the particle and the quantum number ξ describes the internal state of the particle, e.g. the internal spin state. We will revisit the S-matrix later in order to derive analytical properties of the pseudopotential approximation as well as to describe the multichannel scattering problem for collisions of ^{133}Cs atoms.

Stationary scattering states and time-independent scattering theory

Another important concept in scattering theory is the one of the stationary scattering states, which are defined by

$$|\mathbf{p}\pm\rangle \equiv \hat{\Omega}_{\pm} \, |\mathbf{p}\rangle \ , \tag{2.13}$$

where $|\mathbf{p}\rangle$ is the plane wave state of a free particle. The stationary scattering states are (improper [51]) eigenstates of the total Hamiltonian $H = H^0 + V$. If for example, we consider an orbit with "out" asymptote $|\chi\rangle$,

$$|\chi\rangle = \int d^3p \chi(p) \, |\mathbf{p}\rangle \ , \tag{2.14}$$

then the state at $t = 0$ is described by

$$|\chi-\rangle = \int d^3p \chi(p) \, |\mathbf{p}-\rangle \ . \tag{2.15}$$

Therefore, the stationary states are a convenient basis for the expansion of scattering states at $t = 0$. Since the states $|\mathbf{p}\pm\rangle$ are eigenstates of the total Hamiltonian H, they are solutions to the time independent Schrödinger equation (T. I. S. E.) given by the Lippmann-Schwinger equation for $|\mathbf{p}+\rangle$,

$$\langle \mathbf{r}|\mathbf{p}+\rangle \overset{r\to\infty}{\sim} (2\pi)^{-\frac{3}{2}} \left(e^{i\mathbf{pr}} + f\frac{ipr}{r} \right) . \tag{2.16}$$

The coefficient f of the outgoing spherical wave is the scattering amplitude mentioned earlier. The stationary scattering states, which obey the T. I. S. E., bridge the gap between the time-*dependent* picture of scattering theory as discussed in the introduction of the S-matrix and the time-*independent* scattering theory which we will use in the following sections and chapters.

Partial waves, threshold behavior, and scattering length

The plane wave basis of the stationary scattering states discussed in the last section is not the most convenient basis for all problems. For central potentials, a partial-wave expansion in spherical waves is more appropriate. Expanding the free particle Hamiltonian in a spherical basis with r, θ, and ϕ, we write the free particle partial-wave solutions as

$$\psi_{E,l,m}(\mathbf{r}) = R_l(r)Y_l^m(\theta,\phi) . \tag{2.17}$$

General solutions to the free radial Schrödinger equation are then combinations of the spherical Bessel functions

$$R_l(r) = A_l j_l(kr) + B_l n_l(kr) . \tag{2.18}$$

In 3D, the wave function has to be regular at the origin, that is the reduced radial wave function $rR_l(r)$ has to vanish a the origin. This boundary condition is only fulfilled by the Bessel j_l function which behaves as r^l close to the origin. Asymptotically

far away, the free particle partial waves behave like

$$R_l(r) = A_l j_l(kr) \overset{r\to\infty}{\sim} \frac{\sin\left(kr - \frac{l\pi}{2}\right)}{kr}\,. \tag{2.19}$$

For interaction potentials that fall of sufficiently fast according to C_n/r^{-n} with $n \geq 3$, the stationary scattering solutions $j_l^{(+)}(kr)$ are obtained from the Lippman-Schwinger equation for partial waves [51]

$$j_l^{(+)}(kr) \overset{r\to\infty}{\sim} j_l(kr) + \frac{f_l(E)}{r} e^{i(kr - l\pi/2)}\,. \tag{2.20}$$

We see that the interaction leads to an additional outgoing spherical wave (second term), where the partial-wave scattering amplitudes $f_l(E)$ can be calculated from the S-matrix.

To this end, we expand the S-matrix in the partial-wave basis. Since the S-matrix commutes with H, it is diagonal in this basis,

$$\langle E', l', m'| S |E, l, m\rangle = s_l(k)\delta(E' - E)\delta_{l'l}\delta_{m'm}\,. \tag{2.21}$$

Because of the unitarity of the S-matrix, the diagonal elements are $s_l(k) = e^{2i\delta_l(k)}$, where $\delta_l(k)$ is the scattering phase shift. The scattering amplitude can be calculated via $s_l(k)$

$$f_l(E) = \frac{s_l(k) - 1}{2ik} = \frac{\sin\delta_l(E) e^{i\delta_l(E)}}{k}\,. \tag{2.22}$$

The physical interpretation of the scattering phase shift $\delta_l(E)$ can be seen when $f_l(E)$ is inserted into the scattering solutions,

$$j_l^{(+)}(kr) \overset{r\to\infty}{\sim} j_l(kr) + \frac{\sin\delta_l(E) e^{i(kr - l\pi/2 + \delta_l(E))}}{kr} \overset{r\to\infty}{\sim} e^{i\delta_l(E)} \frac{\sin\left(kr - \frac{l\pi}{2} + \delta_l(E)\right)}{kr}\,. \tag{2.23}$$

We see that the scattering solutions for $r \to \infty$ are phase shifted relative to the free case, Eq. (2.19), by $\delta_l(E)$. Usually an attractive potential "pulls" the wave

function in, resulting in a positive phase shift ($\delta_l(E) > 0$), whereas a repulsive potentials "pushes" the wave function out ($\delta_l(E) < 0$). This is not generally true if the attractive potential is strong enough to support bound states, in which case the potential may act repulsive or attractive depending on the location of the last bound state closest to dissociation (see Fig. 2.2).

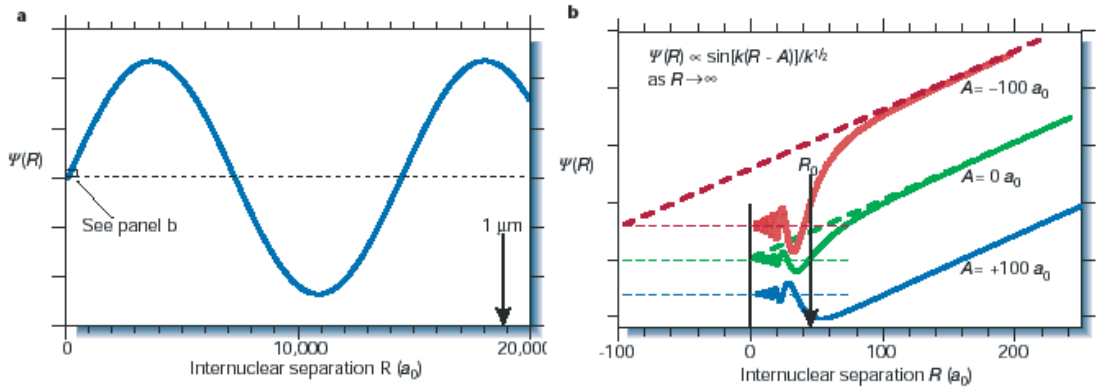

Figure 2.2: Graphs of typical s-wave scattering wave functions $\Psi(R)$ as a function of internuclear separation R. Fig. (a) shows the long-range behavior of the wave function. Fig. (b) show a blow-up of short-range behavior of Ψ for three different scattering phase shifts. The phase shift of the long-range wave function is strongly influenced by the exact behavior of the wave function in the inner region for $R < R_0$. The extension of the asymptotic wave function to the intersection with the R-axis indicates the scattering length $a = A$ measured in Bohr radii a_0 for the three different scenarios with $A = -100a_0$, $A = 0$, and $A = +100a_0$. The scattering length and scattering phase shift are closely related to the location of the last bound state below dissociation. Although the potential is generally attractive, the scattering length is large and positive for a bound state just below dissociation and negative for a quasi-bound state just above dissociation. Figure courtesy of Burnett [1].

In general, this expansion into partial waves represents a convenient basis for representing the Hamiltonian and the scattering solutions. For cold collisions, the partial-wave expansion becomes even more important: near zero temperature s-wave (i.e. $l = 0$) scattering typically dominates due to the centrifugal barrier for higher partial waves. This behavior is quantified in the Wigner threshold law. For small

energies $E = \hbar^2 k^2/2m$ and long deBroglie wavelengths $\lambda_{\mathrm{dB}} = 2\pi/k$, the scattering phase shift is proportional to $\delta_l(k) \propto -k^{2l+1}$ (see Ref. [51]). For s waves and in the zero energy limit, it is therefore helpful to define a new constant parameter, the s-wave scattering length a, via

$$a = -\lim_{k\to 0} \frac{\tan \delta_l(k)}{k} \,. \tag{2.24}$$

The physical interpretation of this scattering length is easily seen in Fig. 2.2. In this picture the scattering length is given by the node closest to the origin if one extends the asymptotic wave functions (2.23) all the way to intersect with the x-axis. Since the scattering length is defined through the negative phase shift, it is usually negative for attractive potentials and positive for repulsive potentials. However, if an attractive potential is strong enough to support bound states, the sign of the scattering length is strongly correlated with the position of the last bound state close to dissociation [52]. If the last bound state is very close to dissociation at energy E_b, the scattering is positive and large with

$$a^2 = \frac{\hbar^2}{2\mu E_b} \,. \tag{2.25}$$

On the other hand, the scattering length is negative and large in magnitude if the interaction potential has a quasi-bound state just above dissociation. If the bound state is located exactly at zero-energy with respect to dissociation, then the potential has a zero-energy scattering resonance and a is infinite. The scattering length is of great importance in the description of ultracold collisions, since it contains the nature of the interaction (i.e. repulsive vs. attractive and strength, as well as the location of the last bound state) in a single parameter. For example, in the application to BEC, the scattering length determines the regions of stability of the condensate [1, 11].

More importantly for us, the scattering length allows us to define an effective interaction potential with the aim of replacing the complicated realistic atomic interaction potentials. The main idea here is to replace the realistic interaction by

a pseudopotential that reproduces the exact asymptotic wave function. One possibility, which is apparent from the interpretation of the scattering length as the intersection of the extended asymptotic wave function, would be to place a hard wall (hard sphere) at the intersection point, thus forcing the node of the wave function to be at a. An alternative way is to match the boundary condition of the asymptotic wave function at the origin as it is done in the Fermi-pseudopotential, which is described in the next section.

2.3 The Fermi pseudopotential and its generalizations to higher partial waves

2.3.1 Fermi-pseudopotential

The most widely used approximation to the two-body interaction is the Fermi pseudopotential, which is frequently applied in the modeling of complex Bose or Fermi many-body systems. Enrico Fermi introduced the zero-range pseudopotential in 1936 to model the interaction of electrons with neutrons by replacing the complicated atomic interaction potential by a much simpler potential that mimics the asymptotic stationary scattering wave functions of the realistic potential [53]. Fermi used a δ function centered at the origin with a strength equal to the scattering length a_{scatt} [Eq. (2.24)] as effective potential

$$v_{\text{eff}} = \frac{2\pi\hbar^2}{\mu} a \delta^3(\mathbf{r}) \,. \tag{2.26}$$

The singularity at the origin, with correctly chosen strength a_0, produces the correct asymptotic wave functions of the realistic potential. Later a regularized version of the pseudopotential was introduced to extend the operator domain to wave functions that may be irregular at the origin. The regularization operator $\partial/\partial r\, r$ acts as a

projector onto the set of regular functions, allowing irregular functions that diverge as r^{-1}. The regularized form of the pseudopotential allows one to write down an eigenvalue equation for the pseudopotential, whose eigensolutions have the correct asymptotic behavior.

In this form, the pseudopotential has been extremely valuable for recent applications to ultracold collisions. At ultracold temperatures, s-wave collisions dominate the interaction. In this regime, the Fermi pseudopotential, which captures only s-wave contributions, is an excellent approximation and is widely applied to mean field calculations for Bose-Einstein condensates as well as to ultracold spectroscopy of the interatomic interaction potentials. Recently, further generalizations of the pseudopotential that go beyond the constant scattering length approximation have been proposed. For energies outside the Wigner-threshold regime, the Fermi pseudopotential can be generalized to include an energy-dependent scattering length so that the mean-field and trap energy-level shifts can be calculated in a self-consistent manner [54, 55]. Further generalizations of the pseudopotential are necessary if one considers collisions at higher temperatures, or in anisotropic potentials such as separated traps and quasi 1-D or 2-D systems, or in the case that s-wave collisions are prohibited due to symmetry considerations as in the case of identical fermions. Then higher partial-wave contributions beyond s waves become important. In the following we will discuss the generalization of the Fermi-pseudopotential to higher partial waves as well as the inclusion of an energy-dependent scattering length.

2.3.2 Huang and Yang's higher partial-wave pseudopotential

The first attempt to derive a generalized pseudopotential was made by K. Huang and C. N. Yang [56, 57]. Given a central force, the true radial asymptotic wave function

$R_l(r)$ for each l wave is supposed to follow from a contact potential,

$$v_{\text{eff}}^{(l)}(r) = \frac{2\pi\hbar^2}{\mu}\frac{(l+1)[(2l-1)!!]}{[(2l)!!]}a_l^{2l+1}\frac{\delta^3(\mathbf{r})}{r^l}\frac{\partial^{2l+1}}{\partial r^{2l+1}}r^{l+1}\,, \tag{2.27}$$

where a_l is the scattering length generalized to higher partial waves. In the following, we will review the original derivation in some more detail, before we discuss the problems of the pseudopotential that have been found by Roth and Feldmeier [58]. This detailed original derivation will also be instructive for our later derivation of a correct form of the higher partial-wave pseudopotential.

Schrödinger equation for spherically symmetric potential

The objective is to replace the exact potential $V(r)$ at all energies and for all partial waves by a zero-range pseudopotential [56]. The general idea for deriving the pseudopotential is to match the boundary condition of the asymptotic solution at the origin through a zero-range pseudopotential. The Schrödinger equation for a central potential $V(r)$ in the relative coordinate system is given by

$$\left[-\frac{\hbar^2}{2\mu}\nabla^2 + V(\mathbf{r})\right]\psi(\mathbf{r}) = E_k\psi(\mathbf{r}) \tag{2.28}$$

with $E_k = \hbar^2k^2/2\mu$. Defining $v(\mathbf{r}) = \mu/\hbar^2\,V(\mathbf{r})$ this can be written in unitless representation as

$$\frac{1}{2}\left(\nabla^2 + k^2\right)\psi(\mathbf{r}) = v(\mathbf{r})\psi(\mathbf{r})\,. \tag{2.29}$$

For spherically symmetric potentials we can expand the wave function in partial waves $\psi(\mathbf{r}) = R_l(r)Y_l^m(\Omega)$. The Schrödinger equation for the radial solution is

$$\begin{aligned}\frac{1}{2}\left(\nabla_r^2 - \frac{l(l+1)}{r^2} + k^2\right)R_l(r) &= v(r)R_l(r)\,;\\ \frac{1}{2}D_lR_l(r) &= v(r)R_l(r)\,,\end{aligned} \tag{2.30}$$

where we have defined the derivative operator D_l and

$$\nabla_r^2 = \frac{1}{r}\frac{\partial^2}{\partial r^2} r \,. \tag{2.31}$$

As before, we assume that the realistic potential $v(r)$ has finite range R, i.e. for $r > R$ the potential $v(r)$ is identical to zero. Outside the range R of the potential $v(r)$, the radial solution is given by

$$R_l(r) = A_l \left[j_l(kr) - \tan \delta_l(k) n_l(kr) \right] \text{for } r > R, \tag{2.32}$$

where $\delta_l(k)$ is the l-wave scattering phase shift for the true interaction and $j_l(kr)$ and $n_l(kr)$ are the spherical Bessel functions.

Schrödinger equation for zero-range potential

We would now like to extend the solution (2.32) all the way to the origin by replacing the exact potential by an effective zero-range interaction potential $v_{\text{eff}}^{(l)}(r)$ for each l. The radial Schrödinger equation for this zero-range potential is

$$\begin{aligned} \frac{1}{2} D_l R_l(r) &= \quad 0 \quad && \text{for } r \neq 0, \\ \frac{1}{2} D_l R_l(r) &= v_{\text{eff}}^{(l)} R_l(r) && \text{for } r = 0. \end{aligned} \tag{2.33}$$

This Schrödinger equation has the solution Eq. (2.32), defined everywhere except at $r = 0$.

$$R_l(r) = A_l \left[j_l(kr) - \tan \delta_l(k) n_l(kr) \right] \text{for } r > 0. \tag{2.34}$$

The problem is now reduced to finding a pseudopotential for which the solution Eq. (2.34) fulfills the Schrödinger equation (2.33).

Derivatives of Bessel and Neumann functions

In order to solve the Schrödinger equation for the pseudopotential (2.33), we need the radial solution around the origin. The expansions of the Bessel and Neumann functions around $r = 0$ are [59]

$$\begin{aligned} j_l(kr) &\rightarrow \frac{(kr)^l}{(2l+1)!!}, \\ n_l(kr) &\rightarrow -\frac{(2l-1)!!}{(kr)^{l+1}}\,. \end{aligned} \tag{2.35}$$

These expansions are necessary to evaluate the derivative operator acting on the radial solution. The Bessel function is the solution to the free Schrödinger equation. Applying the derivative operator D_l on the spherical Bessel function results in

$$D_l j_l(kr) = 0 \text{ for all } r. \tag{2.36}$$

The Neumann function is not a good solution to the free equation at the origin and is only a solution for $r \neq 0$. The derivative of the spherical Neumann function is

$$D_l n_l(kr) = 0 \text{ for } r \neq 0. \tag{2.37}$$

What remains is to calculate the derivative of the Neumann function at the origin. Consider therefore the following integration in a small volume around the origin.

$$\int_V d^3r\, r^l D_l n_l(kr) = \int_V d^3r\, r^l \nabla_r^2 n_l(kr) - \int_V d^3r\, r^l \frac{l(l+1)}{r^2} n_l(kr) + \int_V d^3r\, r^l k^2 n_l(kr)\,. \tag{2.38}$$

Using Green's theorem,

$$\int_V u\nabla^2 v dV = \int_S u\boldsymbol{\nabla} v d\boldsymbol{\sigma} - \int_V \nabla u \nabla v dV\,, \tag{2.39}$$

and using the expansion of the Neumann function, Eq. (2.35), we can evaluate the first term in Eq. (2.38) to be

$$\begin{aligned}\int_V d^3r\, r^l \nabla_r^2 n_l(kr) &= \int_S d\boldsymbol{\sigma}\, r^l \boldsymbol{\nabla}_r n_l(kr) - \int_V d^3r l r^{l-1} \nabla_r n_l(kr) \qquad (2.40)\\ &= \int_S d\boldsymbol{\sigma}\mathbf{e}_r\, r^l \frac{(l+1)(2l-1)!!}{k^{l+1}r^{l+2}} - \int_V d^3r l r^{l-1} \frac{(l+1)(2l-1)!!}{k^{l+1}r^{l+2}}\,.\end{aligned}$$

Here, the first term is given by

$$\int_S d\boldsymbol{\sigma}\mathbf{e}_r\, \frac{(l+1)(2l-1)!!}{k^{l+1}r^2} = 4\pi \frac{(l+1)(2l-1)!!}{k^{l+1}}\,. \qquad (2.41)$$

The second term in Eq. (2.40) is of equal magnitude and opposite sign relative to the second term (centrifugal term) in Eq. (2.38) and therefore cancels

$$\int_V d^3r\, r^l \frac{l(l+1)}{r^2} n_l(kr) = \int_V d^3r l \frac{(l+1)(2l-1)!!}{k^{l+1}r^3}\,. \qquad (2.42)$$

The last term in Eq. (2.38) vanishes as $r \to 0$ and in summary we can write

$$D_l n_l(kr) = \frac{(l+1)(2l-1)!!}{k^{l+1}} \frac{\delta(r)}{r^{l+2}} \qquad (2.43)$$

since

$$\int_V d^3r\, r^l D_l n_l(kr) = 4\pi \frac{(l+1)(2l-1)!!}{k^{l+1}} = \int_V d^3r\, \frac{(l+1)(2l-1)!!}{k^{l+1}} \frac{\delta(r)}{r^2}\,. \qquad (2.44)$$

Pseudopotential

We can now rewrite the left side of the zero-range Schrödinger equation (2.33). Using Eqs. (2.36) and (2.37) we get

$$\begin{aligned}\frac{1}{2} D_l R_l(r) &= 0 && \text{for } r \neq 0,\\ \frac{1}{2} D_l R_l(r) &= -A_l \tan\delta_l(k)\, D_l n_l(kr) && \text{for } r = 0. \qquad (2.45)\end{aligned}$$

Inserting Eq. (2.43), we can evaluate the differential operator applied to the full wave function,

$$\frac{1}{2}D_l R_l(r) = -\frac{1}{2}A_l(l+1)(2l-1)!!\frac{\tan\delta_l(k)}{k^{l+1}}\frac{\delta(r)}{r^{l+2}}\,. \tag{2.46}$$

Comparing this to the Schrödinger equation (2.33), we can write the pseudopotential as the following operator identity [56]

$$v_{\text{eff}}^{(l)} = -\frac{1}{2}A_l(l+1)(2l-1)!!\frac{\tan\delta_l(k)}{k^{l+1}}\frac{\delta(r)}{r^{l+2}}\,. \tag{2.47}$$

The normalization constant A_l remains to be determined in the next section.

Sometimes, instead of the 1-D δ function in r, the three-dimensional $\delta^{(3)}(\mathbf{r})$ function is used according to

$$\delta^3(\mathbf{r}) = \frac{\delta(r)}{4\pi r^2}\,. \tag{2.48}$$

However, one has to carefully treat this three-dimensional δ-function in spherical coordinates, since at the origin the angles θ and ϕ are not defined. Using the three-dimensional δ-function the pseudopotential is then written as [60]

$$v_{\text{eff}}^{(l)} = -2\pi A_l(l+1)(2l-1)!!\frac{\tan\delta_l(k)}{k^{l+1}}\frac{\delta^{(3)}(\mathbf{r})}{r^l}\,. \tag{2.49}$$

Normalization of pseudopotential according to Huang

The correct asymptotic wave functions of a realistic potential are determined only by the correct phase shifts. Instead of matching the phase shifts of the true asymptotic wave functions by ensuring a node (zero) of the wave function at $r = a$, the δ function enforces the matching of the boundary condition at the origin. However, in this case the amplitude of the wave function has to be well defined by A_l. Since scattering eigenstates states are not normalizable, it is necessary to specify the derivative of

the wave function at the origin. As stated before, the radial solution Eq. (2.34) can be expanded around the origin $r = 0$

$$R_l(r) = A_l \left[\frac{(kr)^l}{(2l+1)!!} - \tan\delta_l(k) \frac{(2l-1)!!}{(kr)^{l+1}} \right] \text{for } r > 0. \tag{2.50}$$

The normalization constant can be found by evaluating the $(2l+1)$-th derivative of the r^{l+1}-weighted radial solution at the origin,

$$\begin{aligned} \left[\frac{\partial^{2l+1}}{\partial r^{2l+1}} r^{l+1} R_l(r) \right]_{r=0} &= A_l \left[\frac{\partial^{2l+1}}{\partial r^{2l+1}} \frac{k^l r^{2l+1}}{(2l+1)!!} - \tan\delta_l(k) \frac{\partial^{2l+1}}{\partial r^{2l+1}} \frac{(2l-1)!!}{k^{l+1}} \right], \\ &= A_l \frac{(2l+1)!}{(2l+1)!!} k^l. \end{aligned} \tag{2.51}$$

The normalization is then given by

$$A_l = \frac{(2l+1)!!}{(2l+1)!} \frac{1}{k^l} \left[\frac{\partial^{2l+1}}{\partial r^{2l+1}} r^{l+1} R_l(r) \right]_{r=0}. \tag{2.52}$$

Here, the regularization also acts as a projector on the subspace of regular functions. In this form, the pseudopotential can then be used on the space of all regular and irregular functions. The pseudopotential can be rewritten as [56, 57]

$$\begin{aligned} v_{\text{eff}}^{(l)} &= -\frac{1}{2} \frac{(l+1)[(2l+1)!!]^2}{(2l+1)(2l+1)!} \frac{\tan\delta_l(k)}{k^{2l+1}} \frac{\delta(r)}{r^{l+2}} \frac{\partial^{2l+1}}{\partial r^{2l+1}} r^{l+1}, \\ &\approx \frac{1}{2} \frac{(l+1)[(2l-1)!!]}{[(2l)!!]} a_l^{2l+1} \frac{\delta(r)}{r^{l+2}} \frac{\partial^{2l+1}}{\partial r^{2l+1}} r^{l+1}. \end{aligned} \tag{2.53}$$

Here, the l-wave scattering length is defined as

$$a_l^{2l+1} = -\lim_{k\to 0} \frac{\tan\delta_l(k)}{k^{2l+1}} \tag{2.54}$$

with units of length. Of course, we could have defined an energy-dependent scattering length without the zero energy limit and applied the self-consistent method discussed later in this chapter. Note that this definition of a_l differs by a factor of $[(2l+1)!!]^2/(2l+1)$ from other authors [61]. For the particular case of a hard sphere

potential, the scaled length $[(2l+1)!!]^2/(2l+1)a_l$ coincides with the radius of the hard sphere.

For s waves ($l = 0$), the potential reduces to the well known energy-dependent regularized δ-potential,

$$v_{\text{eff}}^{(0)} = \frac{1}{2} a \delta(r) \frac{\partial}{\partial r} r = 2\pi a \delta^3(\mathbf{r}) \frac{\partial}{\partial r} r \,, \tag{2.55}$$

where the s-wave scattering length is defined by

$$a = a_{l=0} = -\lim_{k \to 0} \frac{\tan \delta_0(k)}{k} \,. \tag{2.56}$$

Alternative normalization of pseudopotential

The normalization constant has been determined analogous to Huang *et al.* [56]. However, the use of the $(2l+1)$-th partial derivative is not the only way for determining A_l. For example A_l can be also written as

$$A_l = \frac{(2l+1)!!}{(2l+1)} \frac{1}{k^l} \left[\frac{1}{r^{2l}} \frac{\partial}{\partial r} r^{l+1} R_l(r) \right]_{r=0} \,. \tag{2.57}$$

Generally, A_l can be determined using any derivative of order one to $2l+1$ so that the pseudopotential seems to have several different possible definitions for $l > 0$. However, only the original operator with the $(2l+1)$-th partial derivative acts as a proper projector on the l-wave radial function subspace. Of course, one can always use a different order derivative if this is more convenient and add an additional projector $\hat{P}_l$ instead.

2.3.3 Effective contact interaction potential by Roth and Feldmeier

Recently, Roth and Feldmeier [58] uncovered difficulties with the pseudopotential derived by Huang and Yang, noting that the perturbative energy shifts of interacting

atoms in a trap are incorrect by a factor of $(l+1)/(2l+1)$. This can easily be seen if one solves for the exact energy spectra of two interacting particles in a 3D well with an infinite wall at the radius Λ. Because of this auxiliary boundary condition, the asymptotic wave functions (2.32) have to vanish at $r = \Lambda$,

$$R_l(\Lambda) = A_l \left[j_l(k\Lambda) - \tan\delta_l(k) n_l(k\Lambda) \right] \equiv 0 \,. \tag{2.58}$$

This leads to discrete energy levels with energy E_{nl} and discrete momenta $k = q_{nl}$, which for the noninteracting case $\delta_l(k) = 0$ are given by

$$q_{nl}\,\Lambda = \pi \left(n + \frac{1}{2} \right) , \tag{2.59}$$

$$E_{nl} = \frac{\hbar^2 q_{nl}^2}{2\mu} = \frac{\hbar^2 \pi^2}{2\mu\Lambda} \left(n + \frac{1}{2} \right) . \tag{2.60}$$

Here, we used the asymptotic expansion of the spherical Bessel function $j_l(k\Lambda)$ for large Λ. For the interacting case, the momenta $\bar{q}_{nl}$ are given by [58]

$$\bar{q}_{nl}\,\Lambda = -\delta_l\,\bar{q}_{nl} + \pi \left(n + n_l^b + \frac{1}{2} \right) , \tag{2.61}$$

where $\delta_l(k = \bar{q}_{nl})$ is the phase shift due to the interaction. The additional phase πn_l^b is the phase due to the number n_l^b of bound states according to Levinson's theorem [51]. The energy shifts due to the interaction are then given by [58, 61]

$$\frac{\Delta E_{nl}}{E_{nl}} = -\frac{2}{\Lambda} \frac{\delta(q_{nl})}{q_{nl}} \approx \frac{2}{\Lambda} q_{nl}^{2l} a_l^{2l+1} \,, \tag{2.62}$$

where our definition of scattering length a_l^{2l+1} does not include the prefactors $[(2l+1)!!]^2/(2l+1)$ used in Ref. [58, 61].

If the energy shifts are calculated in first order perturbation theory using the higher partial-wave pseudopotentials $v_{\text{eff}}^{(l)}$ derived by Huang and Yang,

$$\langle n, l, m |\, v_{\text{eff}}^{(l)} \,| n, l, m \rangle = -\frac{2}{\Lambda} \frac{(l+1)}{(2l+1)} q_{nl}^{2l} a_l^{2l+1} \,. \tag{2.63}$$

Here, the unperturbed wave functions were given by $\langle x|n,l,m\rangle = A_l j_l(q_{nl}r)Y_l^m$ with normalization $A_l^2 = 2q_{nl}^2/\Lambda$ [58]. Comparing the result to the exact energy shifts, one finds a discrepancy corresponding to a factor of $(l+1)/(2l+1)$ in $v_{\text{eff}}^{(l)}$. Roth and Feldmeier therefore concluded that the generalized pseudopotential derived by Huang and Yang is not a proper effective interaction to use in a mean-field description of dilute quantum gases [58]. Roth and Feldmeier [58] proposed that a distinct effective contact interaction (ECI) is needed to calculate energy level shifts in perturbation theory.

The construction of the ECI is quite different from the pseudopotential construction since it does not try to capture the asymptotic wave function. Instead, their derivation starts with the requirement that the expectation values of a proper ECI have to equal the exact energy shifts for interacting particles in Eq. (2.62) so that

$$\langle n,l,m|\, v_{\text{ECI}}^{(l)}\, |n,l,m\rangle = \Delta E_{nl}\,. \tag{2.64}$$

Roth and Feldmeier insert the following ansatz for the ECI,

$$v_{\text{ECI}}^{(l)} = \frac{\overleftarrow{\partial^l}}{\partial r^l}\gamma_l\delta^3(\mathbf{r})\frac{\overrightarrow{\partial^l}}{\partial r^l}\,, \tag{2.65}$$

into Eq. (2.64) and (2.62) and obtain the ECI interaction strength

$$\gamma_l = 2\pi\frac{(2l+1)}{(l!)^2}\frac{[(2l+1)!!]^2}{(2l+1)}a_l^{2l+1}\,. \tag{2.66}$$

Using this form of the ECI, it is easy to show that the correct energy shifts are obtained. However, due to the nature of the derivation and the application of the potential to only matrix elements, it is unclear whether this potential could result in the correct asymptotic wave function and phase shift. We will show later that the distinction between the pseudopotential and a mean field ECI is unnecessary. Rather, the disagreement is due to a fundamental problem in Huang's original derivation of the pseudopotential [57].

2.3.4 Omont's pseudopotential

Another different formulation of the pseudopotential has been derived by Omont [62]. This higher partial-wave potential has been originally derived to capture the effect of a neutral perturber on an excited electron in a Rydberg atom and is given by

$$v^{(l)}_{\mathrm{Omont}} = 2\pi(2l+1)a_l^{2l+1}k^{2l}P_l\left(\frac{\overleftarrow{\nabla}\cdot\overrightarrow{\nabla}}{k^2}\right)\delta^3(\mathbf{r})\,, \tag{2.67}$$

where the ∇ operator in spherical coordinates r, θ, ϕ,

$$\nabla = \frac{\partial}{\partial r}\mathbf{e}_r + \frac{1}{r}\frac{\partial}{\partial\theta}\mathbf{e}_\theta + \frac{1}{r\cos\theta}\frac{\partial}{\partial\phi}\mathbf{e}_\phi\,, \tag{2.68}$$

acts to the left or right wave function as designated by the arrow. Here, P_l are the Legendre polynomials. This zero-range pseudopotential uses the three-dimensional $\delta^3(\mathbf{r})$, which cannot be strictly defined in spherical coordinates. Just as in the Huang potential, the limiting procedure is not clearly given. If, for example, the 3D δ-function is replaced by a radial δ-function according to $\delta^3(\mathbf{r}) = \delta(r)/4\pi$ [see Eq. (2.48)], then the calculated perturbation energy shifts are incorrect by a factor of $1/3$ for $l = 1$. Our pseudopotential approach, which we will present in the next section, corrects this different formulation of the contact interaction as well and clarifies the limiting procedure for the δ-function.

2.4 Derivation of correct pseudopotential based on δ shell

2.4.1 Ansatz for δ-shell pseudopotential

In the contact potential construction, as used by Fermi and later by Huang and Yang, one takes the asymptotic radial wave function associated with a given partial

wave $R_l(r) = A_l\,[j_l(kr) - \tan\delta_l(k) n_l(kr)]$, valid only outside the range of the true potential, and extends it to all r (see Section 2.3). The boundary condition at the origin is set by the zero-range potential, parameterized by the l-wave asymptotic phase shift $\delta_l(k)$. As before we assume that the realistic potential has a finite range, valid when it falls off like $1/r^3$ or faster. The scattering phase shift can be calculated directly via numerical or analytic solution to the Schrödinger equation or may be obtained through spectroscopic data. We will now show that the problems with the pseudopotential that Roth and Feldmeier found [58] are due to a fundamental problem in Huang's original derivation of the pseudopotential when dealing with the δ-function at the origin.

In order to treat the multipole singularity of the δ potential at the origin correctly, we write the pseudopotential as the limit of a δ shell with its radius approaching zero (see Fig. 2.3),

$$v^{(l)}_{\text{shell}}(r) = \lim_{s\to 0} \delta(r-s)\hat{O}_l(r)\,, \tag{2.69}$$

where the operator $\hat{O}(r)$ contains the correct prefactors and regularization. To derive the correct form of $\hat{O}(r)$ we solve the radial Schrödinger equation,

$$\begin{aligned} \frac{1}{2}\left(\nabla^2 + k^2\right) R_l(r) &= v^{(l)}_{\text{shell}}(r) R_l(r)\,, \\ \frac{1}{2}\left(\frac{1}{r}\frac{\partial^2}{\partial r^2} r - \frac{l(l+1)}{r^2} + k^2\right) R_l(r) &= v^{(l)}_{\text{shell}}(r) R_l(r)\,. \end{aligned} \tag{2.70}$$

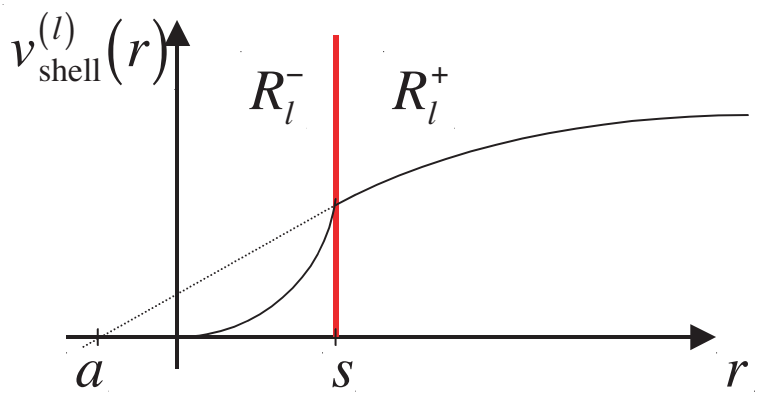

Figure 2.3: Pseudopotential (red vertical line) based on a δ shell with radius s. The inside R_l^- and outside R_l^+ wave function are shown (solid lines) as well as the extension of the asymptotic outside wave function to its intersection with the r-axis. This intersection marks the scattering length a of the interaction.

2.4.2 Radial solutions to the δ-shell potential

The familiar inside and outside solutions expressed in spherical Bessel and Neumann functions are

$$R_l^-(r) = B_l\,[j_l(kr)] \qquad \text{for } r < s, \tag{2.71}$$

$$R_l^+(r) = A_l\,[j_l(kr) - \tan\delta_l(k) n_l(kr)] \qquad \text{for } r > s. \tag{2.72}$$

In the spirit of the pseudopotential approximation, the outside solution to the shell potential coincides with the actual asymptotic wave function of the true potential for large r. Requiring continuity of the wave function at $r = s$ fixes

$$\begin{aligned} \frac{B_l}{A_l} &= \frac{[j_l(ks) - \tan\delta_l(k) n_l(ks)]}{j_l(ks)}\,, \\ &\approx \frac{\frac{(ks)^l}{2l+1)!!} + \tan\delta_l(k)\frac{(2l-1)!!)}{(ks)^{l+1}}}{\frac{(ks)^l}{2l+1)!!}}\,, \\ &\approx 1 + \tan\delta_l(k)\frac{(2l+1)!!(2l-1)!!)}{(ks)^{2l+1}}\,. \end{aligned} \tag{2.73}$$

In the second step, we have used the asymptotic forms of the Bessel functions in the limit $ks \ll 1$ given by Eq. (2.35). Integrating the radial equation over the δ function gives us a second boundary condition (take the limit $s \to 0$ later).

$$\begin{aligned}
\lim_{\epsilon\to 0}\int_{s-\epsilon}^{s+\epsilon}\frac{1}{2}\left(\frac{1}{r}\frac{\partial^2}{\partial r^2}r-\frac{l(l+1)}{r^2}+k^2\right)R_l(r)dr &= \lim_{\epsilon\to 0}\int_{s-\epsilon}^{s+\epsilon}v_{\text{eff}}(r)R_l(r)dr\,,\\
\lim_{\epsilon\to 0}\int_{s-\epsilon}^{s+\epsilon}\frac{1}{2}\frac{1}{r}\frac{\partial^2}{\partial r^2}rR_l(r)dr &= \left[\hat{O}(r)R_l(r)\right]_{r=s}\,,\\
\frac{1}{2}\left(\left[\frac{\partial}{\partial r}R_l^+(r)\right]_{r=s}-\left[\frac{\partial}{\partial r}R_l^-(r)\right]_{r=s}\right) &= \left[\hat{O}(r)R_l(r)\right]_{r=s}\,, \qquad (2.74)
\end{aligned}$$

where the integration on the left side was performed as integration by parts. We can then evaluate the left side of this equation, once again using the expansions of the Bessel and Neumann functions around the origin, Eq. (2.35).

$$\frac{1}{2}A_l\left(\frac{lk^ls^{l-1}}{(2l+1)!!}+\tan\delta_l(k)\frac{-(l+1)(2l-1)!!}{k^{l+1}s^{l+2}}-\frac{B_l}{A_l}\frac{lk^ls^{l-1}}{(2l+1)!!}\right)=\left[\hat{O}(r)R_l(r)\right]_{r=s}. \qquad (2.75)$$

We insert the ratio B_l/A_l [Eq. (2.73)] and obtain

$$-\frac{1}{2}A_l\left((l+1)+l\right)\tan\delta_l(k)\frac{(2l-1)!!}{k^{l+1}s^{l+2}}=\hat{O}_l(s)R_l(s)\,. \qquad (2.76)$$

The first term in this equation is due to the outside wave function, whereas the second term is due to the inside part. We can fulfill the above condition by choosing

$$\hat{O}(r)=-\frac{1}{2}\frac{(2l+1)!!}{(2l)!!}\frac{\tan\delta_l(k)}{k^{2l+1}}\frac{1}{s^{l+2}}\frac{\partial^{2l+1}}{\partial r^{2l+1}}r^{l+1}\,. \qquad (2.77)$$

Here, the normalization A_l and the regularization operator were chosen analog to the detailed discussion in Section 2.3.2.

2.4.3 The generalized δ-shell pseudopotential

With the reduced mass μ and $\hbar$ scaled to one, the pseudopotential is then

$$v_{\text{shell}}^{(l)}(r)=-\lim_{s\to 0}\frac{1}{2}\frac{(2l+1)!!}{(2l)!!}\frac{\tan\delta_l(k)}{k^{2l+1}}\frac{\delta(r-s)}{s^{l+2}}\frac{\partial^{2l+1}}{\partial r^{2l+1}}r^{l+1}\,. \qquad (2.78)$$

Comparing this to the original Huang and Yang pseudopotential, we see that they differ by a factor $(l+1)/(2l+1)$. This occurs because the original derivation ignores the inside wave function contribution of weight $+l$ in Eq. (2.76) when evaluating the derivative of the Neumann function in Eq. (2.37). In the original derivation Huang and Yang considered an integration in a small volume around the origin resulting in Eq. (2.44),

$$\int_V d^3r\, r^l D_l n_l(kr) = 4\pi \frac{(l+1)(2l-1)!!}{k^{l+1}}\,. \tag{2.79}$$

During this volume integration in Section 2.3.2, the inside wave function is ignored, resulting in the wrong $(l+1)$ factor in the term on the right side of Eq. (2.79). The δ-shell potential approach circumvents the singularity at the origin, allowing one to correctly capture higher multipoles. Furthermore, the δ-shell potential also enforces the correct ordering of limits, taking $s \to 0$ as the final step. With this correction, we reproduce the perturbative mean-field energy level shifts found by Roth and Feldmeier [58] with a mathematically rigorous contact potential that also yields the correct asymptotic eigenfunctions. Another advantage of the δ-shell potential is that its radial solutions R_l are in principle normalizable for finite shell radius whereas the solutions for $s = 0$ diverge as r^l and cannot be normalized.

2.4.4 Pseudopotential and Hermiticity

In the above form, the δ-shell potential is not Hermitian since the derivative operator is not. The regularization we choose is necessary in order to extend the domain of the corresponding Hamiltonian to irregular functions that diverge as $1/r^{l+1}$ when $r \to 0$. Although this does not cause a problem in most applications, in general one must be cautious. In order to make the potential Hermitian on the whole domain, including both regular and irregular functions, an additional regularization operator $\left[r^l/(2l+1)!\right]\left(\partial^{2l+1}/\partial r^{2l+1}\, r^{l+1}\right)$ can be added that acts to the left (i.e. on the bra) as

projector onto the regular function subspace. Such dual regularization is cumbersome and so we generally choose to work with only a single regularization operator.

2.4.5 Note on angular part of pseudopotential and wave functions

Including the angular part, the zero-range pseudopotential is written in the operator form

$$\hat{v}(r) = \sum_l |l,m\rangle v_{\text{shell}}^{(l)}(r) \langle l,m| \,. \tag{2.80}$$

Here, $v_{\text{shell}}^{(l)}(r)$ is the derived l- wave radial pseudopotential and $\langle x|l,m\rangle = Y_{l,m}(\theta,\phi)$ are the spherical harmonics. For the calculation of matrix elements, this means that the angular part of the wave function has to be projected out first. This is trivial if the wave function is written in the spherical harmonics basis. In general, matrix elements are calculated as

$$\begin{aligned} \langle \psi_1|\hat{v}(r)|\psi_2\rangle &= \sum_l \langle \psi_1|l,m\rangle v_{\text{shell}}^{(l)}(r) \langle l,m|\psi_2\rangle \,, & (2.81)\\ &= \int d\Omega \psi_1^* Y_{l,m} \quad v_{\text{shell}}^{(l)}(r) \quad \int d\Omega Y_{l,m}^* \psi_2 \,. & (2.82) \end{aligned}$$

This is of particular importance for perturbation theory calculations for atoms in separated traps, where the interaction potential acts on a non-spherically symmetric wave function (displaced harmonic oscillator). Furthermore, in these cases, it is important to use the Hermitian form of the operator with a regularization operator to the left, since ψ_1 usually includes a regular and irregular part. The regularization operator to the left projects ψ_1 back onto the l-wave regular function subspace.

2.5 Energy-dependent scattering length approximation

2.5.1 Energy-dependent scattering length

Our form of the δ-shell potential depends on the energy-dependent phase shift $\delta_l(k)$, which can usually be approximated in the Wigner-threshold regime by a constant scattering length. We find it more useful here, however, to define a fully energy-dependent l-wave scattering length that captures not only corrections due to the effective range [56], but all higher order terms,

$$a_l^{2l+1}(k) = -\frac{\tan\delta_l(k)}{k^{2l+1}}\,. \tag{2.83}$$

This introduction of an energy-dependent scattering length into the pseudopotential approximation has been studied in great detail for the s-wave case [54,55]. Just as in the s-wave case, the general l-wave δ-shell potential exactly reproduces the correct energy-dependent scattering phase shift $\delta_l(k)$ that arises from the true potential and therefore exactly reproduces the correct asymptotic wave functions for all partial waves at all energies. In fact, using an energy-dependent scattering length for higher partial-wave scattering has added benefits since the Wigner-threshold law may not hold for all l, leading to strong energy dependence of the scattering length Eq. (2.83) near zero energy. For example, for power law potentials of the form C_n/r^n, the phase shift is not proportional to k^{2l+1} for $l > n/2$, but instead behaves as k^n [46]. Although the generalized scattering length at low energies is not constant, the full energy-dependent solution will hold. A general breakdown of the pseudopotential approximation only occurs in cases where the realistic potential does not have a finite range and an outside wave function cannot be defined as in Eq. (2.71). In the case of ground state collisions, the van der Waals interaction potentials behave as $-C_6/r^6$ and an asymptotic regime can always be defined. If the collision includes excited

state atomic potentials, as for example in the case of a dipole-dipole interaction where the interaction potentials fall of as $-C_3/r^3$, the asymptotic region is moved out to larger r and is more difficult to define. For Coulomb potentials which behave as $-C_2/r^2$, a description using asymptotic scattering theory fails completely [51].

2.5.2 Self-consistent solution

The introduction of an energy-dependent scattering length into the pseudopotential approximation causes the corresponding Hamiltonian to be energy dependent. Therefore one must use great care for handling such problems. In particular, the solutions to this Hamiltonian are not orthonormal anymore. For bound solutions, one can solve for the discrete eigenvalues of the energy-dependent Hamiltonian derived from an energy-dependent pseudopotential using a self-consistent procedure [54]. To this end, the eigenspectrum of the system is first calculated as a function of a constant scattering length, giving $E(a)$. Then the effective scattering length is calculated as a function of kinetic energy $E_K = E - V$ for the interaction potential alone, yielding $a(E)$. Simultaneous solutions are then found numerically. Examples of the self-consistent method can be found in later sections and chapters. The primary advantage of this two-step procedure is to split up a difficult problem into two manageable tasks. First is the calculation of the energy spectrum for a δ interaction. Second is the separate calculation of scattering length, which includes the correct energy-dependent boundary conditions in a single parameter. This procedure is particularly important for the accurate calculation of the energy spectra of interacting trapped atoms when the interaction range and width of the trap wave functions are orders of magnitude different, as is typically the case.

2.6 Energy-dependent scattering length approximation at negative energies

2.6.1 Bound states and poles in the S-matrix

So far, we have only discussed the positive energy scattering spectrum with respect to the pseudopotential. We will show in the following that the pseudopotential approximation remains valid even for the bound-state spectrum if the scattering length is continued to negative energies. For the discussion of the analytic properties of the pseudopotential at negative energies, it is helpful to use the relationship between the S-matrix and the bound states of an interaction potential. For bound states, the radial functions j_l and n_l both diverge as $r \to \infty$. It is therefore helpful to use the set of spherical Hankel functions instead

$$h_l^{(1)}(kr) = j_l(kr) + in_l(kr)\,, \tag{2.84}$$

$$h_l^{(2)}(kr) = j_l(kr) - in_l(kr)\,. \tag{2.85}$$

Rewriting the asymptotic radial solutions of the true potential in terms of Hankel functions, we get

$$j_l^{(+)}(r) \overset{r\to\infty}{\sim} \frac{A_l}{2}\left[J_l(k)h_l^{(2)}(kr) + J_l(k)^* h_l^{(1)}(kr)\right]\,, \tag{2.86}$$

where the k-dependent coefficients are the Jost functions $J_l(k)$ and their complex conjugates $J_l(k)^*$. The Jost functions are in general analytic functions of k and can be analytically continued to negative energies and complex k. The S-matrix element $s_l(k) = e^{2i\delta_l(k)}$ is then related to the Jost functions via [51]

$$s_l(k) = e^{2i\delta_l(k)} = \frac{J_l(k^*)^*}{J_l(k)} = \frac{J_l(-k)}{J_l(k)}\,. \tag{2.87}$$

Here, the last step is the Schwarz reflection principle for analytic functions.

For negative energies, the wave vector k is purely imaginary, $k = i\kappa$, and the Hankel functions behave as $h_l^{(2)}(kr) \overset{r\to\infty}{\sim} e^{+\kappa r}$ and $h_l^{(1)}(kr) \overset{r\to\infty}{\sim} e^{-\kappa r}$. If we assume a bound state at $E_b = -\hbar^2\kappa_b^2/2m$, its wave function has to be exponentially decreasing so that the Jost function has to be zero at the bound-state energy,

$$J_l(k) = J_l(i\kappa_b) = 0 \quad \Longleftrightarrow \quad \text{bound state.} \tag{2.88}$$

The S-matrix element $s_l(k)$ has a pole for $k = i\kappa$,

$$s_l(k) = s_l(i\kappa_b) = e^{2i\delta_l(i\kappa)} \to \infty \quad \Longleftrightarrow \quad \text{bound state.} \tag{2.89}$$

This is the important correspondence between the zeros of the Jost function, poles of the S-matrix and the bound states of the true interaction [51].

2.6.2 Analytic continuation of the scattering length and bound states

We will show in this section that the self-consistent method discussed earlier can be applied to the interaction potential itself if the scattering length is analytically continued to negative energies. For negative energies, $k = i\kappa$ is purely imaginary and the scattering length is given by

$$a_l^{2l+1}(\kappa) = \frac{\tanh\left[i\delta_l(i\kappa)\right]}{\kappa^{2l+1}}\,. \tag{2.90}$$

This analytic continuation allows us to capture both the positive energy spectrum of the interaction as well as the bound states of the true interaction potential itself. Consider the radial wave function for negative energies,

$$R_l(r) = \frac{A_l}{2}\left[h_l^{(1)}(i\kappa r)\{1 + \tanh\left[i\delta_l(i\kappa)\right]\} + h_l^{(2)}(i\kappa r)\{1 - \tanh\left[i\delta_l(i\kappa)\right]\}\right]. \tag{2.91}$$

Strictly speaking these solutions are only allowed for normalizable wave functions, the true bound states of the δ-shell potential. These occur when $\tanh\left[i\delta_l(i\kappa)\right] = 1$

since then the coefficient of the exponentially increasing $h_l^{(2)}$ vanishes. At these energies, $a_l = 1/\kappa$. The δ-function bound states are thus located at

$$E_\delta = -\frac{\hbar^2\kappa^2}{2\mu} = -\frac{\hbar^2}{2\mu a_l^2}\,, \tag{2.92}$$

just as in the s-wave case. For constant scattering length this means that the pseudopotential has only a single bound state [63]. For an energy-dependent scattering length, the pseudopotential can have several bound states as given by the implicit equation $E_\delta = -\hbar^2/(2\mu a_l^2(E_\delta))$. The condition for a δ-function bound state, $\tanh\left[i\delta_l(i\kappa)\right] = 1$, is fulfilled only when the phase shift has a pole on the imaginary axis, $\delta_l(i\kappa) = -i\infty$. This occurs at each of the negative energies at which the S-matrix of the true interaction potential has a pole [Eq. (2.89)], i.e., at the energies of each of its bound states as discussed in the previous section. The generalized l-wave pseudopotential with an energy-dependent scattering length thus provides an accurate description of the entire energy spectrum of the true interaction potential, bound and scattering.

2.7 Summary

We have derived a generalized zero-range pseudopotential for higher partial-wave interactions that captures both the scattering solutions and bound-state spectrum self consistently. By employing a limiting procedure on a finite-radius δ-shell potential, we have provided a rigorous correction to the long standing error in Huang's and Yang's pseudopotential. We have also shown that the self-consistent solution together with an analytical continuation of the scattering length to negative energies make it possible to capture both the scattering and bound state spectrum of the true interaction, even outside the Wigner threshold regime and for cases where the scattering length is strongly energy dependent. The pseudopotential has applications to many-body problems as well as for modeling of controlled collisions, which play an

important role in quantum information processing and will be discussed in a later chapter.

Chapter 3

δ-shell potential and application to trapped atoms

3.1 Collisions of trapped atoms

3.1.1 Introduction

Laser cooling and subsequent trapping of neutral atoms has been a rapidly developing field over the past decade. Atoms in traps have become the playground for atomic physics, condensed matter physics, and more recently quantum information physics [1]. The progress in atom traps has led to the observation of Bose Einstein condensation (BEC) in several atomic species, the controlled creation of molecules, degenerate Fermi Gases, trapped atoms in optical lattices [2], the observation of quantum phase transitions [6], coherent transport of atoms [39], and many-body entanglement of atoms [40]. For many of these systems, interactions between atoms play a crucial role and the trapping environment can have a large effect on the interaction between atoms. As discussed in Section 1.1.2, the effects of strong confinement

in one or more dimensions have led to an interesting field of research [18, 20, 24]. As a consequence, scattering models for the description of the interatomic interaction have been adapted and modified to produce accurate results, even under strong confinement [54, 55, 64–66].

In the following chapter, we will discuss some of the issues of modeling cold collisions in a trapping environment. In particular, we will apply the δ-shell pseudopotential derived in the previous chapter to two atoms in an isotropic trap. Here the pseudopotential approach allows us to directly derive analytical solutions and eigenvalue equations by simply matching boundary conditions across the δ shell.

3.1.2 Length scales and other basic considerations for interacting trapped atoms

The basic Hamiltonian for two interacting trapped atoms is

$$\hat{H} = \frac{\hat{\mathbf{p}}_1^2}{2m_1} + \frac{\hat{\mathbf{p}}_2^2}{2m_2} + \hat{V}_{\text{trap}}(\mathbf{r}_1) + \hat{V}_{\text{trap}}(\mathbf{r}_2) + \hat{V}_{\text{int}}(\mathbf{r}_2 - \mathbf{r}_1)\,, \tag{3.1}$$

where $\hat{V}_{\text{trap}}(\mathbf{r}_i)$ describes the trapping potential and $\hat{V}_{\text{int}}$ describes the interaction between atoms. Several length scales play an important role in this system. We assume atoms are well-localized near a potential minimum and thus, we can approximate the trapping potential by a harmonic potential $\hat{V}_{\text{trap}} = m_i\omega^2 r_i^2/2$. The confinement of atoms (see section 1.1.1) is measured by the Lamb-Dicke parameter η, given by $\eta = k_l\bar{r}_0 = \sqrt{E_r/\hbar\omega}$. The width $\bar{r}_0$ of the harmonic oscillator ground state for a single atom is

$$\bar{r}_0 = \sqrt{\hbar/(2m\omega)}\,. \tag{3.2}$$

k_l is the wave vector of the trapping laser light, $E_r = \hbar^2 k_l^2/2m$ is the recoil energy. If we assume an interaction potential, which behaves at long range as

$$\hat{V}_{\text{int}} = -\frac{C_n}{r^n}\,, \tag{3.3}$$

then the characteristic length for the range of interaction is

$$\beta_n = \frac{1}{2}\left(\frac{2\mu C_n}{\hbar^2}\right)^{\frac{1}{n-2}} . \tag{3.4}$$

The characteristic interaction length scale β_n is nicely reviewed in the appendix of Ref. [67]. β_n is approximately the length scale of the breakdown of the semiclassical WKB approximation for the collisional phase shift [67]. β_n is further close to the mean scattering length for a $-\frac{C_n}{r^n}$ potential as defined by Ref. [50]. The other important parameter that we discussed in detail in the previous chapter is the s-wave scattering length a, which is mainly determined by the location of the last bound state of the interaction potential. For alkali atoms, the magnitude of the scattering length can be anywhere in the range from about 100 Bohr radii in ^{87}Rb to several 1000 Bohr radii in ^{133}Cs .

The interaction length scale β_n for ground state collisions is typically on the order of a few nm and much smaller than typical experimental trap sizes, which can range from $10-100$ nm ($\eta = 0.1-1$) in optical lattices and strong dipole traps to several 100 nm for magneto-optic traps. On the other hand, the scattering length a can be many times the size of the trap $\bar{r}_0$ as is naturally the case in ^{133}Cs or for any other alkali close to a scattering resonance. Since $\beta_n \ll \bar{r}_0$ we can safely approximate the interaction through a Fermi pseudopotential or our generalized pseudopotential. $\beta_n \ll \bar{r}_0$ replaces the requirement that the deBroglie wavelength $\beta_n \ll \lambda_{\mathrm{dB}}$ in the free case. The Wigner law is defined only in the energy regime with

$$k \ll \frac{\pi}{2\,|a|}\,, \tag{3.5}$$

for which $\delta_0 = -ka$ is a good approximation. For large scattering lengths as in ^{133}Cs , the collisional energies $3\hbar\omega/2$ for tight traps are already outside the Wigner threshold regime and the constant scattering length approximation breaks down. In this case an energy-dependent pseudopotential approximation needs to be employed [54, 55].

3.1.3 Analytic solutions for interacting trapped atoms: "Busch" solutions

Only very recently, exact analytic solutions have been found for atoms in harmonic traps that interact through Fermi pseudopotential [64]. The Hamiltonian for two atoms with the same mass $m_1 = m_2 = m$ in a harmonic trap of frequency ω is

$$\hat{H} = \frac{\hat{\mathbf{p}}_1^2}{2m} + \frac{\hat{\mathbf{p}}_2^2}{2m} + \frac{1}{2}m\omega^2\mathbf{r}_1^2 + \frac{1}{2}m\omega^2\mathbf{r}_2^2 + \frac{4\pi\hbar^2}{m}a\delta^3(\mathbf{r}_2 - \mathbf{r}_1)\frac{\partial}{\partial r}r\,. \tag{3.6}$$

Because of the quadratic form of both, the kinetic energy term and the potential term, we can transform this Hamiltonian to the center of mass (CM) frame with CM and relative coordinates

$$\begin{aligned} \mathbf{R} &= \frac{m_1\mathbf{r}_1 + m_2\mathbf{r}_2}{M} = \frac{\mathbf{r}_1 + \mathbf{r}_2}{2}\,, \\ \mathbf{r} &= \mathbf{r}_2 - \mathbf{r}_1\,. \end{aligned} \tag{3.7}$$

The total mass M and the reduced mass μ are

$$\begin{aligned} M &= m_1 + m_2 = 2m\,, \\ \mu &= \frac{m_1 m_2}{m_1 + m_2} = \frac{m}{2}\,. \end{aligned} \tag{3.8}$$

The Hamiltonian separates into two parts, one trivial Hamiltonian for the CM motion and one Hamiltonian for the relative coordinate motion, which includes the interaction.

$$\begin{aligned} \hat{H}_{CM} &= \frac{\hat{\mathbf{p}}_R^2}{2M} + \frac{1}{2}M\omega^2\mathbf{R}^2, \\ \hat{H}_{rel} &= \frac{\hat{\mathbf{p}}_r^2}{2\mu} + \frac{1}{2}\mu\omega^2\mathbf{r}^2 + \frac{2\pi\hbar^2}{\mu}a\delta^3(\mathbf{r})\frac{\partial}{\partial r}r\,. \end{aligned} \tag{3.9}$$

From now on we will discuss only the relative coordinate motion (and drop the subscript). Scaling energies by $\hbar\omega$ and all lengths by the characteristic harmonic

oscillator length scale $r_0 = \sqrt{\hbar^2/\mu\omega} = 2\bar{r}_0$, we get

$$\hat{H} = \frac{\hat{\mathbf{p}}_r^2}{2} + \frac{1}{2}\mathbf{r}^2 + 2\pi a\delta^3(\mathbf{r})\frac{\partial}{\partial r}r\,. \tag{3.10}$$

Without following the derivation by Busch *et al.* in detail, one expands the solutions to this Hamiltonian in the well known orthonormal radial Laguerre-Gaussian harmonic oscillator basis, which diagonalizes the first part of the Hamiltonian without interaction. Inserting this into the Schrödinger equation, one can determine the expansion coefficients using the generating functions of the Laguerre polynomials and derive an implicit equation for the shifted energy eigenvalues. (Note: An analogous version of this derivation, using our δ-shell pseudopotential for all higher partial waves, is given in the Appendix A.) The eigenvalue equation is

$$2\frac{\Gamma(-\nu)}{\Gamma(-\nu-1/2)} = \frac{1}{a}\,, \tag{3.11}$$

where the noninteger index ν is related to the energy eigenvalues in harmonic oscillator units via $E = 2\nu + 3/2$. The s-wave eigenfunctions are

$$\psi_l(r) = Ae^{-\frac{r^2}{2}}\Gamma(-\nu)U(-v, 3/2, r^2)\,, \tag{3.12}$$

where U are the hypergeometric Kummer U functions [59]. The normalization is determined in Appendix A to be

$$A^2 = \frac{1}{\frac{\partial}{\partial\nu}\left(\frac{2\Gamma(-\nu)}{\Gamma(-\nu-1/2)}\right)}\,; \tag{3.13}$$

or, after some more algebra, expressed in terms of the scattering length

$$A^2 = \frac{-a}{\frac{2\pi}{\sin(2\pi\nu)} + \Phi(\nu+1) - \Phi(\nu+3/2)}\,, \tag{3.14}$$

where $\Phi(x) = \Gamma(x)'/\Gamma(x)$ is the digamma function. For no interaction and $a = 0$, the index ν is integer, $\nu = n$. The hypergeometric U-functions then reduce to the regular Laguerre polynomials $L_n^{l+1/2}$ so that the regular spherical harmonic oscillator

solutions and eigenvalues are obtained. We will discuss the implicit $l = 0$ eigenvalue equation for interacting trapped atoms in more detail later when we discuss the general higher partial-wave equations.

In order to generalize this approach and results to higher partial waves, one could choose an analogous path for the derivation as presented in the appendix (see Appendix A). However, in the following section, we will discuss an alternative approach that is unique to the δ-shell interaction potential formulation.

3.2 Derivation of "Busch" solutions for general l-wave interactions using the δ-shell potential

Our δ-shell approach offers a direct method for obtaining analytic solutions to a scattering problem by simply matching boundary conditions across the δ shell. We will now demonstrate this by employing the energy-dependent δ shell to find all partial-wave solutions to the Schrödinger equation for two particles in an isotropic harmonic trap interacting through a central potential. We separate out the center of mass motion and all distances are scaled to the characteristic harmonic oscillator length $r_0 = \sqrt{\hbar/(\mu\omega)}$ as discussed in the previous section. The scaled Hamiltonian in units of $\hbar\omega$ is

$$\hat{H} = \frac{\hat{\mathbf{p}}_r^2}{2} + \frac{1}{2}\mathbf{r}^2 + \lim_{s\to 0}\frac{1}{2}\frac{(2l+1)!!}{(2l)!!}a_l^{2l+1}\frac{\delta(r-s)}{s^{l+2}}\frac{\partial^{2l+1}}{\partial r^{2l+1}}r^{l+1}\,. \tag{3.15}$$

We make the Ansatz $\psi_{\nu,l,m} = R_{\nu,l}(r)Y_l^m(\theta,\phi)$ with

$$R^{\pm}_{\nu,l}(r) = r^l exp(-r^2/2)w^{\pm}_{\nu,l}(r) \tag{3.16}$$

for the relative coordinate radial wave function inside and outside the shell (see Fig. 3.1). The Schrödinger equation for the radial wave function,

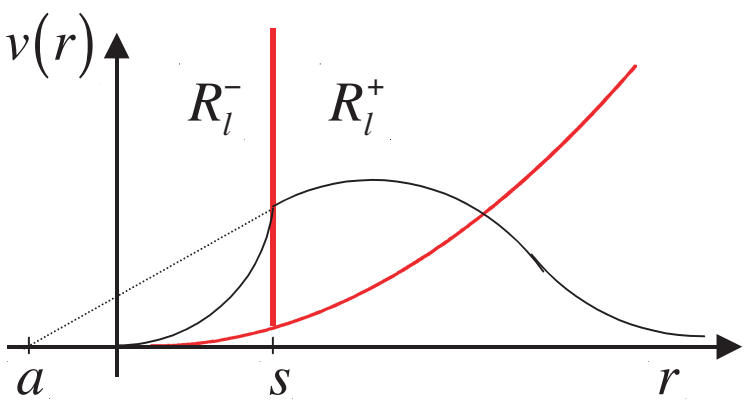

Figure 3.1: Pseudopotential approach for trapped atoms based on a δ shell with radius s (red vertical line). The trapping potential (solid red line) is assumed to be harmonic. The inside $R^-_{\nu,l}$ and outside $R^+_{\nu,l}$ wave function are shown (solid lines) as well as the extension of the asymptotic outside wave function to its intersection with the r-axis. This intersection marks the scattering length a of the interaction.

$$\frac{1}{2}\left(-\frac{1}{r}\frac{\partial^2}{\partial r^2}r+\frac{l(l+1)}{r^2}+r^2\right)R_{\nu,l}(r)=\left(E-v^{(l)}_{\rm shell}(r)\right)R_{\nu,l}(r)\,, \tag{3.17}$$

reduces to the well known Kummer differential equation [59],

$$zw''(z)+(b-z)w'(z)-aw(z)=0\,, \tag{3.18}$$

in the regions where the interaction potential $v^{(l)}_{\rm shell}$ is zero.

Independent solutions of this equation are the confluent hypergeometric functions, $U(a,b,z)$ and $M(a,b,z)$, where $z=r^2$, $a=-\nu$ and $b=l+3/2$ and $E=2\nu+l+3/2$. The inside solution must be proportional to $r^l\exp(-r^2/2)M(-\nu,l+3/2,r^2)$, which behaves regularly as r^l around the origin, whereas the outside solution must be proportional to $r^l exp(-r^2/2)U(-\nu,l+3/2,r^2)$, which falls of exponentially for large r. The inside and outside solutions are then

$$R^-_{\nu,l}(r) \;= B_l r^l e^{-\frac{r^2}{2}}M(-\nu,l+\tfrac{3}{2},r^2) \quad \text{for } r<s, \tag{3.19}$$

$$R^+_{\nu,l}(r) \;= A_l r^l e^{-\frac{r^2}{2}}U(-\nu,l+\tfrac{3}{2},r^2) \quad \text{for } r>s. \tag{3.20}$$

It will be more convenient to write the U function in terms of M functions, so that we can rewrite the outside solution as

$$R^{+}_{\nu,l}(r) = A'_l \Bigg[r^l e^{-\frac{r^2}{2}} M(-\nu, l+3/2, r^2) + \frac{e^{-\frac{r^2}{2}}}{r^{l+1}} \frac{(-1)^l}{\pi} \frac{[\Gamma(l+3/2)]^2}{l+1/2} \frac{\Gamma(-\nu-l-1/2)}{\Gamma(\nu)} M(-\nu-l-1/2, -l+1/2, r^2) \Bigg] . \tag{3.21}$$

In this form, we can very nicely see the analogy to the wave functions in the free case. The first term is analog to the regular spherical Bessel function $j_l(kr)$ and proportional to r^l, whereas the second term is analog to the irregular spherical Neumann functions $n_l(kr)$ and proportional to $r^{-(l+1)}$. The ratio between the two functions, as we will see later, is proportional to $\tan\delta_l$, just as in the free case.

We again require continuity of the wave function at $r = s$ with

$$\begin{aligned} \frac{B_l}{A'_l} &= 1 - \frac{1}{s^{2l+1}} \frac{(-1)^l}{\pi} \frac{[\Gamma(l+3/2)]^2}{l+1/2} \frac{\Gamma(-\nu-l-1/2)}{\Gamma(\nu)} \frac{M(-\nu-l-1/2, -l+1/2, r^2}{M(-\nu, l+3/2, r^2)}, \\ &\approx 1 - \frac{1}{s^{2l+1}} \frac{(-1)^l}{\pi} \frac{[\Gamma(l+3/2)]^2}{l+1/2} \frac{\Gamma(-\nu-l-1/2)}{\Gamma(\nu)} , \end{aligned} \tag{3.22}$$

where the second line is in the limit $ks \ll 1$. Integrating the radial equation over the δ-function gives us a second boundary condition

$$\frac{1}{2} \left(\frac{\partial}{\partial r} R^{+}_{\nu,l}(r) \Big|_{r=s} - \frac{\partial}{\partial r} R^{-}_{\nu,l}(r) \Big|_{r=s} \right) = \hat{O}(r) R_{\nu,l}(r) \Big|_{r=s} . \tag{3.23}$$

Taking $s \ll 1/k$ and inserting the previous results for B_l/A'_l of Eq. (3.22), the derivatives of the outside and inside radial solutions are

$$\begin{aligned} \frac{1}{A_l} \frac{\partial}{\partial r} R^{+}_{\nu,l}(r) \Big|_{r=s} &\approx l s^{l-1} + \tfrac{(-1)^l}{\pi} \tfrac{[\Gamma(l+3/2)]^2}{l+1/2} \tfrac{\Gamma(-\nu-l-1/2)}{\Gamma(\nu)} \tfrac{l+1}{s^{l+2}}, \\ \frac{1}{A_l} \frac{\partial}{\partial r} R^{-}_{\nu,l}(r) \Big|_{r=s} &\approx l s^{l-1} - \tfrac{(-1)^l}{\pi} \tfrac{[\Gamma(l+3/2)]^2}{l+1/2} \tfrac{\Gamma(-\nu-l-1/2)}{\Gamma(\nu)} \tfrac{l}{s^{l+2}} . \end{aligned} \tag{3.24}$$

Note that the first two terms are the same, while the last two differ only by a multiplicative factor. Applying the operator $\hat{O}(r)$ in Eq. (2.77) to (3.20) for small s, we can evaluate the right side of the Eq. (3.23) ,

$$\hat{O}(r)R_{\nu,l}(r)\Big|_{r=s} = \frac{1}{2}\frac{[(2l+1)!!]^2}{s^{l+2}}a_l^{2l+1}A'_l\,. \tag{3.25}$$

Inserting Eq. (3.24) and (3.25) into (3.23), we arrive at the implicit eigenvalue equation,

$$\frac{\pi}{2}\frac{(-1)^l[(2l+1)!!]^2}{(\Gamma(l+3/2))^2}\frac{\Gamma(-\nu)}{\Gamma(-\nu-l-1/2)} \;=\; \frac{1}{a_l^{2l+1}}\,. \tag{3.26}$$

This is the general eigenvalue equation for the l-partial wave interaction that must be solved self-consistently for the energy-dependent a_l as described above. For $l = 0$, this reduces to the known s-wave eigenvalue equation (3.11) derived by Busch *et al.* [64]. The corresponding wave functions are the inside and outside wave functions noted above where the ratio B_l/A'_l is fixed by Eq. (3.22). For finite shell radius, these wave functions are in principle numerically normalizable unlike solutions obtained with a δ potential at the origin, where the unnormalizable solutions diverge as $r^{-(l+1)}$ for $r \to 0$.

During the course of our research, we have learned of alternative approaches for deriving Eq. (3.26). A very nice quantum-defect theory approach for deriving the general Eq. (3.26) was presented by Peach *et al.* [68]. In concurrent theoretical work by Kanjilal and Blume [69], the $l = 1$ special case of Eq. (3.26) has been derived using a corrected $l = 1$ pseudopotential, based on Omont's pseudopotential [62], and applied to 1D- and 3D-confined fermions.

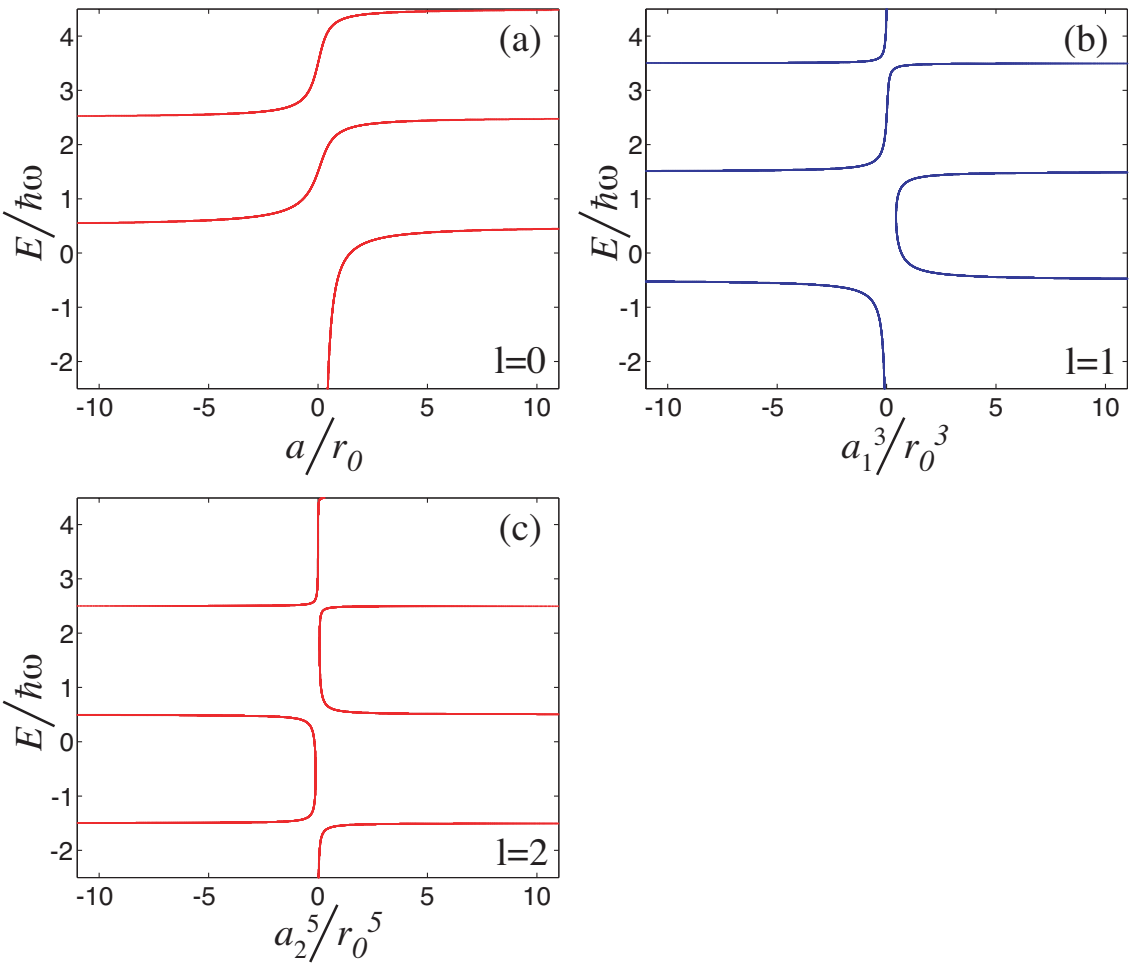

Figure 3.2: Eigenvalues for interacting atoms in traps for $l = 0$, $l = 1$, and $l = 2$ interaction potentials. The solutions to Eq. (3.26) are plotted as a function of the l-wave scattering length.

3.3 Energy spectra for interacting trapped atoms

Figure 3.2 shows numerical solutions to the derived general eigenvalue equation for trapped atoms interacting with an l-partial wave pseudopotential. The results for $l = 0$ are identical to the ones in Ref. [64]. For no interaction, i.e. $a = 0$, one recovers

the unshifted harmonic oscillator energy levels with $(2n+3/2)\hbar\omega$. For infinity positive and negative scattering lengths, these energy levels are shifted maximally by $\pm\hbar\omega$, respectively. More precisely, the energy level for n that is shifted up by $\hbar\omega$ asymptotes to the same energy value as the next energy level with $n+1$ that is downshifted by $\hbar\omega$. This behavior just reflects the fact that $a \to -\infty$ and $a \to \infty$ describe the same physical effect, i.e. a phase shift of the asymptotic solution by $\pi/2$. The wave function in both cases has to be the same, even under confinement. For positive scattering length, one can further identify the δ-function bound state that is originally located at $E_b = -\hbar^2/(2\mu a_0^2)$ and shifted up by the trapping potential. If this bound state is extremely close to dissociation in the free case, the scattering length a is large and positive and the extension of the bound state without trap is measured by a. For $a \gg r_0$, the size of this bound state will be limited by the trap and consequentially, the bound state is pushed to positive energies up to a maximum value of $\hbar\omega/2$.

The energy spectra for $l = 1$ and $l = 2$ are similar to the $l = 0$ case. The usual harmonic oscillator energy levels with $(2n + l + 3/2)\hbar\omega$ can again be shifted at most by $\pm\hbar\omega$. The behavior of the bound state and its link to the trap spectrum has intriguing features, though. The constant scattering length δ-function potential has a single bound state for even l in the case of positive scattering length and for odd l in the case of negative scattering lengths, as seen in the Fig. 3.2 for $l = 1$ and $l = 2$. Intuitively we would expect the correspondence between bound states and the scattering length to be the same for all three cases: a bound state close to dissociation results in a node of the scattering states for large positive r and a corresponding large scattering length. Whereas for $l = 2$, just as for $l = 0$, this is indeed the case, for odd $l = 1$ the δ-function potential has no bound states for positive scattering length. This property of the δ-potential is therefore in stark contrast to our intuitive expectations. The resolution of this paradox follows from considering true potentials with an energy-dependent scattering length, as shown in the next section. If the δ-shell potential is used self-consistently, we observe the same

correspondence between the bound states and the scattering length for $l = 1$ as for $l = 0$, just as predicted by our intuitive arguments. We will revisit this paradox in more detail in Section 3.4.3.

3.4 Breakdown of pseudopotential approximation for trapped atoms: Test example

3.4.1 Spherically symmetric step potential

In order to verify the accuracy of the higher partial-wave energy spectra, we choose a spherically symmetric step potential well with range d and depth V_0 as a test [see Fig. 3.3 (a)]. The potential is given by

$$\begin{aligned} \hat{V}_{\text{test}} &= -V_0 \quad \text{for } r < d, \\ &= \quad 0 \quad \text{for } r > d. \end{aligned} \tag{3.27}$$

This step-potential well is particularly convenient because it can be solved analytically. In the regions of constant potential, we can make the same ansatz for the radial wave function as in the case of the δ shell. $R^{\pm}_{\nu,l}(r) = r^l exp(-r^2/2) w^{\pm}_l(r)$ for $r < d$ (-) and $r > d$ (+) so that the radial equation reduces again to the Kummer differential equation Eq. (3.18). The inside solution must be proportional to $r^l exp(-r^2/2) M(-\nu - V_0/2, l + 3/2, r^2)$ where the index ν is now shifted by $-V_0/2$, accounting for the offset in potential energy. The outside solution is the same as before. The inside and outside solutions are then

$$R^{-}_{\nu,l}(r) = \quad B_l r^l e^{-\frac{r^2}{2}} M(-\nu - \tfrac{V_0}{2}, l + \tfrac{3}{2}, r^2) \quad \text{for } r < d, \tag{3.28}$$

$$R^{+}_{\nu,l}(r) = \qquad A_l r^l e^{-\frac{r^2}{2}} U(-\nu, l + \tfrac{3}{2}, r^2) \qquad \text{for } r > d. \tag{3.29}$$

Matching the boundary conditions across d leads to an implicit equation that can be solved numerically e.g. with Mathematica. Note that, here, a small r expansion of the inside wave function is not possible, since the wave function may be highly oscillatory on the inside depending on the depth of the potential. We compare this

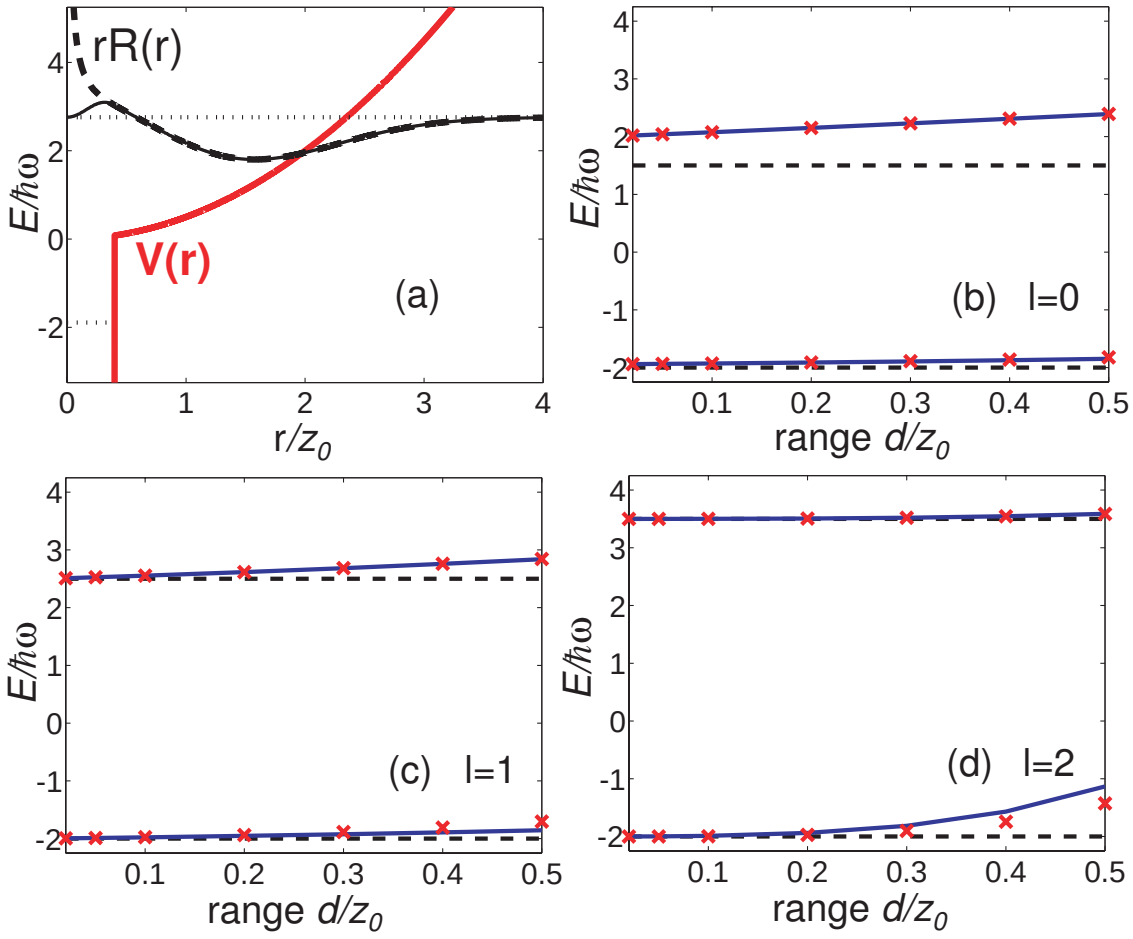

Figure 3.3: (a) Step-well test interaction potential with range $d = 0.4z_0$ and depth $V_0 = 34.95\hbar\omega$ in a harmonic trap, $l = 1$ eigenstates (dotted lines) and corresponding reduced wave function (solid line). The δ-shell solution in the limit of the shell radius $s \to 0$ (dashed line) coincides with the actual eigenstates outside the range d. (b)-(d) Comparison between exact eigenvalues (solid lines) of the step-well interaction plus harmonic trap and pseudopotential eigenvalues (crosses) as a function of the range of the well potential and for $l = 0, 1, 2$ states. The unshifted interaction bound states (fixed at $E_b = -2$) and trap eigenstates are shown as dashed lines.

exact solution with the δ-shell approximation, where the eigenvalues are found self-consistently using the energy-dependent scattering length. For $l = 0$, the s-wave phase shift is given explicitly by

$$\delta_0 (E_K, V_0) = \arctan (k \tan(qR)/q) - kR \,, \tag{3.30}$$

where $q = \sqrt{2\mu(E_K + V_0)/\hbar^2}$ [70]. The energy-dependent scattering length is evaluated using Eq. (2.83) as a function of E. For $l = 1$ and $l = 2$, the phase shift and the scattering length can be solved for analytically as well and has been evaluated using Mathematica.

Figures 3.3(b)- 3.3(d) show a comparison of the exact eigenspectra and the δ-shell approximation for wells with different finite range d. In particular, we chose a well with an l-wave bound state close to dissociation to emphasize the accuracy of the approximation even in the regime of strongly energy-dependent scattering lengths a_l where the Wigner-threshold law does not hold. We find good agreement for relatively large ranges d of the well test potential as shown in Fig. 3.3.

3.4.2 Breakdown of pseudopotential approximation

The breakdown of the pseudopotential approximation at larger ranges is due to the modification of the interaction potential over its finite range by the harmonic trap. As long as the trapping potential is flat across the range d of interaction potential, the self-consistent pseudopotential solutions are exact. If the trap is not constant in this region, one can estimate the difference between the energy shift with and without this modification for the interaction bound states in first order perturbation theory,

$$\Delta E = \langle \psi_{\text{shell}} | r^2/2 | \psi_{\text{shell}} \rangle - \langle \psi_{\text{well}} | r^2/2 | \psi_{\text{well}} \rangle \,. \tag{3.31}$$

Here, ψ_{well} is the exact bound state associated with the step-well potential bound state and ψ_{shell} is the bound-state wave function of the δ-function bound state. For

$l = 1$ and $l = 2$, these two wave functions differ more substantially than for s waves, resulting in a bigger deviation of the pseudopotential approximation as the range d becomes large [Figs. 3.3 (b)-(d)]. In the case of ultracold collisions, the energy-dependent pseudopotential will therefore be a good approximation as long as the characteristic interaction length scale of the van der Waals interaction β_6 is much smaller that the characteristic length scale of the trap r_0. This has been analyzed and tested in detail in Refs. [54, 55].

3.4.3 Odd partial-wave bound state of the spherical step-potential well

In the previous section, we considered a spherical step-potential well with an $l = 1$ bound state at $E_b = -2$. Although the scattering length is positive at zero energy, the potential has a bound state. This is in contrast to the property of the δ-potential discussed earlier and the statement made in the literature that an interaction potential with a positive $l = 1$ scattering length cannot have a bound state close to dissociation [69, 71]. In fact, as shown by the step-potential and as predicted intuitively, exactly the opposite appears to be true. In the higher partial wave case, one needs to consider the energy-dependent scattering length, as shown for the step-well example in Figure 3.4. Here, the energy-dependent scattering length changes sign between the bound state and zero energy. This change in the scattering length seems to be a general feature for realistic interactions where the close by bound state results, just like in the s-wave case, in a repulsive positive energy behavior. A more in depth study of the connection between $l = 1$ bound states and the positive zero-energy scattering length, as well as a study of the resonant like character of the scattering length just below zero energy is planned future investigation.

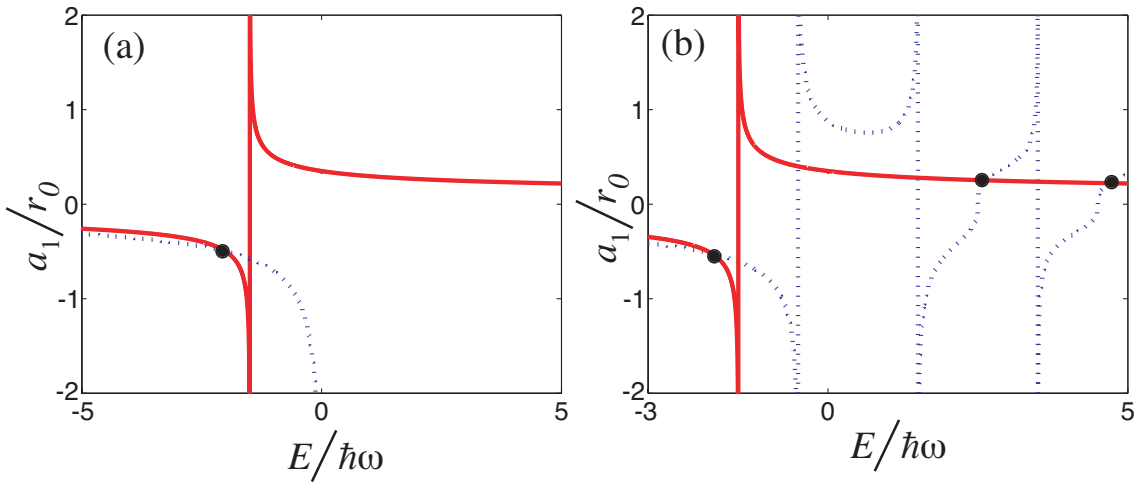

Figure 3.4: $l = 1$ scattering length for the spherical step-well potential (red solid lines). (a) δ-function bound state as a function of scattering length according to $E_b = -\frac{\hbar^2}{2\mu a_1^2}$ (dotted blue line). The intersection between the two curves (black dot) shows the self-consistent solution for the $l = 1$ bound state in the "free" case. (b) $l = 1$ "Busch"-eigen values as a function of scattering length (dotted blue line). The intersection between the two curves (black dots) shows the self-consistent solution for the $l = 1$ bound state and the energy shifted trap eigenstates. The obtained eigenvalues correspond to the $\Delta z = 0$ eigenvalues in Fig, 3.3(c).

3.5 Summary

In Chapter 2 we have derived a generalized zero-range pseudopotential for higher partial-wave interactions that captures both the scattering solutions and bound-state spectrum self consistently. Here, we were able to put this pseudopotential to good use and apply the developed pseudopotential to a system of interacting trapped atoms. The δ-shell potential offers a direct method to analytically solve the Schrödinger equation, as demonstrated for the case of interacting trapped atoms, where we derived the higher partial-wave energy spectrum and obtained normalizable eigenfunctions. This is of special interest for degenerate gases of identical fermions where $l = 1$ scattering is the primary contribution to the interaction and for Bose systems

where noncentral forces play an important role. Our accurate modeling of interacting trapped atoms and the analytical calculation of the eigenenergies should provide new avenues for studying degenerate gases of interacting ultracold atoms in tightly confining traps [1], such as in optical lattices [6]. Beyond its application to many-body problems, the accurate modeling of the interaction of trapped atoms plays an important role in quantum information processing as we will show in later chapters. Other interesting problems include collisions in non-spherically symmetric trapping potentials. For example, "confinement induced resonances" have been predicted for 1D and 2D trapped bose gases [18, 20, 23, 24]. Another interesting and important effect occurs for collisions in separated traps in form of trap-induced resonances. In the next chapter, we will built on our existing models and discuss these new kind of resonances.

Chapter 4

Trap-induced shape resonances in ultracold atomic collisions

4.1 Introduction

The ability to arbitrarily manipulate the quantum state of a many-body ensemble represents the ultimate control of a physical system. The standard approach to modeling and designing coherent states of matter has its foundations in condensed matter theory, where one considers solutions to the entire many-body Hamiltonian. An alternative viewpoint arises from a fundamental theorem of quantum information theory [9]: an *arbitrary* state of a many-body system can be reached entirely through operations on single bodies and pairwise interactions. This provides a direct approach to engineering mesoscopic states through the application of a "quantum circuit" [72, 73]. Moreover, one requires only a *single* two-body interaction (e.g. CPHASE or CNOT gate) that entangles the "particles" to contribute to a universal set of quantum logic gates.

In the context of ultracold neutral atoms, whereas manipulating the quantum

state of an individual atom is a very mature technique, arbitrary unitary mapping of a two-atom system has not yet been achieved. Neutrals, by their very nature, do not strongly couple to anything. This may be an advantage for avoiding noise, but it implies that the two-body interaction will generally require close overlap of the atomic wave packets. By bringing two atoms within the same well of a tightly confining microtrap, one can achieve this strong coupling while remaining in the electronic ground state. Proposals for two-atom control in such a geometry have been considered using ground state s-wave collisions [28], including Feshbach resonances [74] and laser induced Raman transitions [75]. At such close range, the atoms lose their individual identities and instead must be described as a molecular dimer, which generally does not respect the atomic symmetries. This constrains the possible encodings of quantum information such that two-body logic gates can be performed within a well-defined "logical basis". This constraint can be overcome by placing the particles in distinguishable locations where the atomic quantum numbers are conserved asymptotically. Under typical conditions, such separated atoms would generally encounter very weak interactions. The coupling between atoms can be dramatically increased, however, when a resonance of the two-body system is excited, resulting in long-range interactions. An example of this is induced electric dipole-dipole interactions associated with excited electronic states [32, 35].

In this chapter, we describe the physics at the foundation of these protocols by considering ultracold collisions between trapped but *separated* atoms. In this setting, resonances can occur between eigenstates of the trap and molecular bound states, allowing us to overcome the generally very weak interactions associated with the van der Waals potential. These "trap-induced resonances" (TIR) can be substantial and provide a new tool for molecular dimer control (e.g. the production of cold molecules) and the design of two-atom quantum logic gates.

4.2 Hamiltonian and pseudopotential interaction

4.2.1 Hamiltonian for interacting atoms in separated traps

Our model system consists of two atoms in separated traps that interact through the molecular potential $\hat{V}_{\rm int}$. It is described by a Hamiltonian,

$$\begin{aligned}\hat{H} &= \frac{\hat{\mathbf{p}}_1^2}{2m} + \hat{V}_{\rm trap}\left(\mathbf{r}_1 + \frac{\Delta\mathbf{z}}{2}\right) \\ &\quad + \frac{\hat{\mathbf{p}}_2^2}{2m} + \hat{V}_{\rm trap}\left(\mathbf{r}_2 - \frac{\Delta\mathbf{z}}{2}\right) + \hat{V}_{\rm int}(\mathbf{r}_1 - \mathbf{r}_2)\,, \end{aligned} \tag{4.1}$$

where Δz is the separation of the traps (chosen in the z-direction). In the case $\Delta z = 0$ this system reduces to the one discussed in the previous chapter. The trapping potential $\hat{V}_{\rm trap}$ for the two atoms could be, for example, the state-dependent trap of a three-dimensional optical lattice potential [2]. In this system, Δz can be continuously controlled by the angle between the polarization vectors of the counter propagating laser beams [2,39] (see Section 1.1.1). We again assume atoms are well-localized near potential minima that are approximated as isotropic and harmonic with frequency ω. Just as in non-separated case, the Hamiltonian separates because of the quadratic form of the potential term into one for the center-of-mass moving in an isotropic harmonic potential, and one for relative coordinate dynamics, described by (see Appendix B for detailed derivation),

$$\begin{aligned}\hat{H}_{\rm CM} &= \frac{\hat{\mathbf{p}}_R^2}{2M} + \frac{1}{2}M\omega^2\mathbf{R}^2, \\ \hat{H}_{\rm rel} &= \frac{\hat{\mathbf{p}}_{\rm rel}^2}{2\mu} + \frac{1}{2}\mu\omega^2\left(\mathbf{r} - \Delta\mathbf{z}\right)^2 + \hat{V}_{\rm int}(\mathbf{r})\,. \end{aligned} \tag{4.2}$$

The reduced mass $\mu = m/2$ moves under the combined effects of a harmonic trap centered at $\Delta\mathbf{z}$ and a central interatomic potential (Fig. 4.1). The Hamiltonian can

be expressed in spherical coordinates with r, θ, and ϕ as

$$\hat{H}_{\rm rel} = -\frac{\hbar^2}{2\mu}\frac{1}{r}\frac{\partial^2}{\partial r^2}r - \frac{\hbar^2 l(l+1)}{2\mu r^2} + \frac{1}{2}\mu\omega^2 r^2 - \mu\omega^2\Delta z r\cos\theta + \frac{1}{2}\mu\omega^2\Delta z^2 + \hat{V}_{\rm int}(r)\,. \quad (4.3)$$

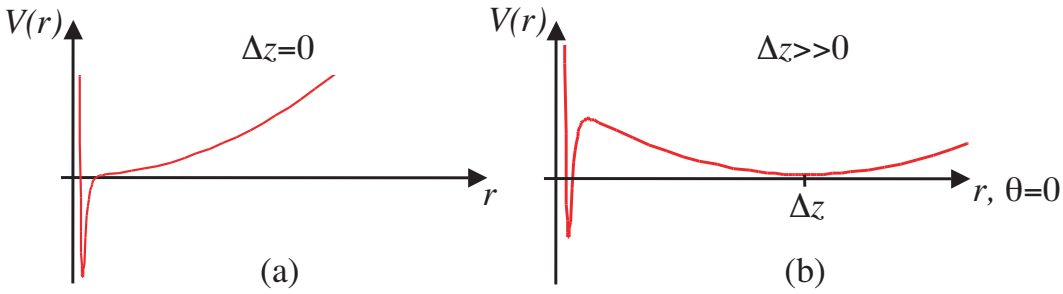

Figure 4.1: Sum of the harmonic trapping potential and chemical binding potential (red line) in the relative coordinate r for zero trap separation (a) and larger trap separation $\Delta z \gg r_0$ (b). For $\Delta z \gg r_0$ the interaction potential is pushed up in energy by the trapping potential at the origin.

4.2.2 Discussion of pseudopotential approximation for separated traps

The harmonic trap is characterized by the characteristic scale $r_0 = (\hbar/\mu\omega)^{1/2}$, while the interatomic potential has a much shorter characteristic length scale β. For the ground state van der Waals interaction $\hat{V}_{\rm int}(r) = -C_6/r^6$, $\beta = \beta_6 = (2\mu C_6/\hbar^2)^{1/4}/2$ (see Section 2.2.1). As we have discussed in 3.4.2, the pseudopotential breaks down if the trapping potential is not constant over the characteristic range of the interaction β. This distortion of the interaction by the separated trap varies with direction. It is greatest along the z-axis and is due to the $\frac{1}{2}\mu\omega^2\Delta z r\cos\theta$ term in the Hamiltonian 4.3. This term is comparable to the long-range interaction,

$$\left|\frac{1}{2}\mu\omega^2 r_{\rm dist}\Delta z\right| = \left|\frac{C_6}{r_{\rm dist}^6}\right|\,, \quad (4.4)$$

at

$$r_{\rm dist} = \left(\frac{2C_6\mu r_0^4}{\hbar^2\Delta z}\right)^{\frac{1}{7}} = \left(\frac{(2\beta_6)^4 r_0^4}{\Delta z}\right)^{\frac{1}{7}} . \tag{4.5}$$

At $r_{\rm dist}$, the distortion due to the trap can no longer be neglected. For a useful pseudopotential approximation, we require $r_{\rm dist} \gg \beta_6$. In an optical lattice system, the largest separation between traps that we need to consider is $\Delta z = \lambda/4$, where λ is the wavelength of the applied light field. For this maximum value of the separation, the pseudopotential approximation holds as long as the confinement parameter η is larger than

$$\eta = k_l \bar{r}_0 = k_l \frac{r_0}{2} > \frac{\pi}{2\sqrt{2}} \left(\frac{\beta_6}{\lambda}\right)^{\frac{3}{4}} . \tag{4.6}$$

For typical values of $\beta_6 = 5$nm and $\lambda = 852$nm for ^{133}Cs, this requires that $\eta > 0.024$, which is true for all current experimental systems.

Further, we will only consider s-wave scattering, which typically dominates for ultracold collisions, and discuss the effects of higher partial interactions later. Under these conditions, the interatomic interaction $\hat{V}_{\rm int}(\mathbf{r})$ can be replaced by the standard s-wave pseudopotential discussed earlier

$$\hat{V}_{\rm eff}(\mathbf{r}, E_K) = \frac{2\pi\hbar^2}{\mu} a_{\rm eff}(E_K)\delta(\mathbf{r})\frac{\partial}{\partial r} r \, . \tag{4.7}$$

Here, $E_K = (\hbar k)^2/(2\mu)$ is the kinetic energy of relative motion for two atoms in an asymptotic scattering state with momentum $\hbar k$. As argued in the previous chapter, the collisional energies $3/2\,\hbar\omega$ for tight traps are outside the Wigner threshold regime and an energy-dependent scattering length needs to be used

$$a_{\rm eff}(E_K) = -\frac{\tan\delta_0(E_K)}{k} , \tag{4.8}$$

where $\delta_0(E_K)$ is the s-wave collisional phase shift. The eigenvalues of this trapped system must thus be solved self-consistently as described in Section 2.5.2. As discussed in Section 2.6, this method not only accurately reproduces the scattering

behavior but also the molecular bound-state spectrum. This is particularly important for the trap-induced resonance described below. Since we limited ourselves only to s-wave interactions, only bound states with s-wave symmetry are included in the description.

4.2.3 Hamiltonian in the "Busch"-basis

Using these approximations, the problem is reduced to solving the Schrödinger equation for the relative coordinate Hamiltonian in Eq. (4.3) with a δ-function interaction. To this end, we represent the Hamiltonian for arbitrary Δz in the basis corresponding to the solutions with $\Delta z = 0$ and a *fixed* scattering length a (i.e. not the self-consistent solution). This basis set, derived by Busch *et al.* [64], consists of 3D-harmonic-oscillator-like solutions and has been discussed in detail in Chapter 3. Since we only include an s-wave pseudopotential we need to consider only the irregular radial waves for $l = 0$, which include the pseudopotential bound state at negative energy. The $l \geq 1$ wave functions are the regular 3D-harmonic oscillator wave functions. The first three terms of the Hamiltonian plus the interaction potential are diagonal in this basis

$$\langle \psi_{\nu',l'}| - \frac{\hbar^2}{2\mu}\frac{1}{r}\frac{\partial^2}{\partial r^2}r + \frac{\hbar^2 l(l+1)}{2\mu r^2} + \frac{1}{2}\mu\omega^2 r^2 + \hat{V}_{\rm int}(r)\,|\psi_{\nu,l}\rangle = E_{\nu l}\delta_{\nu'\nu}\delta_{l'l} \tag{4.9}$$

with

$$E_{\nu l} = \hbar\omega\left(2\nu + l + \frac{3}{2}\right). \tag{4.10}$$

The trap-potential separation term, proportional to $r\cos\theta = \sqrt{4\pi/3}rY_{10}$, is axially symmetric and dipolar, thereby preserving the magnetic quantum number of the relative motion and coupling the partial waves $l, m = 0$ to $l \pm 1, m = 0$. The $m = \pm 1$ states vanish at the origin and are therefore not affected by the interaction. Hence, the $m = \pm 1$ energy levels do not shift and can be trivially included at the end of the calculation.

A detailed derivation of the separation matrix elements is given in Appendix B. The regular matrix elements can be calculated using n- and l-ladder operators given in [24]. Using these ladder operators, the nonvanishing matrix elements are obtained after some basic operator algebra (see Appendix B).

$$\begin{aligned} \langle n,l|r\cos\theta|n,l+1\rangle &= (l+1)\sqrt{\frac{(n+l+3/2)}{(2l+1)(2l+3)}}\,, \\ \langle n,l|r\cos\theta|n-1,l+1\rangle &= -(l+1)\sqrt{\frac{n}{(2l+1)(2l+3)}}\,. \end{aligned} \tag{4.11}$$

For the irregular $l = 0$ solutions, we only need to evaluate the matrix elements $\langle n,1|\, r\cos\theta\,|\nu,0\rangle$. To this end, we use the expansion of the irregular solutions in terms of the regular harmonic wave functions $|nl\rangle$ as in the original derivation of the "Busch" solutions (see Appendix A). The sought-after matrix element is then

$$\langle n,1|\, r\cos\theta\,|\nu,0\rangle = a_\nu\sqrt{\frac{2\Gamma(n+\frac{5}{2})}{\pi\Gamma(n+1)}}\left(\frac{1}{n-\nu}-\frac{1}{n+1-\nu}\right)\,. \tag{4.12}$$

Including all elements, the Hamiltonian matrix (4.3) is tri-diagonal. The diagonal elements are determined through Eq. (3.11); the off-diagonal elements are given by Eq. (4.11) and (4.12). The sparse Hamiltonian matrix is diagonalized in this basis at each trap separation Δz using the numerical program discussed in Appendix C.

4.3 Trap-induced resonances

4.3.1 Energy spectra

The resulting energy spectra for two atoms are shown in Fig. 4.2 and 4.3 for both positive and negative scattering lengths as a function of Δz. The results of first-order perturbation theory for $a = \pm 0.5$ are also shown for comparison. For $\Delta z \gg r_0$, we recover the expected unperturbed 3D harmonic oscillator eigenenergies. As

the separation between traps is decreased, perturbation theory predicts a negative ($a < 0$) or positive ($a > 0$) energy shift to the ground state. The expected behavior is seen for negative a, but an unexpected solution is seen for positive scattering lengths.

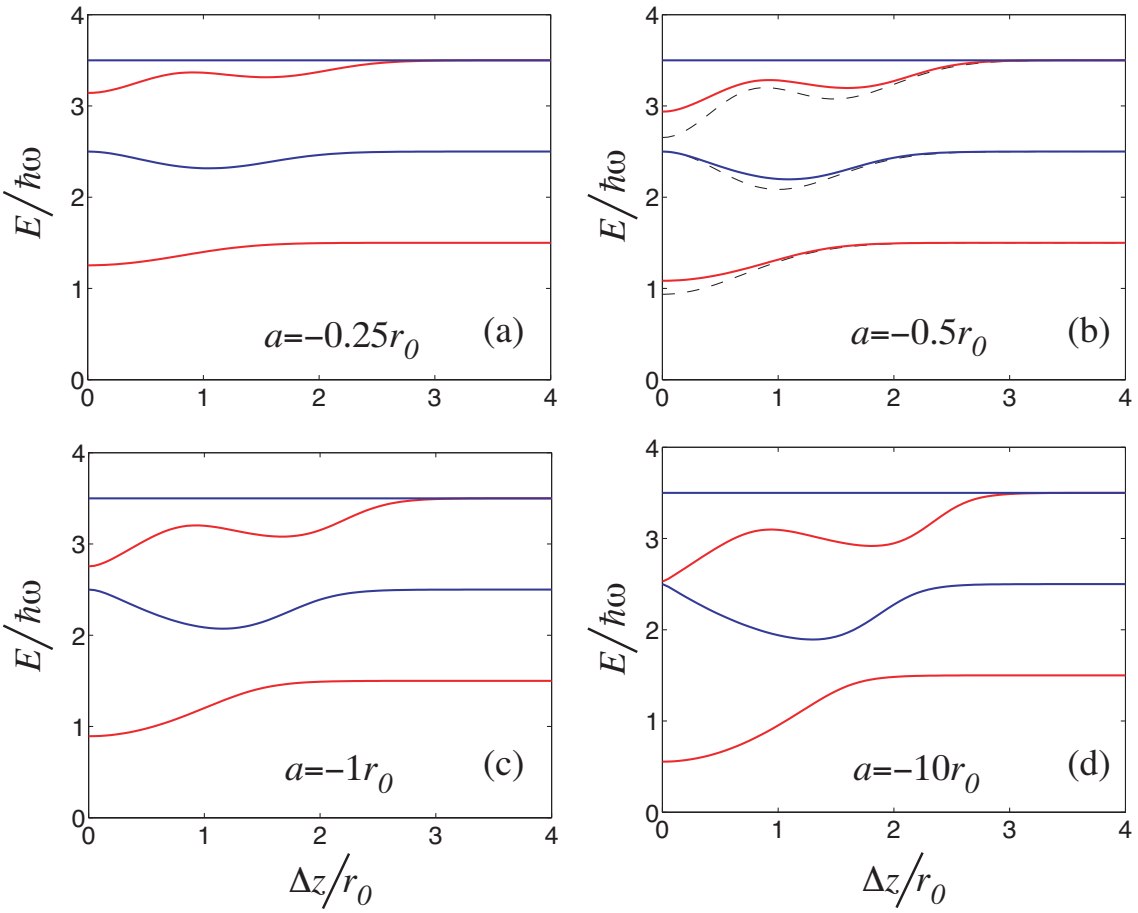

Figure 4.2: Energy spectra as a function of separation Δz between traps for negative scattering lengths $a = -0.25r_0$, $a = -0.5r_0$, $a = -1r_0$, and $a = -10r_0$. The results of perturbation theory are shown as dashed lines for $a = -0.5r_0$.

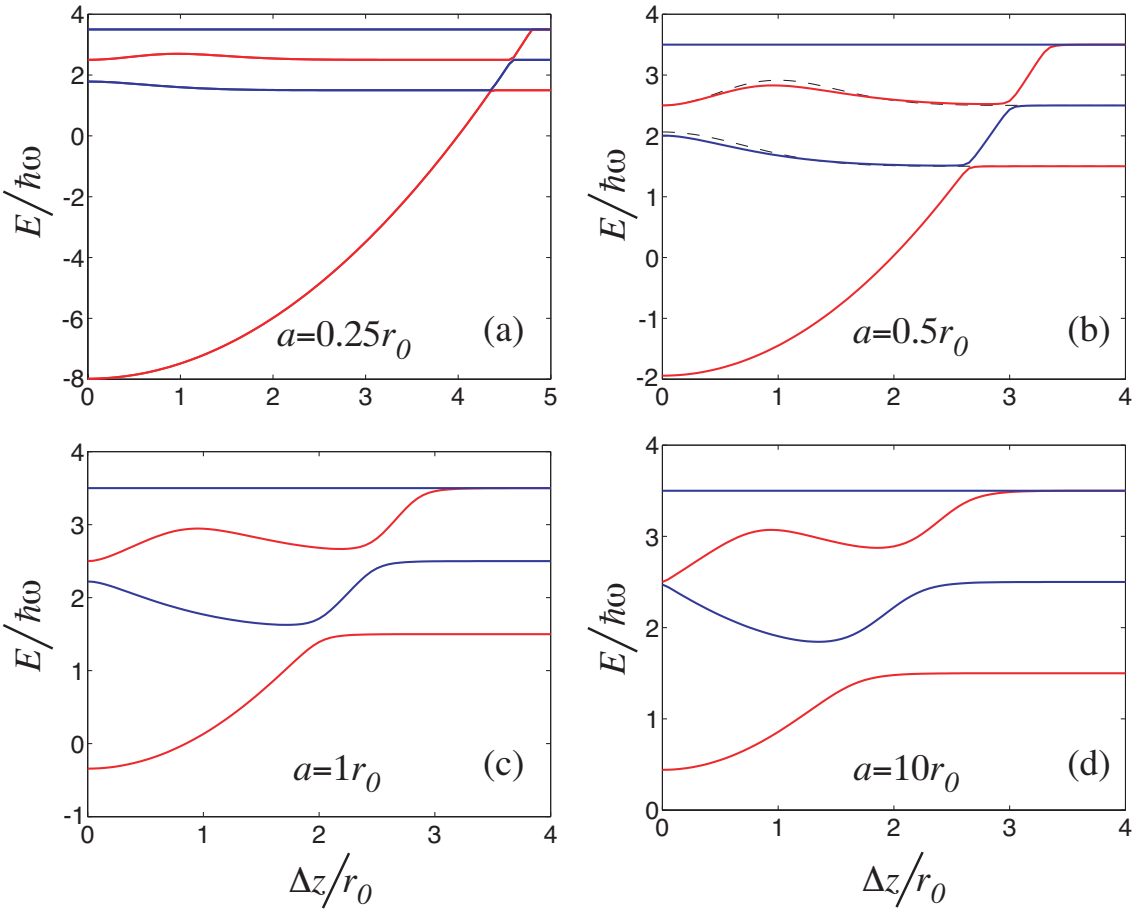

Figure 4.3: Energy spectra as a function of separation Δz between traps for positive scattering lengths $a = 0.25r_0$, $a = 0.5r_0$, $a = 1r_0$, and $a = 10r_0$. The results of perturbation theory are shown as dashed lines for $a = 0.5r_0$. For positive scattering length, one can easily identify the parabolic energy shift of the molecular bound state due to the harmonic trapping potential and the avoided crossings associated with the TISR.

4.3.2 Molecular bound states and trap-induced resonances

The results for the positive scattering length are explained as follows. As discussed in 2.2.2, for large positive a, there is a molecular bound state close to dissociation. As Δz is increased, the interatomic potential, located at very small internuclear dis-

tances, is raised in energy by $\mu\omega^2\Delta z^2/2$ due to the parabolic trapping potential in Eq. (4.3). That is, in order for the separated atoms to collide, they must overcome the potential barrier created by the trap (see Fig. 4.4). When the molecular bound

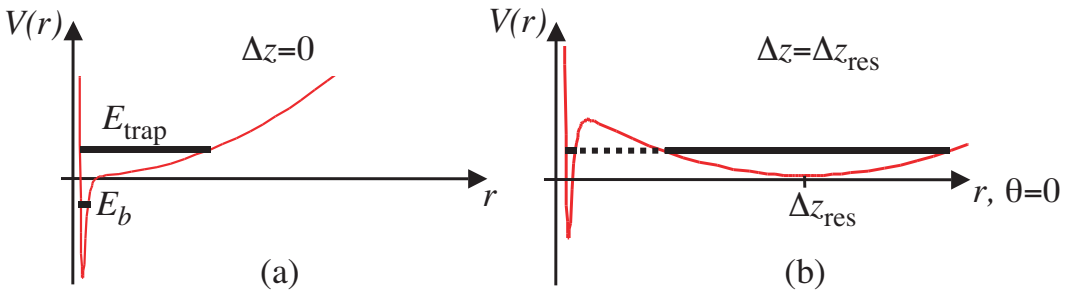

Figure 4.4: Schematic of trap-induced resonanance. Fig. (a) shows the sum of the harmonic trapping potential and chemical binding potential (gray line) in the relative coordinate z for zero trap separation. Fig (b). The molecular bound state at E_b and trap eigenstate at $E_{\rm trap}$ can become resonant at a critical separation $\Delta z_{\rm res}$.

state becomes resonant with the lowest trap eigenstate, an avoided crossing occurs in the energy spectrum(see Fig. 4.3). As the separation is increased even further, the molecular bound state becomes resonant with higher-lying trap states and more avoided crossings occur. This is a new "shape resonance" for s-wave collisions, in which the trap barrier plays the role of the centrifugal barrier in a standard free-space shape resonance for higher partial waves. Analogous, Feshbach-like, "confinement induced resonances" have recently been predicted for 1D and 2D trapped Bose gases [18, 20, 23, 24] and for delocalized states in 3D-optical lattices [76]. Note that the expression "shape resonance" can be quite confusing in this context, since the trap-induced shape resonance does not necessarily imply higher partial-wave scattering, as this is the case in atomic and molecular physics. In fact, the term "shape" refers to the sensitivity of this trap-induced resonance to the shape of the trapping potential and to the fact that the resonance occurs in a single channel as opposed to Feshbach resonances. In the remainder, we will refer to this new kind of a resonance as trap-induced resonance (TIR) in order to avoid further confusion.

4.3.3 Characterization of the trap-induced resonance

The separation at which the lowest resonance occurs, $\Delta z_{\rm res}$, is easily estimated by equating the sum of the molecular binding energy and trapping potential at the origin, $E_b + \mu\omega^2\Delta z^2/2$, to the vibrational ground state energy of the oscillator, $3\hbar\omega/2$, yielding $\Delta z_{\rm res}/r_0 = \sqrt{3 + r_0^2/a^2}$. The location and gap of the avoided crossing depends strongly on the molecular binding energy. For a deeply bound state, but still positive scattering length, corresponding to $0 < a \ll r_0$, the resonance occurs at much larger separations and with an exponentially small energy gap. This corresponds to the small probability for the atoms to tunnel from the trap into the chemical binding potential. Using a standard variational approach [70] based on

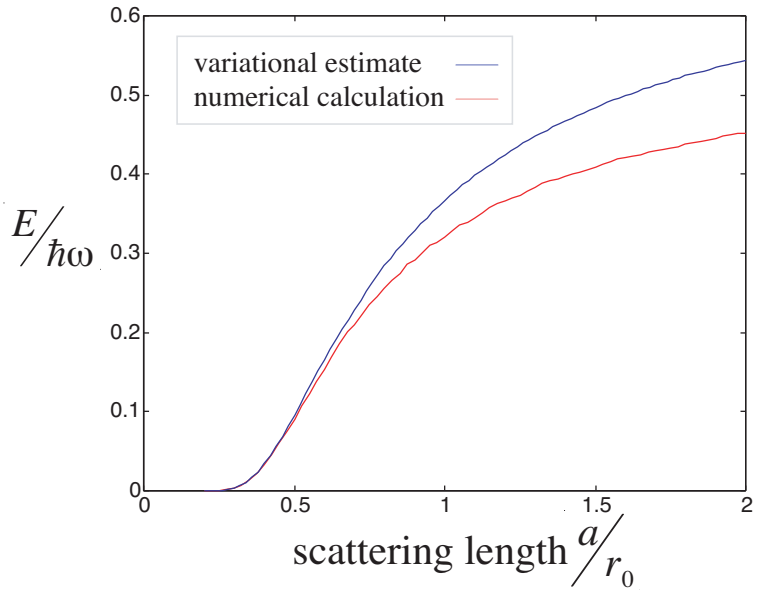

Figure 4.5: The figure shows the energy gap ΔE for the two lowest energy levels at resonance as a function of scattering length a calculated from energy spectra at the different scattering lengths. A variational estimate of the energy gap is shown as the dashed line.

symmetric and anti-symmetric combinations of the $\Delta z = 0$ bound state [64] and the trap ground state, we find that for $0 < a < 0.2r_0$ the gap is smaller than $10^{-4}\hbar\omega$.

For $a \gg r_0$ the energy gap asymptotes to a large value, $\Delta E_{\max} = 0.5640\hbar\omega$ (see Fig. 4.5). The shape resonance can therefore be easily observed for large positive scattering lengths, where the bound state would be close to dissociation. This can be achieved in tight traps, where the scattering length is on the order of r_0 and the energy gap approaches a significant fraction of $\hbar\omega$ (see Fig. 4.5). For example, in an optical lattice of ^{133}Cs atoms the large scattering lengths of the singlet and triplet Born-Oppenheimer potentials, $280a_0$ to $2400a_0$, are comparable to typical trap sizes in an optical lattice, corresponding to a modest Lamb-Dicke parameter $\eta = k_l\bar{r}_0 = k_l r_0/2 = 0.2$. A substantial TIR will result.

4.4 Trap-induced resonances and self-consistent energy spectra

To obtain a more accurate spectrum in the case of trapped alkali atoms, we must account for the energy-dependence of the scattering length in the self-consistent model described in Section 2.5.2. As a test case, we consider again the simplest possible interatomic potential – a step-potential of radius R and depth V_0 with a single s-wave bound state. We have previously discussed this potential and its semianalytical solution for the case of anisotropic traps in 3.4.1. The s-wave phase shift is given explicitly by

$$\delta_0\left(E_K, V_0\right) = \arctan\left(k\tan(qR)/q\right) - kR\,, \tag{4.13}$$

where $q = \sqrt{2\mu(E_K + V_0)/\hbar^2}$ [70]. The energy-dependent scattering length is evaluated using Eq. (4.8) as a function of E_K. The relative kinetic energy of the colliding atoms is given by the total energy eigenvalue E minus the trap potential at the origin given by $\Delta z^2/2$. Figure 4.6 shows the self-consistent energy spectrum as a function of well separation Δz. These approximate eigenvalues are compared with

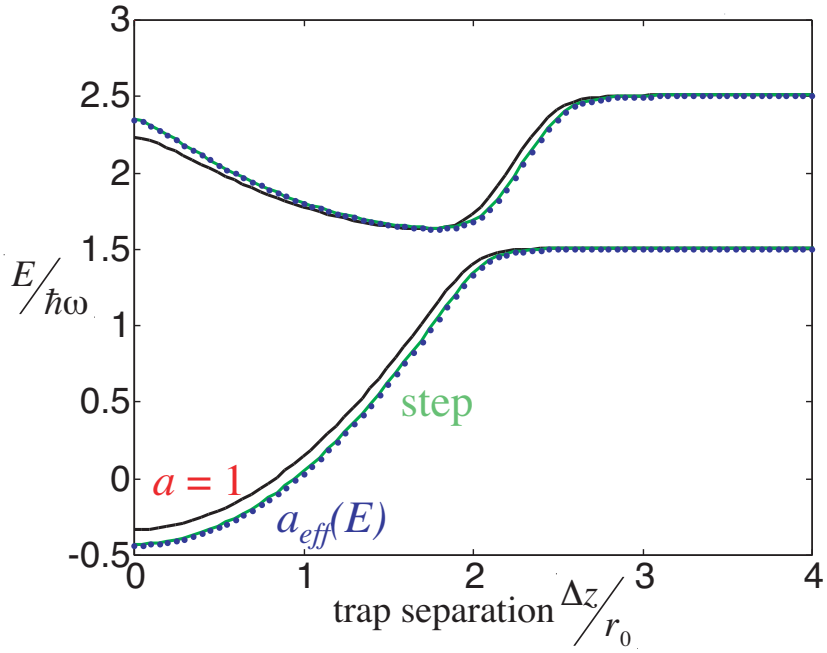

Figure 4.6: Comparison between the energy spectrum of the test step-potential and that of the pseudopotential approximation. The two lowest energy curves are shown for the step-potential (solid), the pseudopotential with an energy-dependent scattering length $a_{\rm eff}$ (circles) and constant a (dashed).

the exact solution for the step-potential ($V_0 = 36.79\hbar\omega$ and $R = 0.2r_0$) plus harmonic potential, calculated numerically. We accomplish this by expanding the total Hamiltonian in isotropic 3D-harmonic oscillator wave functions and diagonalizing the matrix (see numerical codes in Appendix C. Figure 4.6 also shows a plot of the constant scattering length approximation, using the zero-energy scattering length $a = a_{\rm eff}(0)$. As expected, this approximation fails to capture the correct bound-state energy and therefore the correct location of the shape resonance. In contrast, the self-consistent solution using the energy-dependent pseudopotential shows excellent agreement with the exact calculation, even for a well that was chosen to have a fairly long range, $R = 0.2r_0$. The agreement only breaks down when the range of the potential becomes on the order of trap size, $R > 0.5r_0$.

4.5 Higher partial-wave trap-induced resonances

In general, the trap-induced resonance can occur for bound state with any l-wave symmetry. Since the energy-dependent s-wave pseudopotential only captures s-wave bound states self-consistently, we need to consider the higher partial-wave pseudopotential based on the δ shell. This case of separated atoms interacting via the higher partial-wave pseudopotential is left for future work. However, as a proof of principle, we again consider the spherical step-well potential, this time with an $l = 1$ bound state close to zero energy. The energy-dependent scattering length for our example potential is shown in Fig. 3.4. The energy spectrum as a function of separation is shown in Fig. 4.7. Just as in the $l = 0$ case, the $l = 1$ bound state does cause an avoided crossing through a trap-induced resonance. Interestingly though, the "resonance" in the scattering length just below zero-energy as seen in Fig. 4.7 does not affect the energy spectrum in this self-consistent approximation [77].

4.6 Collisions in separated anisotropic traps

In the previous sections, we have limited ourselves to the discussion of collisions in isotropic traps. In general, the trapping potential is not necessarily isotropic. For example in an optical lattice, there will be a slight anisotropy in the direction of separation due to the state-dependent trapping potential. Even worse, the anisotropy usually does not stay constant as the separation between atoms is changed when rotating the polarization angle between the counter propagating laser beams. Alternatively, one could choose less confinement in x-y-directions, since the trap-induced resonance only requires strong confinement along the direction of separation in the z-direction. This can be important if experiments are limited in laser power or in case one needs to reduce the photon scattering rate by detuning further from the

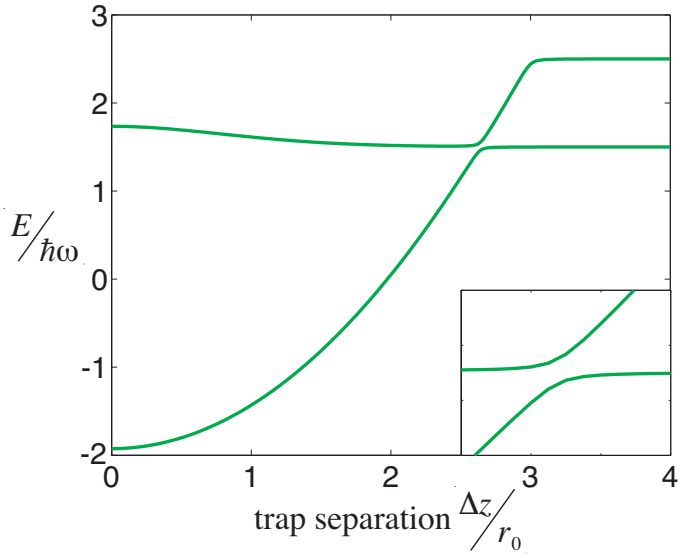

Figure 4.7: Energy spectra as a function of separation Δz for spherical step-well potential with a $l = 1$ bound state. We again identify the parabolic energy shift of the molecular bound state due to the harmonic trapping potential and the avoided crossings associated with the TISR. The inset shows a close-up of the avoided crossing.

excited-state potential.

4.6.1 Hamiltonian

The Hamiltonian for two atoms of the same mass $m_1 = m_2 = m$ in identical anisotropic separated traps $\hat{V}_{\rm trap}(r_i)$ interacting via $\hat{V}_{\rm int}(r)$ is

$$\hat{H} = \frac{\hat{\mathbf{p}}_1^2}{2m} + \frac{\hat{\mathbf{p}}_2^2}{2m} + \hat{V}(\mathbf{r}_1) + \hat{V}(\mathbf{r}_2) + \hat{V}_{\rm int}(\mathbf{r}_2 - \mathbf{r}_1)\,. \tag{4.14}$$

In our model, we approximate the anisotropic trapping potential as harmonic with frequencies $\omega_\perp$ and ω_z in the transverse and z-direction. Because of the quadratic term of both, the kinetic energy term and the potential term, the Hamiltonian can again be separated into a Hamiltonian for the center of mass (CM) motion and the

relative coordinate motion as described in Appendix B.1,

$$\begin{aligned}\hat{H}_{\rm CM} &= \frac{\hat{\mathbf{p}}_R^2}{2M} + \frac{1}{2}M\omega_\perp^2\left(X^2+Y^2\right) + \frac{1}{2}M\omega_z^2 Z^2\,,\\ \hat{H}_{\rm rel} &= \frac{\hat{\mathbf{p}}_r^2}{2\mu} + \frac{1}{2}\mu\omega_\perp^2\left(x^2+y^2\right) + \frac{1}{2}\mu\omega_z^2\left(z-\Delta z\right)^2 + \hat{V}_{\rm int}(r)\,. \end{aligned} \tag{4.15}$$

Here, X, Y, and Z are the Cartesian CM coordinates, x, y, and z the Cartesian relative coordinates. The CM Hamiltonian has the usual anisotropic trap solutions. The relative coordinate Hamiltonian describes an anisotropic trap centered at Δz and the interaction potential centered at the origin. We can rewrite the Hamiltonian for the relative coordinate motion using the spherical harmonics

$$Y_{10} = \sqrt{\frac{3}{4\pi}}\cos\theta\,, \tag{4.16}$$

$$Y_{20} = \sqrt{\frac{5}{16\pi}}\left(3\cos\theta^2-1\right)\,. \tag{4.17}$$

With $z = r\cos\theta$, we can write the Hamiltonian as

$$\hat{H}_{\rm rel} = \frac{\hat{\mathbf{p}}_r^2}{2\mu} + \frac{1}{2}\mu\omega^2 r^2\left(1-\Lambda\sqrt{\frac{16\pi}{5}}Y_{20}\right) - \mu\omega_z^2\Delta z r\sqrt{\frac{4\pi}{3}}Y_{10} + \frac{1}{2}\mu\omega_z^2\Delta z^2 + \hat{V}_{\rm int}(r)\,. \tag{4.18}$$

Here, we defined the "mean" frequency ω,

$$\omega^2 = \left(\frac{2}{3}\omega_\perp^2 + \frac{1}{3}\omega_z^2\right)\,, \tag{4.19}$$

and the parameter Λ,

$$\Lambda = \frac{\omega_z^2-\omega_\perp^2}{3\omega^2} = \frac{\omega_z^2-\omega_\perp^2}{2\omega_\perp^2+\omega_z^2}\,. \tag{4.20}$$

The interatomic interaction $\hat{V}_{\rm int}(r)$ is again replaced by the s-wave pseudopotential

$$\hat{V}_{\rm eff}(\mathbf{r}, E_K) = \frac{2\pi\hbar^2}{\mu}a_{\rm eff}(E_K)\delta(\mathbf{r})\frac{\partial}{\partial r}r \tag{4.21}$$

with an energy-dependent scattering length $a_{\rm eff}(E_K)$.

4.6.2 Matrix elements in anisotropic traps

We represent the relative coordinate Hamiltonian in the same basis as in the isotropic case. This "Busch" basis consists of the irregular $l = 0$ solutions and the regular harmonic oscillator solutions for $l \geq 1$. The first three terms of the Hamiltonian plus the interaction potential are diagonal in this basis

$$\langle \psi_{\nu',l'}| -\frac{\hbar^2}{2\mu}\frac{1}{r}\frac{\partial^2}{\partial r^2}r + \frac{\hbar^2 l(l+1)}{2\mu r^2} + \frac{1}{2}\mu\omega^2 r^2 + \hat{V}_{\rm int}(r)\,|\psi_{\nu,l}\rangle = E_{\nu l}\delta_{\nu'\nu}\delta_{l'l} \tag{4.22}$$

with

$$E_{\nu l} = \hbar\omega\left(2\nu + l + \frac{3}{2}\right). \tag{4.23}$$

The remaining important terms are the Λ anisotropic term and the Δz separation term. The first one couples partial waves with $l - l' = 0, \pm 2$, the second, dipolar term couples partial waves with $l - l' = 0, \pm 1$. The term with Δz^2 only adds a constant energy. The potential is again cylindrically symmetric, just as in the isotropic case. The $m = \pm 1$ levels are again not affected by the interaction and hence, do not shift. They can be trivially included at the end of the calculation.

The regular $l \geq 1$ non-vanishing matrix elements for the anisotropic term are given by

$$\langle nl|\, r^2\, |n, l+2\rangle = \frac{1}{2}\sqrt{(2n+2l+3)(2n+2l+5)}\,, \tag{4.24}$$

$$\langle n+1, l|\, r^2\, |n, l+2\rangle = -\sqrt{2(n+1)(2n+2l+5)}\,, \tag{4.25}$$

$$\langle n+2, l|\, r^2\, |n, l+2\rangle = \sqrt{(n+1)(n+2)}\,. \tag{4.26}$$

For the special case of $l = 0$, we do not need the matrix elements $\langle \nu, 0|\, r^2\, |\nu, 0\rangle$ since the angular part of the integration $I_{l=0,l=0}$ vanishes (see Appendix B). Only the matrix elements $\langle n, 2|\, r^2\, |\nu, 0\rangle$ have to evaluated. To this end, we use the expansion of the irregular solutions in terms of the regular harmonic wave functions $|nl\rangle$ (see

also Appendix A). The nonvanishing irregular matrix elements are given by

$$\langle n, 2| \, r^2 \, |\nu, 0\rangle = a_\nu \sqrt{\frac{\partial \nu_n}{\partial a}} \sqrt{\frac{2\Gamma(n+\frac{7}{2})}{\pi\Gamma(n+1)}} \left(\frac{1}{n-\nu_n} - \frac{2}{n+1-\nu_n} + \frac{1}{n+2-\nu_n} \right) . \tag{4.27}$$

The separation term results in the matrix elements presented in Section 4.2.3, Eqs. (4.11) and (4.12). For a given anisotropy A, the sparse Hamiltonian matrix is diagonalized in this basis at each trap separation Δz using the numerical program discussed in Appendix C.

4.6.3 Energy spectra and discussion

Figure 4.8 shows examples of energy spectra for an anisotropic trap with $A = 4$ and different scattering lengths a for the interaction. The anisotropy does not change the essential character of the trap-induced resonance and the corresponding avoided crossing in the energy spectrum. Also note that in both, the isotropic as well as the anisotropic calculations, we neglected the slight additional anisotropy in the optical lattice potential in the z-direction for separated traps.

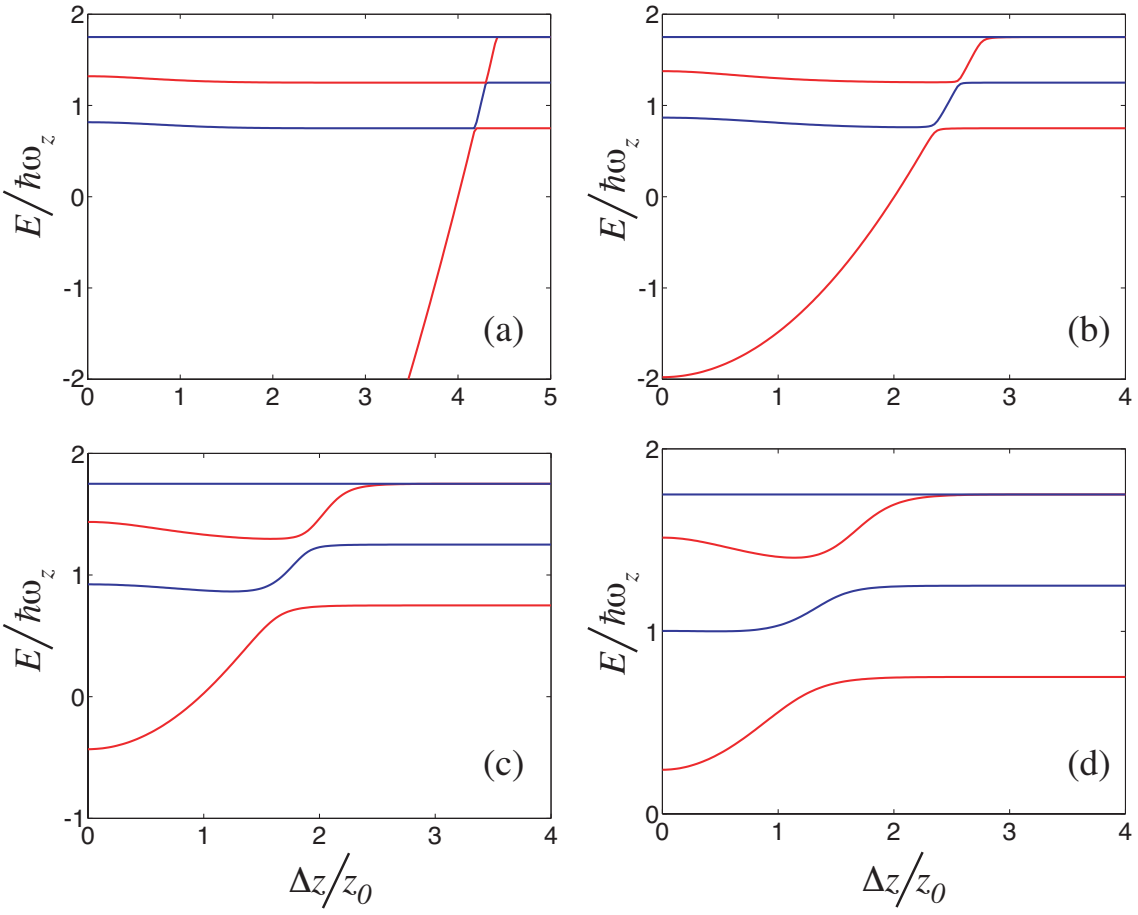

Figure 4.8: Energy spectra as a function of separation Δz for interacting atoms in *anisotropic traps* for (a) $a = 0.25z_0$, (b) $a = 0.5z_0$, (a) $a = 1z_0$, (a) $a = 10z_0$. Here, the anisotropy $A = \omega_z/\omega_\perp = 4$. The energy in each graph is scaled by $\hbar\omega_z$, where ω_z is the trap frequency in the z-direction . The scattering length a and the separation Δz are scaled by the characteristic length in the z-direction $z_0 = \sqrt{\hbar/(\mu\omega_z}$. The parabolic energy shift of the molecular bound state due to the harmonic trapping potential and the avoided crossings associated with the TISR can be identified in each of the graphs.

4.7 Summary

In this chapter, we have applied the self-consistent pseudopotential model to the case of interacting atoms in separated traps. Atoms in separated traps are particularly interesting for use as qubits in quantum computation proposals. The interactions are then necessary to design two-atom quantum logic gates. The use of ultracold ground state collisions was initially considered by Jaksch *et al.* [28] in the non-resonant case, using perturbation theory. Our analysis shows that in principle, for positive scattering lengths, resonances will occur at some atomic separation, and perturbation theory will break down. The resulting avoided crossing in the energy spectrum must be properly accounted for. This is particularly true for atoms with very large scattering lengths, such as ^{133}Cs. The TIR opens the door to new protocols for entangling two-atom logic gates with separated atoms. For example, a 2π Rabi oscillation between the trapped atoms and an auxiliary molecular bound state leads to a phase shift of -1 on the two-atom state (see Figure 4.9). If the acquired

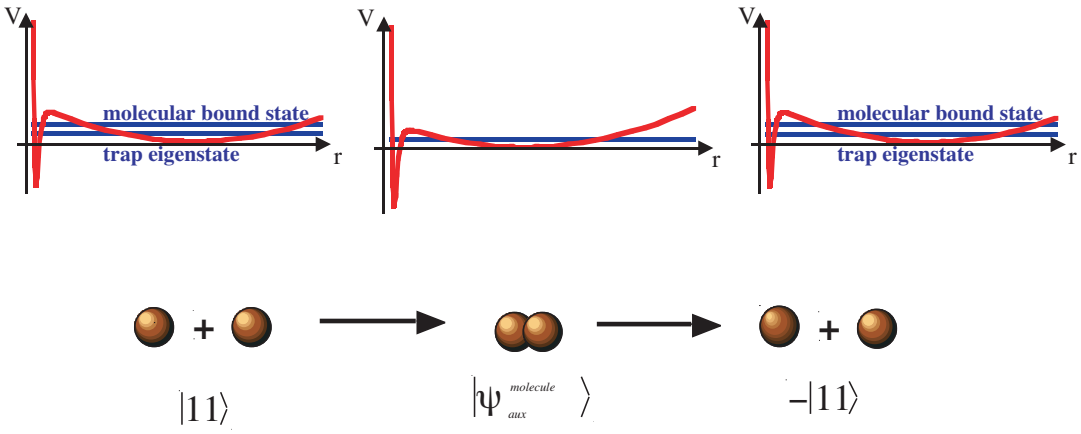

Figure 4.9: The Figure shows the schematic for a two-qubit quantum gate based on the trap-induced resonance. Here, 2π Rabi oscillation between the trapped atoms and an auxiliary molecular bound state leads to a phase shift of -1 on the two-atom state.

phase shift occurs only for one logical encoding of the atoms, the resulting unitary transformation is the so called "CPHASE" two-qubit logic gate [9]. An optimal regime for operation of this protocol is where $r_0 \ll a$. In this regime, the energy gap (Fig.4.5) asymptotes to its maximum value, minimizing the dependence of the cooperative phase shift on the precise value of the trap characteristic length r_0, and hence reducing errors due to trap-laser intensity fluctuations.

More generally, beyond quantum logic, the TIR provides a new avenue for spectroscopy and coherent control of ultracold molecular dimers. Like magnetic Feshbach resonances, these shape resonances can provide new ultra-high precision spectroscopic data on the molecular potential [78], and the production of cold molecules tunable by the trap parameters. More generally, the TIR and the trap eigenstates probe the interaction potential at the bound-state energies and at negative energies in between. For example, a detailed study of the energy spectra of interacting atoms in separated traps, can give information about the analytic continuation of the scattering length to negative energies aside from the location of the interaction bound states.

A complete characterization of these protocols requires a generalization of our model, including the full spin-dependent nature of the collision process via the hyperfine and exchange interactions. In the next chapter we derive a multichannel version of the pseudopotential based on the energy-dependent higher partial-wave δ-shell potential. We also apply this model to collisions in ^{133}Cs for which the observation of trap-induced resonances seems the most promising.

Chapter 5

Trap induced resonances in ^{133}Cs

5.1 Theoretical background

5.1.1 Multichannel scattering and channel state representation

The channel state formalism has been developed initially by F. Mies in [79] as a unifying theory of atomic scattering theory and molecular bound-state spectroscopy. It represents a convenient way to include the influence of bound-states on scattering states as is, for example, the case in Feshbach resonances. Here, the total wave function is expanded in a particular complete set of electronic-rotational states. This particular expansion allows for the asymptotic analysis of the radial part of the wave functions and the calculation of the asymptotic scattering properties in form of the K and S-scattering matrices.

For a two-atom system, the total Hamiltonian is given in a center of mass frame with reduced mass μ, electron coordinates r_{el} and interatomic nuclear coordinate r

as

$$\hat{H} = -\frac{\hbar^2}{2\mu r}\frac{\partial^2}{\partial r^2}r + \frac{\hbar^2 \mathbf{L}_r^2}{2\mu r^2} + \hat{H}_A + \hat{H}_B + \hat{V}_{AB}(\mathbf{r}_{el}, \mathbf{r})\,. \tag{5.1}$$

The first term is the radial kinetic energy operator. The relative coordinate angular momentum $\mathbf{L}_r = -i\mathbf{r} \times \nabla_{\mathbf{r}}$ dependent term is characterized by the partial-wave quantum number l. Of the last three terms, the individual atomic electronic Hamiltonians $\hat{H}_A$ and $\hat{H}_B$ are independent of the interatomic distance r while the interaction potential $\hat{V}_{AB}(\mathbf{r_{el}}, \mathbf{r})$ vanishes for large $r \to \infty$. In this asymptotic limit, the total Hamiltonian $\hat{H}$ becomes completely separable.

A very important feature of atomic scattering theory is the degeneracy of states. At a given positive energy E and for a total angular momentum J with projection M, and given parity Π, there are N_O degenerate scattering states that are energetically accessible. These open channels represent independent orthogonal eigensolutions of the total Hamiltonian

$$(\hat{H} - E)\Psi_\gamma(J, M, \Pi; E) = 0 \quad \text{with} \quad \gamma = 1, N_O\,. \tag{5.2}$$

In this context, a (scattering-) channel is defined by the distinctive quantum numbers J, M, Π. At a given energy E it is often necessary to not only include the energetically accessible states (open channels), but also states that are asymptotically energetically inaccessible (closed channels) in the physical description. This notion of open and closed channels has been initially developed by H. Feshbach in the context of nuclear physics in order to describe the coupling between a molecular bound state to a scattering state [13–15]. This resonance between a molecular bound state that belongs to a closed channel and a scattering state of a different channel has been termed Feshbach resonance (see Fig. 1.3 in Section 1.1.2). Later, with the introduction of general scattering matrices, we will include the closed channels in counting γ. This is of particular importance, since we are interested in the asymptotic scattering properties at negative energies, where the channel of interest is closed.

The solutions to the Schrödinger equation $\Psi_\gamma(J, M, \Pi, E)$ may be expanded using any complete electronic-rotational states $\psi_\alpha(J, M, \Pi; \mathbf{r}_{el}, \hat{r})$ in the following way

$$\Psi_\gamma(J, M, \Pi, E) = \sum_\alpha \psi_\alpha(J, M, \Pi; \mathbf{r}_{el}, \hat{r}) \frac{F_{\alpha,\gamma}(E; r)}{r} \,. \tag{5.3}$$

The $\psi_\alpha(J, M, \Pi; \mathbf{r}_{el}, \hat{r})$ are characterized by the rigorously conserved quantum numbers $J, M, \Pi,$, which will be suppressed in our notation in the following. The functions $\psi_\alpha(\mathbf{r}_{el}, \hat{r})$ span the space of all electron coordinates $\mathbf{r}_{el}$ and further include the angular part of the wave function in the form of spherical harmonics $Y_{l,m}(\hat{r})$ with polar interatomic nuclear coordinates $\hat{r}$. The $F_{\alpha,\gamma}(E; r)$ are reduced radial wave functions that vanish at the origin for a Hermitian interaction potential. The complete set of electronic-rotational states $\psi_\alpha(J, M, \Pi; \mathbf{r}_{el}, \hat{r})$ is predetermined by the Hund's coupling scheme, that is most convenient for expressing the interaction potential $\hat{V}_{AB}(\mathbf{r_{el}}, \mathbf{r})$. Inserting the expansion into the Schrödinger equation, (5.2) we arrive at a set of coupled equations for the radial functions $F_{\alpha,\gamma}(E; r)$

$$\sum_\alpha \langle \psi_\alpha | \, \hat{H} - E \, | \psi_{\alpha'} \rangle \, \frac{F_{\alpha',\gamma}(E; r)}{r} = 0 \,. \tag{5.4}$$

If we ignore the implicit r-dependence of the electronic wave function as in the Born-Oppenheimer approximation described in Section 2.2.1, ψ_α commutes with the radial kinetic energy operator. We can then write the coupled equations as

$$\left(\frac{\hbar^2}{2\mu} \frac{\partial^2}{\partial r^2} - \frac{l(l+1)\hbar^2}{2\mu r^2} + E \right) F_{\alpha,\gamma}(r) - \sum_{\alpha'} \hat{V}_{\alpha,\alpha'}(r) F_{\alpha',\gamma}(r) = 0 \,. \tag{5.5}$$

Although the Hamiltonian $\hat{H}$ becomes separable for large interatomic distances r, the interaction matrix $\hat{V}_{\alpha,\alpha'}$ is not necessarily diagonal in the electronic-rotational basis of choice. We can now define the channel state representation as the particular electronic-rotational basis that diagonalizes the interaction matrix asymptotically. This basis is equivalent to the Hund's case (e) electronic-rotational basis that is usually neglected in molecular theory [49]. The channel states $\psi_\gamma(\mathbf{r}_{el}, \hat{r})$ can be

obtained from the original basis $\{\psi_\alpha\}$ via a simple transformation from the original Hund's case representation to Hund's case (e) according to

$$\psi_\gamma(\mathbf{r}_{el}, r) = \sum_\alpha \psi_\alpha(\mathbf{r}_{el}, r) M_{\alpha,\gamma}(\infty)\,. \tag{5.6}$$

The interaction matrix in the channel state representation is asymptotically diagonal

$$\hat{V}_{\gamma,\gamma'}(r) \overset{r\to\infty}{\sim} \delta_{\gamma,\gamma'} E^\infty_\gamma + \mathcal{O}(r^{-3})\,. \tag{5.7}$$

Thus, in the limit $r \to \infty$, the channel states represent exact solutions to the molecular Hamiltonian with eigenvalue $E^\infty_\gamma = E^\infty_A + E^\infty_B$ and angular momentum quantum number l. For this reason, the channel states are a convenient basis to extract the asymptotic scattering properties of interest. Using the transformation $\mathbf{M}(\infty)$ and rewriting the coupled equations in the channel state representation, we get

$$\left(\frac{\partial^2}{\partial r^2} + k^2_{\gamma'}\right) F_{\gamma',\gamma}(r) - \sum_{\gamma''} U_{\gamma',\gamma''}(r) F_{\gamma'',\gamma}(r) = 0 \tag{5.8}$$

with the asymptotic wave number $k^2_\gamma = 2\mu\hbar^2(E - E^\infty_\gamma)$ and the symmetric interaction matrix $\mathbf{U}$,

$$U_{\gamma',\gamma''} = \frac{2\mu}{\hbar^2}\left(\hat{V}_{\gamma',\gamma''}(r) + \frac{l(l+1)}{r^2}\delta_{\gamma',\gamma''} - E^\infty_{\gamma'}\delta_{\gamma',\gamma''}\right) \overset{r\to\infty}{\sim} \frac{l(l+1)}{r^2}\delta_{\gamma',\gamma''} + \mathcal{O}(r^{-3})\,. \tag{5.9}$$

Following Eq. (5.8), the channel states are only coupled for small internuclear distance r, i.e. at "close range". In the asymptotic limit $r \to \infty$, the "close-coupled" equations (5.8) decouple and we can impose the following boundary conditions on the asymptotic wave functions

$$\left(\frac{\partial^2}{\partial r^2} + k^2_{\gamma'} - \frac{l(l+1)}{r^2}\right) F_{\gamma',\gamma}(r) \overset{r\to\infty}{\sim} 0\,. \tag{5.10}$$

The corresponding asymptotic solutions are linear combinations of the *reduced* spherical Bessel functions $J_{\gamma'}(r)$ and $N_{\gamma'}(r)$

$$F_{\gamma',\gamma}(r) \overset{r\to\infty}{\sim} J_{\gamma'}(r) A_{\gamma',\gamma} + N_{\gamma'}(r) B_{\gamma',\gamma}\,. \tag{5.11}$$

Here, the indices γ and γ' refer to the different "in" and "out" channels of stationary scattering theory (see Section 2.2.2) as will become clear in the discussion of the multichannel S-matrix in the next section.

The reduced radial function $J_\gamma(r)$ is regular at the origin with $J_\gamma(0) = 0$, whereas $N_\gamma(r)$ is irregular at the origin where it diverges as r^{-l}. They are related to the spherical Bessel function j_l and n_l,

$$\begin{aligned} J_\gamma(r) &= \frac{(k_\gamma r)}{|k_\gamma|^{\frac{1}{2}}} j_l(k_\gamma r) \qquad (5.12) \\ &\overset{r\to\infty}{\sim} \frac{1}{|k_\gamma|^{\frac{1}{2}}} \sin\left(k_\gamma r - \frac{\pi l}{2}\right), \\ N_\gamma(r) &= \frac{(k_\gamma r)}{|k_\gamma|^{\frac{1}{2}}} n_l(k_\gamma r) \qquad (5.13) \\ &\overset{r\to\infty}{\sim} -\frac{1}{|k_\gamma|^{\frac{1}{2}}} \cos\left(k_\gamma r - \frac{\pi l}{2}\right). \end{aligned}$$

Note that our definitions of the reduced radial function $J_\gamma(r)$ and $N_\gamma(r)$ differ from the conventions in Ref. [79] by a phase factor. Our different conventions keep the "natural" phase of the wave function, making it easier to analytically continue the different parameters of interest to negative energies. However, we have to keep in mind that in this phase convention, the wave functions are in general complex for closed channels and not real as in Ref. [79].

In scattering theory, we are interested in the asymptotic stationary solutions for large interatomic separation and the appropriate scattering matrices and parameters. Using the asymptotically diagonal channel state basis, the determination of the asymptotic parameters is reduced to determining the r-independent matrix elements $\{A_{\gamma',\gamma}\}$ and $\{B_{\gamma',\gamma}\}$ of Eq. (5.11).

5.1.2 The multichannel K-matrix and S-matrix

In scattering theory, there are several important scattering matrices that characterize the scattering properties of a particular interaction potential. Next, we will discuss the scattering K-matrix and S-matrix in the channel state representation. For simplification, we can write Eq. (5.8) in matrix form,

$$\mathbf{F}''(r) + \left(\mathbf{k}^0\mathbf{k}^0 - \mathbf{U}(r)\right)\mathbf{F}(r) = 0\,. \tag{5.14}$$

Here, the superscript "0" denotes diagonal matrices. The asymptotic reduced radial solutions are

$$\mathbf{F}(r) \overset{r\to\infty}{\sim} \mathbf{J}^0(r)\mathbf{A} + \mathbf{N}^0(r)\mathbf{B}\,. \tag{5.15}$$

Using the matrices $\mathbf{A}$ and $\mathbf{B}$ we can define the K-matrix of scattering theory as

$$\mathbf{K} \equiv -\mathbf{B}\mathbf{A}^{-1}\,. \tag{5.16}$$

Since the set of radial solutions $\mathbf{F}(r)$ is complete, we can always generate a new set of solutions $\mathbf{F}^K(r)$ so that

$$\mathbf{F}^K(r) = \mathbf{F}(r)\mathbf{A}^{-1} \overset{r\to\infty}{\sim} \mathbf{J}^0(r) - \mathbf{N}^0(r)\mathbf{K}\,. \tag{5.17}$$

This form is analogous to the single channel problem discussed earlier where the asymptotic l-wave radial wave function was given by

$$R_l(r) = j_l(kr) - \tan\delta_l n_l(kr)\,. \tag{5.18}$$

The K-matrix is directly related to the tangents of the scattering phase shift. In the next chapter, we will use this analogy to define the scattering length that is used in the pseudopotential approximation with the help of the K-matrix.

Before deriving a multichannel pseudopotential based on the K-matrix, we will first introduce the scattering S-matrix in the channel state representation for completeness of our discussion. The S-matrix describes the coupling of "in" channel to

"out" channels in the scattering process (see review of S-matrix in Section 2.2.2). In our multichannel notation, the "in" channels are denoted by the index γ, the "out" channels by γ'. The S-matrix, just as the K-matrix, can be defined to include both open and closed channels. For closed channels, the reduced radial functions J_γ and N_γ both diverge as $r \to \infty$. It is therefore helpful to introduce the *reduced* spherical Hankel functions as defined by

$$\begin{aligned} H_\gamma^+(r) &= J_\gamma(r) + iN_\gamma(r) \qquad (5.19)\\ &\overset{r\to\infty}{\sim} \frac{-i}{|k_\gamma|^{\frac{1}{2}}} \exp\left[i\left(k_\gamma r - \frac{\pi l}{2}\right)\right], \\ H_\gamma^-(r) &= J_\gamma(r) - iN_\gamma(r) \qquad (5.20)\\ &\overset{r\to\infty}{\sim} \frac{i}{|k_\gamma|^{\frac{1}{2}}} \exp\left[-i\left((k_\gamma r - \frac{\pi l}{2}\right)\right]. \end{aligned}$$

Again, note that we use a slightly different convention than in Ref. [79] and instead define the reduced Hankel functions analogously to the usual definition of the spherical Hankel functions [80]. Writing the reduced spherical Bessel functions in terms of the reduced Hankel functions,

$$\begin{aligned} J_\gamma(r) &= \frac{1}{2}\left[H_\gamma^+(r) + H_\gamma^-(r)\right], \qquad (5.21)\\ N_\gamma(r) &= \frac{1}{2i}\left[H_\gamma^+(r) - H_\gamma^-(r)\right], \qquad (5.22) \end{aligned}$$

we can rewrite the asymptotic reduced radial solutions of Eq. (5.17) as

$$\mathbf{F}^K(r) \overset{r\to\infty}{\sim} \frac{1}{2}\left\{\mathbf{H}^{-0}(r)\left[\mathbf{1}^0 - i\mathbf{K}\right] - \mathbf{H}^{+0}(r)\left[\mathbf{1}^0 + i\mathbf{K}\right]\right\}. \qquad (5.23)$$

Choosing another complete set of solution vectors $\mathbf{F}^S(r)$,

$$\begin{aligned} \mathbf{F}^S(r) &= 2\mathbf{F}^K(r)\left[\mathbf{1}^0 - i\mathbf{K}\right]^{-1} \qquad (5.24)\\ &\overset{r\to\infty}{\sim} \mathbf{H}^{-0}(r) - \mathbf{H}^{+0}(r)\mathbf{S}, \qquad (5.25) \end{aligned}$$

we can define the scattering S-matrix $\mathbf{S}$ for open and closed channels in the usual way as

$$\mathbf{S} \equiv \left[\mathbf{1}^0 + i\mathbf{K}\right]\left[\mathbf{1}^0 - i\mathbf{K}\right]^{-1} . \tag{5.26}$$

If only open channels are present, we can find the scattering phase shifts by a unitary transform that diagonalizes both the S-matrix and the K-matrix,

$$\mathbf{S}_{OO} = \mathcal{U} e^{i2\delta^0} \tilde{\mathcal{U}} , \tag{5.27}$$

$$\mathbf{K}_{OO} = \mathcal{U} \tan\delta^0 \tilde{\mathcal{U}} . \tag{5.28}$$

The scattering phases are determined through the diagonal elements of the K-matrix or S-matrix.

Note that these relationships between the K-matrix, S-matrix and scattering phases are only true for the case of only open channels. Since we are interested in open and closed channels, we can block the K and S-matrix each into four blocks

$$\mathbf{K}\left(N_T \times N_T\right) = \left(\begin{array}{c|c} \mathbf{K}_{OO}\left(N_O \times N_O\right) & \mathbf{K}_{OC}\left(N_O \times N_C\right) \\ \hline \mathbf{K}_{CO}\left(N_C \times N_O\right) & \mathbf{K}_{CC}\left(N_C \times N_C\right) \end{array}\right) \tag{5.29}$$

and

$$\mathbf{S}\left(N_T \times N_T\right) = \left(\begin{array}{c|c} \mathbf{S}_{OO}\left(N_O \times N_O\right) & \mathbf{S}_{OC}\left(N_O \times N_C\right) \\ \hline \mathbf{S}_{CO}\left(N_C \times N_O\right) & \mathbf{S}_{CC}\left(N_C \times N_C\right) \end{array}\right) . \tag{5.30}$$

Following Ref. [79] and expanding Eq. (5.26) for the elements that include an open channel $\mathbf{S}_{OO}$ term,

$$\begin{aligned} \left(\mathbf{S}\mathbf{1}^0 - i\mathbf{S}\mathbf{K}\right) &= \left(\mathbf{1}^0 + i\mathbf{K}\right) , \\ \mathbf{S}_{OO} - i\mathbf{S}_{OO}\mathbf{K}_{OO} - i\mathbf{S}_{OC}\mathbf{K}_{CO} &= \mathbf{1}^0 + i\mathbf{K}_{OO} , \\ \mathbf{S}_{OC} - i\mathbf{S}_{OO}\mathbf{K}_{OC} - i\mathbf{S}_{OC}\mathbf{K}_{CC} &= i\mathbf{K}_{OC} , \end{aligned}$$

we eliminate $\mathbf{S}_{OC}$ from the expressions

$$\mathbf{S}_{OO}\left(\mathbf{1}^0 - i\mathbf{K}_{OO} - \mathbf{K}_{OC}\left(\mathbf{1}^0 - i\mathbf{K}_{CC}\right)^{-1}\mathbf{K}_{CO}\right) = \mathbf{1}^0 + i\mathbf{K}_{OO} - \mathbf{K}_{OC}\left(\mathbf{1}^0 - i\mathbf{K}_{CC}\right)^{-1}\mathbf{K}_{CO}\,. \quad (5.31)$$

We can find a similar relationship as before for the open channel parts of the S and K-matrices.

$$\mathbf{S}_{OO} = \left[\mathbf{1}^0 + i\left(\mathbf{K}_{OO} + \mathbf{K}^R_{OO}\right)\right]\left[\mathbf{1}^0 - i\left(\mathbf{K}_{OO} + \mathbf{K}^R_{OO}\right)\right]^{-1}\,, \quad (5.32)$$

where $\mathbf{K}^R_{OO}$ is defined by

$$\mathbf{K}^R_{OO} = i\mathbf{K}_{OC}\left[\mathbf{1}^0 + i\mathbf{K}_{CC}\right]^{-1}\mathbf{K}_{CO}\,. \quad (5.33)$$

Note that $\mathbf{K}_{CC}$ is anti-Hermitian, and $\mathbf{K}^R_{OO}$ has to be Hermitian so that the unitarity of the open channel S-matrix is preserved. In general, $\mathbf{K}_{OC}$ and $\mathbf{K}_{CO}$ have both Hermitian and anti-Hermitian terms. $\mathbf{K}^R_{OO}$ reflects the effect of the closed channels on the open channel part of the S-matrix. For example, this plays an important role in the case of Feshbach resonances where a scattering state in an open channel can be resonant with a bound state of a closed channel. Furthermore, we can define similar relationships for the eigenphases as before,

$$\mathbf{S}_{OO} = \mathcal{U}e^{i2\delta^0}\tilde{\mathcal{U}}\,, \quad (5.34)$$

$$\left(\mathbf{K}_{OO} + \mathbf{K}^R_{OO}\right) = \mathcal{U}\tan\delta^0\tilde{\mathcal{U}}\,. \quad (5.35)$$

Usually one could choose to define the scattering length through the scattering phases and correspondingly through the S-matrix as this is done in most elementary quantum mechanics textbooks. However, as we will see in the next section it is advantageous and more appropriate in the pseudopotential approximation to define a scattering length matrix through the K-matrix.

5.1.3 Multichannel pseudopotential formalism

In Chapter 2, we have derived a generalized pseudopotential that is based on a δ-shell potential. Here, we would like to extend this formulism to the multichannel problem. The complete single channel pseudopotential is given by

$$\hat{V}(r) = \sum_l |l,m\rangle \hat{v}^{(l)}_{\rm shell}(r) \langle l,m| \,, \tag{5.36}$$

where the l-wave pseudopotential is given by

$$\hat{v}^{(l)}_{\rm shell}(r) = -\lim_{s\to 0} \frac{1}{2}\frac{(2l+1)!!}{2l!!}\frac{\tan\delta_l(k)}{k^{2l+1}}\frac{\delta(r-s)}{r^{l+2}}\frac{\partial^{2l+1}}{\partial r^{2l+1}} r^{l+1} \,, \tag{5.37}$$

$$\hat{v}^{(l)}_{\rm shell}(r) = \lim_{s\to 0} \frac{1}{2}\frac{(2l+1)!!}{2l!!} a_l^{2l+1} \frac{\delta(r-s)}{r^{l+2}}\frac{\partial^{2l+1}}{\partial r^{2l+1}} r^{l+1} \,. \tag{5.38}$$

The derivatives on the right acts as a regularization operator, as defined by

$$\hat{P}_l = \frac{r^l}{(2l+1)!}\frac{\partial^{2l+1}}{\partial r^{2l+1}} r^{l+1} \,. \tag{5.39}$$

This operator acts like an identity operator on a regular wave function. For irregular functions with $l' \leq l$, $\hat{P}_l$ acts as a null operator. We define a multichannel l-wave scattering length matrix $a^{l+l'+1}_{\gamma,\gamma'}$ using the multichannel K-matrix,

$$k_\gamma^{l+1/2} k_{\gamma'}^{l'+1/2} a^{l+l'+1}_{\gamma',\gamma} = K_{\gamma',\gamma} \,. \tag{5.40}$$

Here, lm and $l'm'$ are the sets angular momentum quantum numbers of the channels γ and γ'. We can formulate an ansatz for the multichannel pseudopotential

$$\hat{V}(r) = \sum_{\gamma,\gamma'} |l,m\rangle \, \hat{V}_{\gamma\gamma'}(r) \, \langle l',m'| \tag{5.41}$$

with

$$\hat{V}_{\gamma\gamma'}(r) = \hat{\tilde{P}}_l \left[\lim_{s\to 0} c_{l,l'} a^{l+l'+1}_{\gamma',\gamma} \frac{\delta(r-s)}{r^{l+l'+2}}\right] \hat{P}_{l'} \,. \tag{5.42}$$

Here, we have added an additional projection operator that acts to the left. In case the potential is only acting to the right, the projector on the left can be simply set

equal to the identity operator. The constant $c_{l,l'}$ will be determined later. We rewrite the close-coupled equations for the radial wave functions instead of the reduced wave functions

$$\left(\frac{1}{r}\frac{\partial^2}{\partial r^2}r - \frac{l'(l'+1)}{r^2} + k_{\gamma'}^2\right)\frac{F^{\infty}_{\gamma',\gamma}(r)}{r} = \sum_{\gamma''}\hat{V}_{\gamma',\gamma''}(r)\frac{F^{\infty}_{\gamma'',\gamma}(r)}{r}\,. \tag{5.43}$$

Here, $F^{\infty}_{\gamma'',\gamma}(r)/r$ is the asymptotic wave function (5.11) extended all the way to the shell radius according to

$$F^{\infty}_{\gamma',\gamma}(r) = J_{\gamma'}(r)\delta_{\gamma',\gamma} + N_{\gamma'}(r)K_{\gamma',\gamma}\,. \tag{5.44}$$

Inserting the pseudopotential in the closed coupled equations (5.43) and leaving the limit $s \to 0$ for later, we need to evaluate the left side as

$$\begin{aligned}
\hat{V}_{\gamma',\gamma''}(r)\frac{F^{\infty}_{\gamma'',\gamma}(r)}{r} &= \left[c_{l',l''}a_{\gamma'',\gamma'}^{l'+l''+1}\frac{\delta(r-s)}{r^{l'+l''+2}}\right]\hat{P}_{l''}\frac{F^{\infty}_{\gamma'',\gamma}(r)}{r}\,,\\
&= \left[c_{l',l''}k_{\gamma'}^{-l'-1/2}k_{\gamma''}^{-l''-1/2}K_{\gamma'',\gamma'}\frac{\delta(r-s)}{r^{l'+l''+2}}\right]\hat{P}_{l''}\frac{J_{\gamma''}(r)}{r}\delta_{\gamma'',\gamma}\,,\\
&= \left[c_{l',l''}k_{\gamma'}^{-l'-1/2}k_{\gamma''}^{-l''-1/2}K_{\gamma'',\gamma'}\frac{\delta(r-s)}{r^{l'+l''+2}}\right]\left[\frac{k_{\gamma''}}{|k_{\gamma''}|^{\frac{1}{2}}}\frac{(k_{\gamma''}r)^{l''}}{(2l''+1)!!}\delta_{\gamma'',\gamma}\right]\,,\\
&= \left[c_{l',l''}k_{\gamma'}^{-l'-1/2}K_{\gamma'',\gamma'}\frac{\delta(r-s)}{r^{l'+2}}\right]\left[\frac{\delta_{\gamma'',\gamma}}{(2l''+1)!!}\right]\,.
\end{aligned} \tag{5.45}$$

The regular part of the wave function has been expanded at the origin according to

$$\hat{P}_{l''}\frac{J_{\gamma''}(r)}{r} = \hat{P}_{l''}\left[\frac{1}{|k_{\gamma''}|^{\frac{1}{2}}}(k_{\gamma''})\frac{(kr)^{l''}}{(2l''+1)!!}\right] = \left[\frac{1}{|k_{\gamma''}|^{\frac{1}{2}}}(k_{\gamma''})\frac{(kr)^{l''}}{(2l''+1)!!}\right]\,. \tag{5.46}$$

The derivative operator $\hat{P}_{l''}$ acts like the identity on the regular part of the wave function. Integrating the closed coupled equations around the shell,

$$\lim_{\epsilon\to 0}\int_{s-\epsilon}^{s+\epsilon}\left(\frac{1}{r}\frac{\partial^2}{\partial r^2}r - \frac{l'(l'+1)}{r^2} + k_{\gamma'}^2\right)\frac{F^{\infty}_{\gamma',\gamma}(r)}{r} = \lim_{\epsilon\to 0}\int_{s-\epsilon}^{s+\epsilon}\sum_{\gamma''}\hat{V}_{\gamma',\gamma''}(r)\frac{F^{\infty}_{\gamma'',\gamma}(r)}{r}\,,$$

we obtain

$$\lim_{\epsilon\to 0}\left(\left[\frac{\partial}{\partial r}\frac{F^{\infty}_{\gamma',\gamma}(r)}{r}\right]_{r=s+\epsilon} - \left[\frac{\partial}{\partial r}\frac{F^{\infty}_{\gamma',\gamma}(r)}{r}\right]_{r=s-\epsilon}\right) = \lim_{\epsilon\to 0}\int_{s-\epsilon}^{s+\epsilon}\sum_{\gamma''}\hat{V}_{\gamma',\gamma''}(r)\frac{F^{\infty}_{\gamma'',\gamma}(r)}{r}\,. \quad (5.47)$$

As before in the derivation of the single channel pseudopotential, we expand the Bessel and Neumann functions around the origin. After some algebra similar to the single channel case, we evaluate 5.47 to be

$$\begin{aligned} K_{\gamma',\gamma}\frac{(2l'+1)(2l'-1)!!}{k_{\gamma'}^{l'+1/2}s^{l'+2}} &= \sum_{\gamma''}\left[K_{\gamma'',\gamma'}\frac{c_{l',l''}}{k_{\gamma'}^{l'+1/2}s^{l'+2}}\frac{\delta_{\gamma'',\gamma}}{(2l''+1)!!}\right], \\ K_{\gamma',\gamma}\frac{(2l'+1)!!}{k_{\gamma'}^{l'+1/2}s^{l'+2}} &= K_{\gamma,\gamma'}\frac{c_{l',l''}}{k_{\gamma'}^{l'+1/2}s^{l'+2}}\frac{1}{(2l''+1)!!}\,. \end{aligned} \quad (5.48)$$

Since it has been shown in Ref. [79] that the K-matrix is symmetric $K_{\gamma',\gamma} = K_{\gamma,\gamma'}$, the closed coupled equation set is fulfilled and the constant $c_{l',l''} = (2l'+1)!!(2l''+1)!!$. The generalized multichannel pseudopotential is given by

$$\hat{V}(r) = \sum_{\gamma',\gamma''}|l',m'\rangle\,\hat{V}_{\gamma'\gamma''}(r)\,\langle l'',m''| \quad (5.49)$$

with

$$\hat{V}_{\gamma'\gamma''}(r) = \hat{\tilde{P}}_{l'}\left[\lim_{s\to 0}(2l'+1)!!(2l''+1)!!a^{l'+l''+1}_{\gamma'',\gamma'}\frac{\delta(r-s)}{r^{l'+l''+2}}\right]\hat{P}_{l''}\,. \quad (5.50)$$

Also, note that analog to before we have defined an energy-dependent scattering length matrix by

$$a^{l'+l''+1}_{\gamma'',\gamma'} = K_{\gamma'',\gamma'}k_{\gamma'}^{-l'-1/2}k_{\gamma''}^{-l''-1/2}\,. \quad (5.51)$$

Without proving this in detail, the energy-dependent pseudopotential has the same properties as the single channel pseudopotential in that it should capture the complete scattering and bound-state spectrum of the participating channels. It further allows us to continue the scattering length matrix element for the channel of interest to negative energies, which are crucial in the atoms in separated traps case.

5.2 Calculation of the scattering length in ^{133}Cs for positive and negative energies

5.2.1 Introduction to close-coupling codes

The Mies-Julienne-Sando close-coupling code has been developed over several decades by the Atomic Physics Division at the National Institute of Standards and Technology (NIST), Gaithersburg. In the past, the codes have been used and continuously improved to predict more than 60 experimentally observed magnetic Feshbach resonances in ultracold collisions of ^{133}Cs [44, 45]. The collisional properties of ^{133}Cs have been of particular interest in the past due the enormous collision cross sections in ^{133}Cs and the large clock shifts [81], and due to the difficulty of achieving a BEC in ^{133}Cs [82]. Additionally, the large nuclear spin and the correspondingly large manifold of hyperfine states lead to the richest resonance structure of all alkali atoms, which has been the focus of many experimental and theoretical investigations [44, 45, 78, 83]. The huge progress in resolving these collisional anomalies of ^{133}Cs over the past years and the prediction of low magnetic field Feshbach resonances have finally lead to the BEC of ^{133}Cs [84].

The NIST close-coupling code solves the close-coupled set of equations (5.8) for realistic ^{133}Cs interaction potentials in the presence of a magnetic field. A more detailed description of the codes and our changes made to the code can be found in Appendix D. The realistic interatomic interaction potential can be constructed in a choice of different basis set, defined by the various complete sets of quantum numbers. One convenient choice at close range is the molecular Hund's case (a) basis set [48,49], that is defined by the molecular quantum numbers, $\{|J, M, \Pi; S, m_S, I, m_I\rangle\}$. A convenient basis set at long range is the channel state basis $\{|J, M, \Pi; l, F, f_a, f_b\rangle\}$ which is equivalent to Hund's case (e) basis set [79]. Alternatively a user defined basis

set can be chosen, which in our case is the Hund's case (m) basis [85], defined by the two-atom uncoupled basis states $\{|J, M, \Pi; l, m, f_a, f_b, m_{f_a}, m_{f_b}\rangle\}$. In the presence of a magnetic field, the "dressed" two atom basic states are referred to as dressed state basis set. Although the potential might not be diagonal at finite range in the two-atom basis due to the long-range anomalously large spin-spin and higher-order spin-orbit coupling in ^{133}Cs, the uncoupled two-atom basis allows an easy termination of the close coupling calculations at some finite long-range right stopping point.

The wave function can be propagated from the left starting point to the right end point using either a Numerov [86,87] or a Gordon propagation algorithm [88,89]. At the long-range right stopping point, r_{final}, the scattering boundary conditions are determined for both open and closed channels. There, the logarithmic derivative matrix $m_{\gamma',\gamma}(r_{\text{final}})$ is calculated for the reduced wave functions $F_{\gamma',\gamma}(r)$ according to

$$m_{\gamma',\gamma}(r_{\text{final}}) = \frac{\frac{\partial}{\partial r} F_{\gamma',\gamma}(r)|_{r=r_{\text{final}}}}{F_{\gamma',\gamma}(r_{\text{final}})} \,. \tag{5.52}$$

Matching the logarithmic derivative to the asymptotic wave function,

$$F^{\infty}_{\gamma',\gamma}(r) \overset{r\to\infty}{\sim} J_{\gamma'}(r)\delta_{\gamma',\gamma} + N_{\gamma'}(r)K_{\gamma',\gamma} \,, \tag{5.53}$$

we can determine the K-scattering matrix from $m_{\gamma',\gamma}(r_{\text{final}})$ according to

$$K_{\gamma',\gamma} = \left[N_{\gamma'}(r_{\text{final}})m_{\gamma',\gamma}(r_{\text{final}}) - N'_{\gamma'}(r_{\text{final}})\right]^{-1} \left[J_{\gamma'}(r_{\text{final}})m_{\gamma',\gamma}(r_{\text{final}}) - J'_{\gamma'}(r_{\text{final}})\right] \,. \tag{5.54}$$

Here, $J'_{\gamma'}(r_{\text{final}})$ and $N'_{\gamma'}(r_{\text{final}})$ are the derivatives of the reduced spherical Bessel functions at $r = r_{\text{final}}$. The K-matrix then defines the scattering length matrix that is appropriate for use in the generalized multichannel pseudopotential as discussed in the previous section.

In the case of separated traps where negative energy scattering becomes important and where the scattering channel of interest is closed, we need to extend the

scattering length matrix and therefore the K-matrix to include closed channels (the NIST codes includes only open channels in the calculation of the K-matrix). This can be achieved by simply continuing the reduced spherical Bessel functions $J'_{\gamma'}(kr_{\text{final}})$ and $N'_{\gamma'}(kr_{\text{final}})$ to negative energies by using a purely imaginary wave vector, $k = i\kappa$, and allowing a complex argument of the Bessel functions. This is done via a separate Matlab code that uses the logarithmic derivative matrix for all channels obtained from the NIST codes. The complete K-matrix that includes open and closed channels is again calculated using Eq. (5.54). Alternatively, it is helpful to rewrite the asymptotic wave function in terms of reduced Hankel functions Eq. (5.19),

$$F^{\infty}_{\gamma',\gamma}(r) \overset{r\to\infty}{\sim} \frac{1}{2}\left\{H^{-}_{\gamma}(r)\left[\delta_{\gamma',\gamma} - iK_{\gamma',\gamma}\right] - H^{+}_{\gamma}(r)\left[\delta_{\gamma',\gamma} + iK_{\gamma',\gamma}\right]\right\} . \tag{5.55}$$

For reference, the complete Matlab code can be found in Appendix D.

5.2.2 Calculation of the scattering length in ^{133}Cs for the $|ap\rangle$ channel

Figure 5.1 shows the hyperfine states and magnetic sub-levels in the ^{133}Cs ground state labeled with letters from a to p. The scattering channel of interest is the two atom combination in the stretched states, $|ap\rangle$, with a total angular momentum projection quantum number of $m_{\text{total}} = m_{f1} + m_{f2} = 7$. This channel is of particular interest since in the absence of any spin-motion coupling, conservation of angular momentum implies conservation of these quantum numbers. For this reason, the states a and p are the ones originally considered for entangling atoms via ultracold collisions [28] (see also Section 1.2.1. Also, in the case of ^{133}Cs, this channel has, as we will see later, a large positive scattering length, which is necessary to observe the proposed trap-induced resonance for atoms in separated traps. While the scattering interaction usually preserves the total magnetic quantum number so that the selected two atom channel $|ap\rangle$ does not couple to any other open channels, for interacting

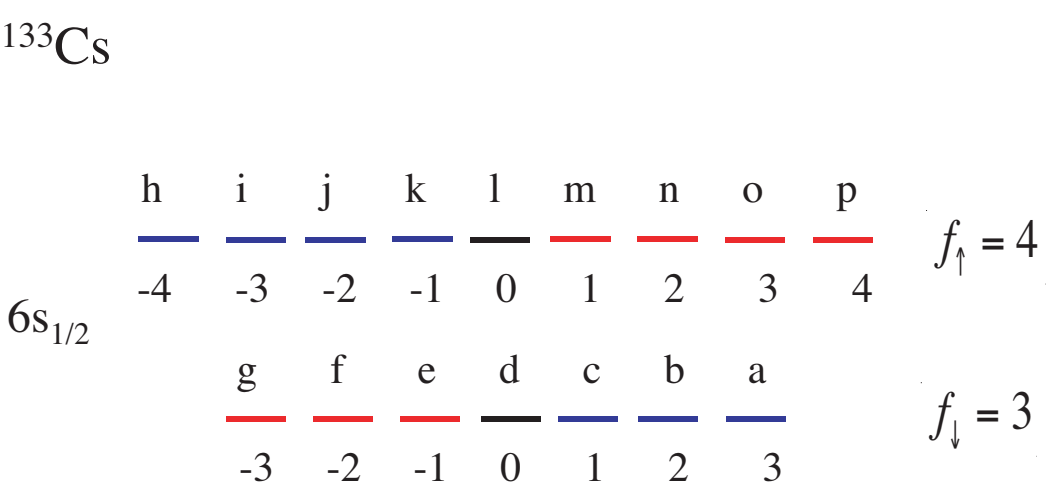

Figure 5.1: Hyperfine levels of the $6s_{1/2}$ ground state of ^{133}Cs . The magnetic sublevels are labeled with letters from a to p.

^{133}Cs atoms, this desirable property, the conservation of m_{total}, is not completely valid due to the strong spin-spin and higher-order spin-orbit coupling in ^{133}Cs [44,45]. Due to this coupling to other channels with higher angular momentum l, there is multitude of open and closed scattering channels that need to be included in the description (see Table 5.1). The set of close-coupled equations for the reduced radial wave functions of the participating channels is integrated from a left starting point r_{initial} to a right stopping point r_{final} using a standard renormalized Numerov method [86, 87]. An example of the variable Numerov grid is shown in Table 5.2 where the right stopping point has been adjusted to $r_{\text{final}} = 10000a_0$, deep in the asymptotic region.

Note that in this case we determine the scattering boundary conditions at r_{final}, which is much larger than the typical size of the ground state in an optical lattice site. This might raise doubts about the validity of the pseudopotential approximation in an optical lattice system, since the range of the interaction, outside which we can define the asymptotic boundary conditions, seems to be much larger than the trap size. However, as shown in Ref. [54, 55], it is the characteristic β_6 length scale that

matters in the δ approximation, not the absolute range of the interaction nor the scattering length a. The pseudopotential approximation only breaks down if the trapping potential is strong enough to distort the interaction across the β_6 length scale and alter the boundary conditions at r_{final} sufficiently. Since $\beta_6 = 100a_0$ in ^{133}Cs , and therefore much smaller than typical trap sizes in tight optical lattices, we can safely approximate the interaction by our pseudopotential.

A plot of the resulting scattering length for the $|ap\rangle$ channel is shown in Fig. 5.2. The calculated scattering length continues smoothly across zero energy and also takes a finite value at the bound-state energy as expected.

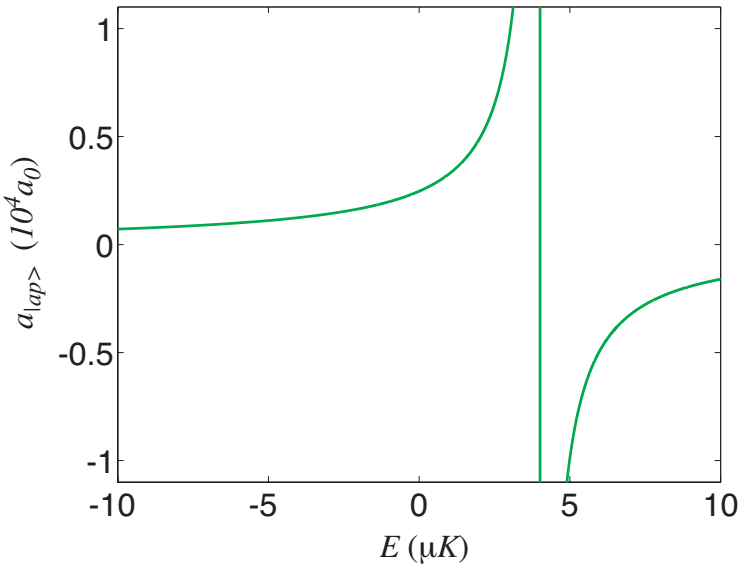

Figure 5.2: Calculations of the diagonal scattering length matrix element for the $|ap\rangle$ channel as a function of energy.

Figures 5.3(a-f) show calculations of the diagonal scattering length matrix element for the $|ap\rangle$ channel as a function of the stopping point r_{final} for various negative energies. At negative energies, we expect the codes to converge in the calculation of $a_{|ap\rangle}$ only for a small range of r_{final}. The closed-coupled equations need to be

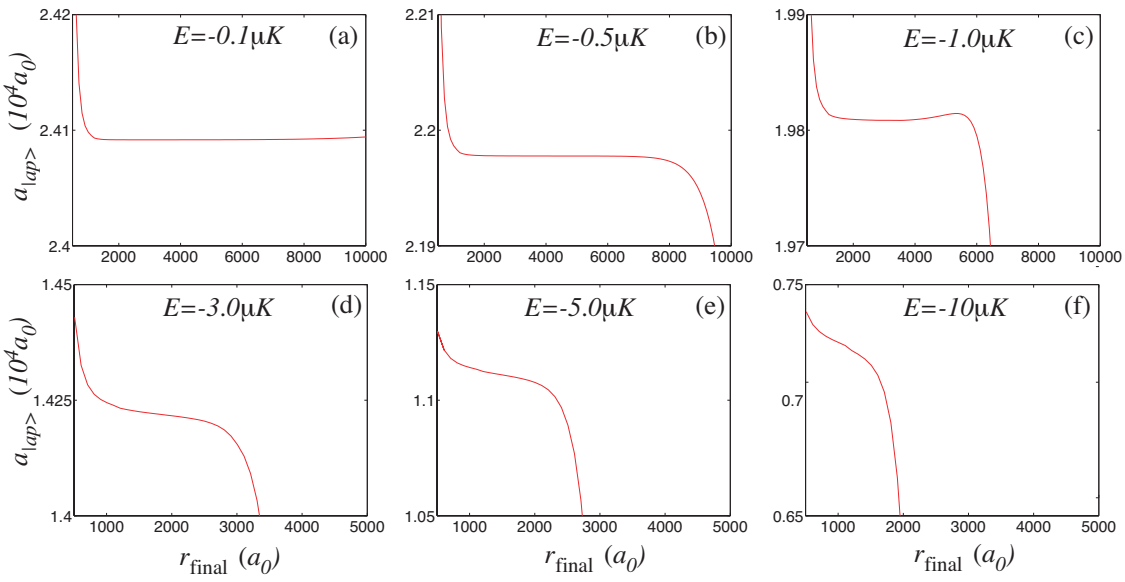

Figure 5.3: Calculations of the diagonal scattering length matrix element for the $|ap\rangle$ channel as a function of the stopping point r_{final} for different negative energies.

integrated far enough into the asymptotic regime where the interaction potential vanishes. However, for very large r, we expect the wave function to diverge exponentially and the codes to become unstable in the matching of boundary condition. We expect the region of convergence to decrease for larger negative energies, since the wave function diverges as $\exp +\kappa r$ (see Figures 5.3) As we can see from Figures 5.3 we can reliably calculate a scattering length for negative energies as low as $-10\mu K$. The calculation errors in the scattering length of Fig. 5.2can be estimated from Fig. 5.3 to be around 5% at $-10\mu K$ whereas for smaller negative energies of around $-1\mu K$ the error can be estimated to be smaller than 0.5%.

We have further examined the magnetic field dependence of the scattering length in the linear Zeeman regime. The background scattering length remains large and constant over a wide range of magnetic fields and shows three small resonances over the calculated range at $11.6G$, $25G$, and $28G$ in Fig. 5.4. An identification of the different resonances, i.e. the labeling of the resonances by the corresponding bound-

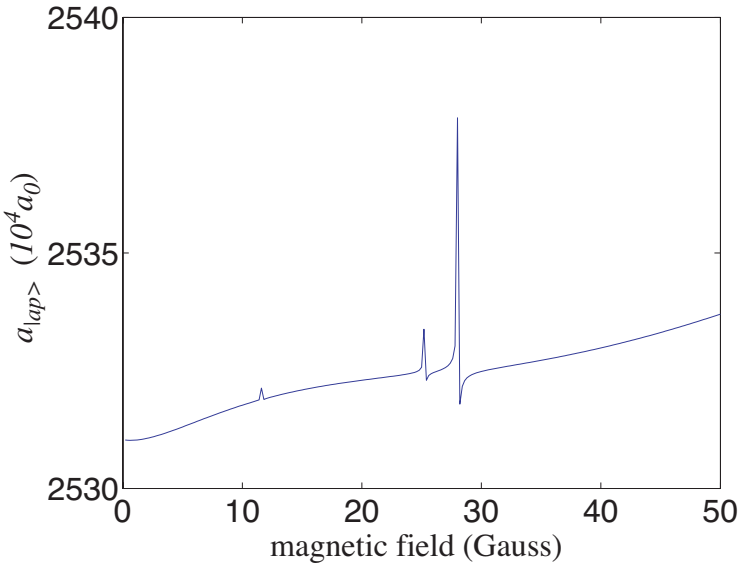

Figure 5.4: Calculations of the diagonal scattering length matrix element for the $|ap\rangle$ channel as a function of magnetic field. Three narrow scattering resonances can be observed for applied magnetic fields in the range from 0 to $50G$.

states, is left for future discussion. Although the resonances are narrow (less than $1G$), they might be useful to tune the interaction from large positive scattering lengths to smaller or even negative scattering lengths.

5.2.3 Complex scattering length in ^{133}Cs for the $|ap\rangle$ channel

In the following, we introduce a complex scattering length defined by the S-matrix that allows us to characterize inelastic collisions. The scattering S-matrix can be calculated from the K-matrix using Eq. (5.26),

$$\mathbf{S} = \left[\mathbf{1}^0 + i\mathbf{K}\right]\left[\mathbf{1}^0 - i\mathbf{K}\right]^{-1} . \tag{5.56}$$

The S-matrix describes the coupling from the different "in"-channels to the various "out"-channels and is generally not diagonal in the channel basis. Any scattering-matrix diagonal element is related to the off-diagonal elements by unitarity of the

S-matrix and therefore of the form

$$S_{\gamma,\gamma} = 1 - \sum_{\gamma'} S_{\gamma',\gamma} = \exp\left[2i\left(\lambda + i\mu\right)\right] = \left|S_{\gamma,\gamma}\right| e^{2i\lambda} \tag{5.57}$$

with a complex phase shift $\delta = \lambda + i\mu$. This complex phase shift can be used to define a complex energy-dependent scattering length [34],

$$\tilde{a}_\gamma = a_\gamma - i\beta_\gamma \equiv -\frac{\tan\left(\lambda + i\mu\right)}{k_\gamma^{2l+1}}\,. \tag{5.58}$$

The imaginary part of the scattering length is a measure of the "loss" from the scattering channel γ to all other open channels. Note that the imaginary part of the scattering length not only measures the inelastic collisions but also includes the coherent couplings to channels in the same hyperfine manifold. Figure 5.5 shows the real and imaginary part of the complex scattering length that has been calculated from the real and imaginary part of the S-matrix as a function of energy for positive energies. For scattering energies far below $4\mu K$, the imaginary part is several orders smaller than the real part of the scattering length. In this regime, couplings to other channels that are due to spin-spin or spin-orbit coupling can be neglected and the total magnetic quantum number m_{total} is approximately conserved.

5.3 Trap-induced shape resonances and quantum information processing in ^{133}Cs

We have shown in Chapter 4 that trap-induced resonances provide new avenues for entangling atoms via ultracold collisions. However, these resonances occur only for circumstances when the scattering length is on the order of the size of the trap ground state. Estimates of the scattering length in ^{87}Rb and ^{133}Cs show that trap-induced resonances in ^{87}Rb at low magnetic fields are going to be difficult to observe due the small scattering length and strong localization needed. ^{133}Cs , on the other

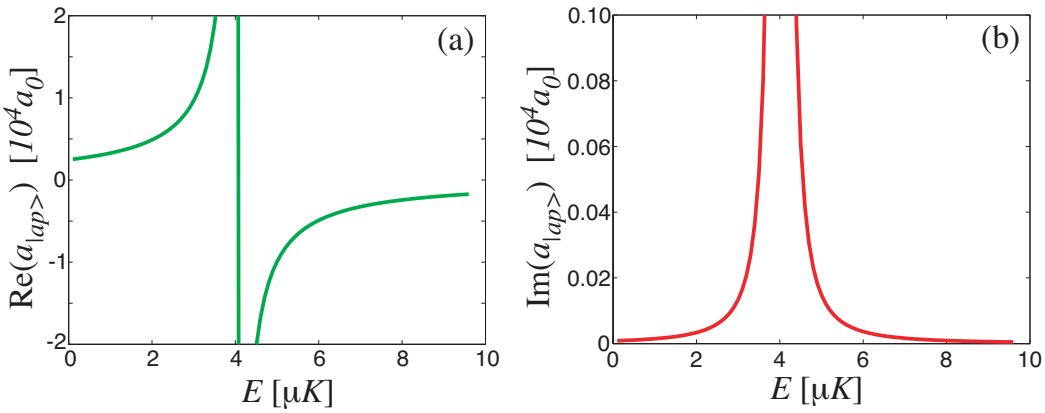

Figure 5.5: S-matrix based calculations of the real and imaginary part of scattering length for the $|ap\rangle$ channel as a function of energy.

hand, with its anomalously large scattering length, provides a natural setting to study separated trap effects on strongly interacting atoms. We will therefore discuss the feasibility for observing these newly predicted resonances under realistic circumstances for ^{133}Cs atoms in 3D-optical lattices.

5.3.1 Optical lattice parameters

We consider a 3D optical lattice, created by three pairs of linearly polarized counter-propagating laser beams as described in Chapter 1.1.1. We approximate the optical lattice wells by harmonic oscillator potentials with frequency ω with

$$\hbar\omega = 2\sqrt{V_{pp}E_R}\,. \tag{5.59}$$

V_{pp} is the peak-to-peak depth of the optical lattice potential and $E_R = \hbar^2 k_l^2/2m$ is the recoil energy of a ^{133}Cs atom of mass m upon absorption of a photon with wave vector $k_l = 2\pi/\lambda$. For ^{133}Cs , the optical lattice is usually generated by laser beams far detuned from the $\lambda = 852$ nm D2 line on the $S_{1/2} \rightarrow P_{3/2}$ transition. The

Lamb-Dicke parameter, which measures the localization of atoms in the lattices is

$$\eta = \sqrt{\frac{E_R}{\hbar\omega}}\,. \tag{5.60}$$

The Lamb-Dicke parameter η is related to the width of the harmonic-oscillator ground state of a single atom, $\bar{r}_0 = \sqrt{\hbar/2m\omega}$ (FWHM), by $\eta = k_l\bar{r}_0$. The characteristic harmonic oscillator length $r_0 = \sqrt{\hbar/\mu\omega} = \sqrt{2\hbar/m\omega}$ used in Chapters 3 and 4 is related to the ground state width via $r_0 = 2\bar{r}_0$.

For the observation of a trap-induced resonance for the $|ap\rangle$-channel, we require r_0 to be on the order of, or much smaller than, the scattering length $a_{|ap\rangle} \approx 2500a_0 \approx$ 132 nm. A second requirement for trap-induced resonances is that the trap potential at the origin, $V_{\Delta z} = \frac{1}{2}\Delta z^2$, is strong enough to raise the molecular bound-state at E_b to positive energies so that $E_b + V_{\Delta z} \geq \frac{3}{2}\hbar\omega$. In an optical lattice with finite depth V_{pp}, $V_{\Delta z}$ is limited by V_{pp}, resulting in $\frac{3}{2}\hbar\omega < V_{\Delta z} < V_{pp}$. An optical lattice with a Lamb-Dicke parameter of $\eta = 0.25$, $V_{pp} = 64E_R$, $\hbar\omega = 16E_R$, and $r_0 \approx 34$ nm fulfills all these requirements and still allows a reliable harmonic approximation to the optical lattice potential. Also, a Lamb-Dicke parameter of $\eta = 0.25$ can easily be achieved experimentally and is used in experiments of our collaborators led by Poul Jessen at the University of Arizona in Tucson.

5.3.2 Trap-induced resonances

Figure 5.6 shows the calculated energy spectrum for ^{133}Cs atoms in separated harmonic isotropic traps as a function of trap separation Δz. Here, we assumed an optical lattice with a Lamb-Dicke parameter of $\eta = 0.25$ as discussed in the previous section. The energy eigenvalues are calculated self-consistently at each separation as described in Section 2.5.2 using the energy-dependent scattering length for ^{133}Cs, which is shown in Fig. 5.6 in harmonic oscillator units. This plot of the scattering

length nicely illustrates the necessity of the application of an *energy-dependent* pseudopotential because of the strong energy dependence of the scattering length in the energy range of interest. A constant scattering length approximation would misestimate the location of the bound-state and therefore the size of the avoided crossing in the energy spectrum. Fig. 5.6 shows the main signature of the trap-induced res-

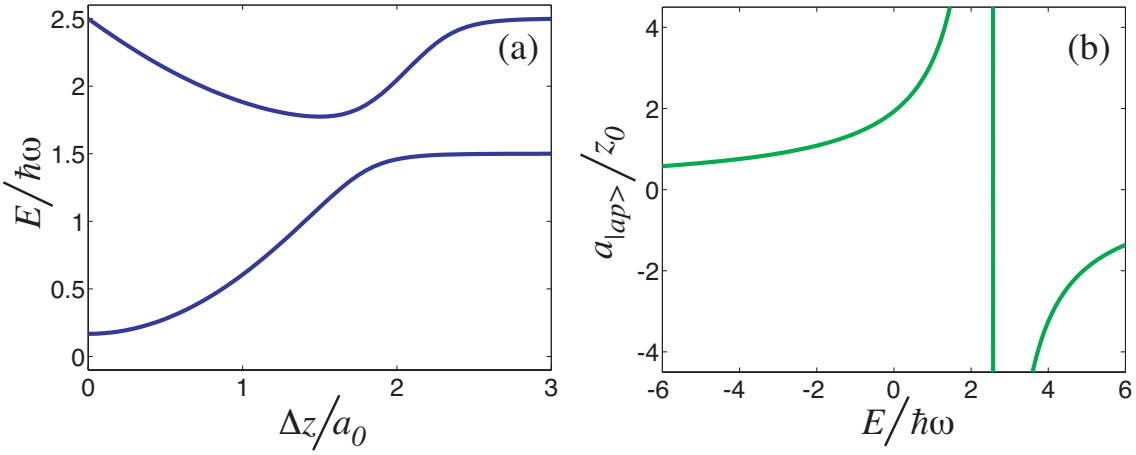

Figure 5.6: (a) Self-consistent energy eigenvalues as a function of trap separation Δz calculated using the scattering length for the $|ap\rangle$-channel in ^{133}Cs , which is shown in (b).

onance in the form of the avoided crossing, which in the case of ^{133}Cs results in an almost maximal energy gap of about $\hbar\omega/2$. Experimentally, the avoided crossing due to the trap-induced resonance can be observed in a Ramsey type controlled collision experiment similar to the experiments by Mandel *et al.* [39]. These experiments have been described in detail in Section 1.2.2. Following the proposal by Jaksch *et al.* [28], the two states of interest $|a\rangle$ and $|p\rangle$ travel on different optical lattice potentials. After preparing the atoms in the $|a\rangle$-state, the atoms are placed in a superposition of $|a\rangle$ and $|p\rangle$ via a microwave $\pi/2$-pulse and then each atom is split into two wave packets by rotating the laser-polarization vectors. Instead of bringing the $|a\rangle$-wave packet of one atom and the $|p\rangle$-wave packet of the other atom into the same well as in the original proposal (see Section 1.2.1), one can keep the atoms separated

and let the atoms acquire a collisonal phase shift using the trap-induced resonance (see Fig. 5.7). For appropriate phase shifts during the interaction time t_{int}, this re-

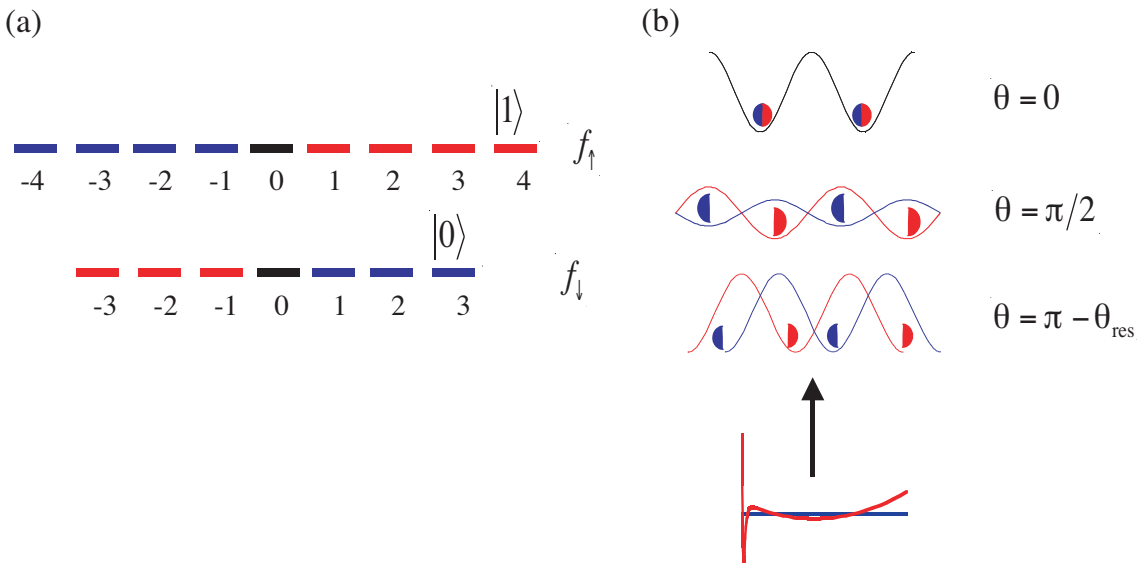

Figure 5.7: Encoding in ^{133}Cs hyperfine structure and schematic of controlled collisions via trap-induced resonances. (a) Hyperfine levels of the $6s_{1/2}$ ground state of ^{133}Cs . The logical basis states $|0\rangle$ and $|1\rangle$ are encoded in the stretched states in order to avoid inelastic collsions. (b) Following the proposal by Jaksch *et al.* [28] atoms travel on different lattice potentials. Unlike in the original proposal, here, the phase shift is acquired for separated atoms using the trap-induced resonance.

sults in entangled atoms, which cannot be disentangled by another $\pi/2$-pulse. In the case of no entanglement, this final $\pi/2$-pulse leads to Ramsey-interference fringes as the phase between the two $\pi/2$-pulses is varied. The disappearing and reappearing Ramsey-fringes as a function of the interaction time are a measure of the acquired phase shift and the corresponding energy shift. A strong measured energy shift for separated traps should be an experimentally observable signature of the trap-induced resonance.

5.3.3 Two-qubit gates via trap-induced resonances in ^{133}Cs

The above scheme is also a viable way to achieve the two-qubit gate necessary for quantum computing. Limits to the fidelity of the gate based on the trap-induced resonance include the limited lifetime of atoms in the optical lattice, the non-perfect cooling to the ground state, leakage to states outside the logical basis through the collisional couplings, loss from the trap due to inelastic collisions, the dephasing of the qubit during the transport and storage. We address these issues in this section.

The timescale for a collisonal gate is generally limited by $t_{\rm int} < \pi/\omega$ since the acquired phase shifts are always smaller than $\hbar\omega$. Furthermore, the adiabatic change of the trap separation must be slower than ω in order to avoid excitation to higher vibrational states. The lifetime of atoms in the optical lattice is limited by the spontaneous emission rate Γ, which should be much smaller than ω. In general, the light shift potential is inversely proportional to the detuning Δ, whereas $\Gamma \propto /\Delta^2$. In practice, the spontaneous emission rate can be suppressed to an almost arbitrary degree using intense trap light tuned very far from atomic resonance [36].

Non-perfect cooling to the ground state or heating results in occupation of higher excited states in the relative coordinate motion. Heating in the transverse direction corresponds to excitation to higher excited states with $l > 0$ and projection quantum number $m \neq 0$. Since $m \neq 0$ states vanish at the origin and are therefore not affected by the interatomic interaction, these states do not shift at all and will limit the fidelity of a quantum gate. The effect of heating along the direction of separation, which corresponds to states with $m = 0$, can be seen in Figs. 4.3 and 5.6. Atoms in these states experience trap-induced resonances at different separations (see the energy gaps in Fig. 4.3) and acquire very different energy and phase shifts as a function of separation between traps. However, for a high-fidelity entangling gate, only the total acquired phase shift during the gate time is of importance. The total phase shift is

acquired at the final trap separation as well as during the slow adiabatic movement of the atoms on the energy surfaces when the atoms are brought together. In principle, it should be possible to design a gate that is robust with respect to heating in the direction of separation. One can vary the two open parameters, the final trap separation and the velocity of moving the atoms, in such a way that the discrepancy between the phase shift acquired in the vibrational ground vs. the first two excited states is minimized. A more detailed discussion of the optimization of two-qubit gates based on the trap-induced resonances is planned for future investigation.

Leakage to states outside the logical basis and inelastic collisonal loss from the trap is minimized by using the stretched-state encoding in the states $|ap\rangle$. Our calculation of the imaginary part of the scattering length verifies this and shows that despite the large spin-spin and spin-orbit coupling in ^{133}Cs , inelastic collisions are down by one or two orders of magnitude as long as the collisional kinetic energy $E \approx \frac{3}{2}\hbar\omega - V_{\Delta z}$ is smaller than $4\mu K$. Here, $V_{\Delta z} = \frac{1}{2}\Delta z^2$ is the trap potential at the origin, which shifts the resonance in the scattering length at $4\mu K$ to higher energies for separated traps. For the particular trap frequency chosen for Fig. 5.6, the first two trap levels are well below $4\mu K$ so that inelastic collisions can be safely neglected.

Using the above encoding into the stretched-states to avoid inelastic collisions comes at the cost of being maximally sensitive to magnetic field- and trap noise due to the opposite sign of the g-factor for the two different states. This was one of the major limiting factors in the Münich experiments [39], where inhomogeneous fluctuations in the optical lattice field lead to dephasing of the individual qubits during transport. An alternative is to use the encoding in the original proposal by Brennen et al. [31]. Here, we consider two different species with logical basis states $|0_+\rangle = |i\rangle$, $|1_+\rangle = |a\rangle$ and $|0_-\rangle = |o\rangle$, $|1_+\rangle = |g\rangle$ (see Fig. 5.8). For these combinations, Zeeman shifts for magnetic fields along the quantization axis and AC Stark shifts are close to identical. The logical states then move on identical

optical potentials and are never split into separated wave packets. This provides excellent immunity against noise, but at a cost: in a two-qubit interaction, all four logical states interact. The challenge then is to engineer a collision to produce a non-separable phase shift without inelastic scattering. Here, collisions in spatially separated traps represent a promising approach to strengthen a single elastic channel and suppress off-resonant inelastic processes. In the case of ^{133}Cs , this would mean designing a trap-induced resonance for the collisions between the states $|1_+\rangle = |a\rangle$ and $|1_-\rangle = |g\rangle$. Off-diagonal couplings to channels with same total $m_{\text{total}} = 0$, such as $|bf\rangle$, $|ce\rangle$, $|dd\rangle$, etc. (see Fig. 5.1), can then be suppressed via the state-dependent trapping potentials. These channels experience a weaker light shift than the $|a\rangle$ and $|g\rangle$ state and leaving them at higher energies effectively causes these other channels to be closed(see Fig. 5.8). One major difficulty in this kind of encoding, especially in

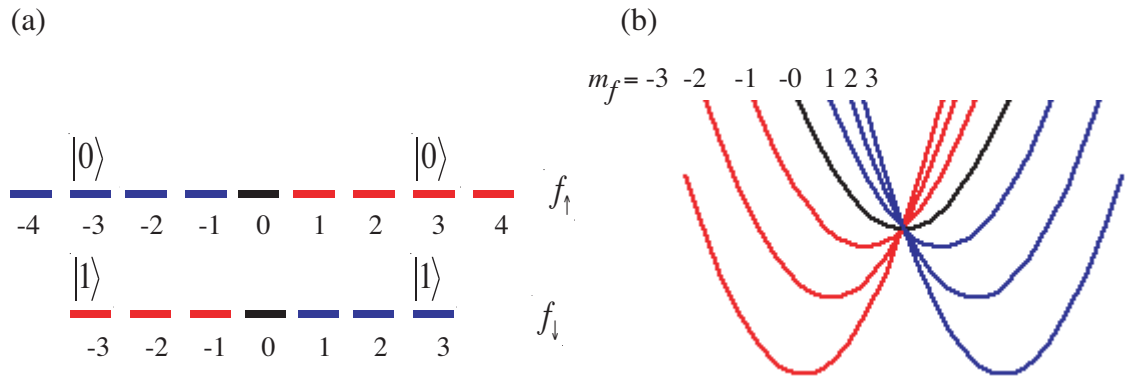

Figure 5.8: Example of robust encoding and schematic of state-dependent trapping potential for the different magnetic sublevels.

the case of ^{133}Cs with its extremely large scattering lengths, is to keep the interaction between atoms in the other logical states small. For ^{133}Cs, these channels could show highly inelastic collision rates, since for the two-qubit combinations, $|ao\rangle$, $|gi\rangle$, and $|io\rangle$, at least one atom is in the higher-energy hyperfine state.

5.4 Summary

In this chapter, we have addressed the important question of whether the trap-induced resonances proposed in Chapter 4 can actually be observed in a realistic setting for a specific alkali, and whether it can be employed as a new avenue for quantum information processing. To study the interaction between atoms of a realistic alkali with hyperfine structure, we generalized our δ-shell pseudopotential to the case of multichannel scattering. In order to match the boundary conditions of the asymptotic multichannel scattering solutions correctly, one has to employ the scattering K-matrix in the definition of the scattering length, not the S-matrix as is usually done in atomic physics.

Using the NIST close-coupling codes, we have calculated the K-matrix for collisions of ^{133}Cs atoms for positive *and negative* collisional energies and correspondingly evaluated the scattering length matrix via analytic continuation for positive and negative energies. We then calculated the energy spectrum for ^{133}Cs atoms in separated traps self consistently using the scattering length matrix element for the stretched states scattering channel. The energy gap in the spectrum provides a signature by which the trap-induced resonance could be experimentally observed. We concluded with a discussion of the use of the trapped induced resonance in ^{133}Cs for feasibly performing two-qubit entangling gates and further addressed some of the limitations to the fidelity of such gates.

Channel	Energy (au)	atom A	m_A	atom B	m_B	m_A+m_B	l
1	-0.139712361591D-05	a	3	a	3	6	2
2	-0.139712361591D-05	a	3	b	2	5	2
3	-0.139712361591D-05	a	3	a	3	6	4
4	-0.139712361591D-05	b	2	b	2	4	4
5	-0.139712361591D-05	a	3	b	2	5	4
6	-0.139712361591D-05	a	3	c	1	4	4
7	-0.139712361591D-05	a	3	d	0	3	4
8	-0.139712361591D-05	b	2	c	1	3	4
9	0.000000000000D+00	p	4	a	3	7	0
10	0.000000000000D+00	p	4	a	3	7	2
11	0.000000000000D+00	p	4	b	2	6	2
12	0.000000000000D+00	p	4	c	1	5	2
13	0.000000000000D+00	o	3	a	3	6	2
14	0.000000000000D+00	o	3	b	2	5	2
15	0.000000000000D+00	n	2	a	3	5	2
16	0.000000000000D+00	p	4	a	3	7	4
17	0.000000000000D+00	p	4	b	2	6	4
18	0.000000000000D+00	p	4	c	1	5	4
19	0.000000000000D+00	p	4	d	0	4	4
20	0.000000000000D+00	p	4	e	-1	3	4
21	0.000000000000D+00	o	3	a	3	6	4
22	0.000000000000D+00	o	3	b	2	5	4
23	0.000000000000D+00	o	3	c	1	4	4
24	0.000000000000D+00	o	3	d	0	3	4
25	0.000000000000D+00	n	2	a	3	5	4
26	0.000000000000D+00	n	2	b	2	4	4
27	0.000000000000D+00	n	2	c	1	3	4
28	0.000000000000D+00	m	1	a	3	4	4
29	0.000000000000D+00	m	1	b	2	3	4
30	0.000000000000D+00	l	0	a	3	3	4
31	0.139712361591D-05	p	4	o	3	7	0
32	0.139712361591D-05	p	4	p	4	8	2
33	0.139712361591D-05	o	3	o	3	6	2
34	0.139712361591D-05	p	4	o	3	7	2
35	0.139712361591D-05	p	4	n	2	6	2
36	0.139712361591D-05	p	4	m	1	5	2
37	0.139712361591D-05	o	3	n	2	5	2
38	0.139712361591D-05	p	4	p	4	8	4
39	0.139712361591D-05	o	3	o	3	6	4
40	0.139712361591D-05	n	2	n	2	4	4
41	0.139712361591D-05	p	4	o	3	7	4
42	0.139712361591D-05	p	4	n	2	6	4
43	0.139712361591D-05	p	4	m	1	5	4
44	0.139712361591D-05	p	4	l	0	4	4
45	0.139712361591D-05	p	4	k	-1	3	4
46	0.139712361591D-05	o	3	n	2	5	4
47	0.139712361591D-05	o	3	m	1	4	4
48	0.139712361591D-05	o	3	l	0	3	4
49	0.139712361591D-05	n	2	m	1	3	4

Table 5.1: Participating channel information. The channel of interest is $|ap\rangle$ (channel 9), which defines the zero of energy. The first thirty channels are open, of which the first eight channels are the ones with both atoms in the lower hyperfine manifold. Channels 31 to 49 are closed channels with both atoms in the $F = 4$ manifold.

Grid No.	No. of Steps	r (initial)	r (final)	Step Size
1	10112	2.999	13.111	0.001
2	1328	13.11	15.766	0.002
3	768	15.764	18.836	0.004
4	512	18.832	22.928	0.008
5	360	22.92	28.68	0.016
6	288	28.664	37.88	0.032
*** Final Step has been Adjusted ***				
6	311894	28.664	10009.272	0.032

Table 5.2: Variable Numerov grid with six regions with different step size. The initial and final radius and the step size are given in units of Bohr radii a_0. R_{final} can be readjusted by the user in the input file of the closed coupled codes (in this case to about $r_{\text{final}} = 10000a_0$).

Chapter 6

Summary and Outlook

6.1 Summary

This thesis is the culmination of a detailed study of controlled collisions of ultracold trapped atoms. In the process of this research, we have developed new methods for modeling and coherently controlling ultracold collisions of atoms in separated traps with the aim of reevaluating and extending existing proposals for entangling atoms for quantum computing purposes. In particular, we have focused on building accurate scattering models for describing cold collisions of trapped atoms to investigate the effect of the trap potential on the atomic interaction. We have identified new trap-induced resonances, where the trapping potential of separated atoms provides a new knob to coherently control atomic interactions.

The modeling of atomic interactions is an old but important problem in atomic physics. In particular, the generalization of Fermi's zero-range pseudopotential to higher partial waves using a δ function at the origin has been quite challenging in the past. We have derived a correct pseudopotential based on a δ-shell potential in the limit as the shell radius approaches zero, that takes into account the higher

multipoles not captured by a δ-function at the origin. Our pseudopotential correctly reproduces the asymptotic scattering behavior of the true interactions. In the case of strong energy-dependent scattering behavior outside the Wigner-threshold regime, we showed that the δ-shell potential could be easily extended to an energy-dependent pseudopotential if an energy-dependent scattering length was employed. Furthermore, an analytic continuation of the scattering length to negative energies allows not only the capture of the complete scattering spectrum of the true interaction, but also includes information about all the bound states as long as the pseudopotential is applied self consistently.

We have successfully applied the generalized pseudopotential for the description of interacting atoms in isotropic harmonic traps. Using the δ-shell approach we derived analytical equations for the energy eigenvalues and the eigensolutions of interacting atoms in isotropic traps. This extends previous work by Busch *et al.* [64], in which the $l = 0$ solutions have been derived, to all higher partial wave solutions. In a detailed comparison of the pseudopotential with a spherical step-well test potential, we show that the pseudopotential captures both the positive and negative energy spectrum. Our results show that the pseudopotential model only breaks down if the range of the true interaction is comparable to the size of the trapping potential so that the true interaction potential is strongly distorted by the trap. Furthermore, we have demonstrated that for realistic interactions, the self-consistent trap solutions using an energy-dependent pseudopotential can be quite important, particularly in the case that a higher partial wave bound state is close to dissociation.

Although our scattering model is applicable to a variety of interesting problems in many-body atomic physics, our primary motivation for developing this model was to investigate controlled collisions of atoms in separated but close traps. Like a 1D system where a confinement induced resonance has a strong effect on the atomic interaction, atoms in *separated* traps can show similar effects. Our prediction of a

new "trap-induced resonance" is the principal result of our research. In very tight traps, as the separation is increased, the trapping potential can be strong enough to raise a bound state of the molecular interaction to positive energies. Avoided crossings occur in the eigenspectrum for certain separations where the energy of this molecular bound state becomes resonant with the eigenstates of the trap potential. This is a new "shape resonance" for s-wave collisions, in which the trap barrier of the separated potential plays the role of the centrifugal barrier in a standard free-space shape resonance for higher partial waves. We have analyzed the properties of these trap-induced resonances in detail for isotropic as well as anisotropic separated traps. We further showed that, in principle, trap-induced resonances can occur due to higher l-wave bound states, making a complete description in terms of a higher partial wave pseudopotential necessary. Comparison with a spherical step-well test potential verified the accuracy of our pseudopotential approximation. Here, the self-consistent solution, which employs an energy-dependent scattering length, is crucial: a constant scattering length approximation does not capture the location of the bound state and the resulting energy gap accurately.

We have studied the feasibility of observing these trap-induced resonances under realistic experimental conditions. Our studies showed that ^{133}Cs is a potentially promising candidate. Using realistic interaction potentials of ^{133}Cs, a detailed multichannel analysis that included higher partial waves and second order spin-orbit coupling, showed an extremely weakly bound state near dissociation. For a complete description of the interaction for a realistic multilevel atom, we extended our δ-shell pseudopotential to the multichannel problem. We showed that, to correctly capture the boundary conditions of the multichannel wave function, we needed to define a scattering length matrix based on the scattering K-matrix. For the particular calculation of the ^{133}Cs interaction parameters, we extended the K-matrix and the corresponding scattering length to negative energies through analytic continuation. We applied the results to calculate the energy spectrum for interacting ^{133}Cs atoms

in the stretched states as a function of the separation between traps. The avoided crossing at the trap-induced resonance and the resulting energy gap in the spectrum provides a possible experimental signature of the trap-induced resonance. We have discussed in detail how this could be done using a Ramsey interference measurement.

Atoms in separated traps are attractive for use as qubits in quantum computation proposals due to the relative ease of manipulating atoms for performing single qubit gates. The interactions between atoms provide the foundation for two qubit entangling gates, which are a necessary ingredient for quantum computation. In this context, we have investigated the possibility of employing the trap-induced resonance for implementing entangling gates under realistic conditions for ^{133}Cs atoms in an optical lattice, and pointed out sources of limitations to the fidelity of such gates.

6.2 Outlook

6.2.1 Further applications of the generalized pseudopotential

The study of interacting trapped atoms in degenerate quantum gases, condensed matter physics, and for the purpose of quantum information processing is an ongoing field of research. The generalized scattering model that we have developed, which is based on a fully generalized multichannel Fermi pseudopotential, is of great interest in several fields. It offers a direct method to analytically solve the Schrödinger equation, as demonstrated for the case of interacting trapped atoms in isotropic traps. The higher partial wave pseudopotential is applicable to all cases in which higher partial wave scattering of trapped particles plays an important role.

Important examples are degenerate gases of identical fermions, an area of current

intense research. In the case of identical Fermions, the s-wave scattering cross section vanishes [90] and p-wave scattering dominates [58]. Moreover, even for bosons, these higher l waves can be resonantly coupled to the dominant $l = 0$ scattering due to noncentral forces [45] such as the dipolar spin-spin interaction [91], second order spin-orbit interaction [92], electric and magnetic dipole-dipole interaction, and/or the forces of an anisotropic trapping potential [24, 69].

We have already seen that anisotropic trapping potentials can be of fundamental importance in the description of trapped gases. In the limit of a 1D or 2D system, interesting confinement induced effects on the interaction can be investigated as in the case of a Tonks-Girardeau gas [18, 20]. In these highly anisotropic settings, the different partial waves are coupled due to the non-spherical symmetry. Higher partial wave resonances and bound states should play an important role in this setting, and the generalized pseudopotential would aid in the general description and study of such systems. In particular, the higher partial wave δ-shell pseudopotential might be useful to solve the problem of interacting atoms in anisotropic traps analytically. Recently, Idziaszek and Calarco [93] presented an analytical solution for s-wave interactions only. The δ-shell pseudopotential should allow for a generalization of these results.

The generalized pseudopotential is not only of key interest to the atomic physics community, but is also of broad interest across various fields of physics where long wavelength scattering plays a central role [94]. Important applications can be found in nuclear [62], electromagnetic [95], and acoustical physics [96].

6.2.2 Trap-induced resonances

Trap-induced resonances provide new possibilities for the quantum control of ultracold atomic collisions. While we have primarily been interested in applications for

quantum information processing purposes, the trap-induced resonance has a general impact on various applications such as, for example, the control of molecular dimers and the production of cold molecules.

An example is the case of ^{133}Cs atoms in an optical lattice system. The trap-induced resonance provides the possibility of producing ultracold molecules by adiabatic change of the separation between traps. A particular nice feature in a sparsely populated optical lattice is that the expected conversion efficiency of two-atom pairs would be very high since the interaction is restricted to two atoms and many-body collisions can be safely neglected. In the case of Feshbach resonances, the trapping potential provides an additional means to fine tune the interaction via the trapping potential or to sweep through the resonance by changing the separation between traps.

Another important example is ultra-high precision spectroscopy. Here, the trap-induced resonance gives direct access to the negative-energy spectrum of the interaction since the energy spectrum of atoms in separated traps directly depends on the scattering length at negative energies. In addition, the trap-induced resonance is a direct probe of the location of the bound states. For example, the high lying bound state in ^{133}Cs that is responsible for the TIR shown in Fig. 5.6 can be exactly determined by mapping the location of the energy gap.

The most important application of trap-induced resonances remains quantum information processing. In Section 5.3.3, we have already made a first attempt to identify sources of error for a two-qubit entangling gate based on trap-induced resonances. A detailed estimate of the gate fidelity is necessary and planned for future work. We are also interested in optimizing the two-qubit gate by varying the two open parameters discussed in Section 5.3.3 in such a way that the discrepancy between the phase shift acquired in the vibrational ground vs. the first two excited states is minimized. This robustness is particularly important since the initial imperfect

cooling to the ground state and subsequent heating during gate operations will result in population of higher excited states.

While the encoding chosen in Section 5.3.3 allows for a direct observation of the trap-induced resonance and proof of principle experiments, it is not the best choice for quantum information processing. The two stretched states are maximally sensitive to fluctuations in the magnetic field or the trap-laser field. An alternative is to use the encoding proposed in Section 5.3.3. These combinations provide excellent immunity against noise, but are not robust with respect to spin-changing collisions. In Section 5.3.3, we proposed to use the state-dependent trapping potential to suppress these inelastic collisions and energetically close these channels. With this in mind, it will be necessary to extend our model of the interaction. Here, the difficulty is that the state-dependent trapping potential cannot be included in the pseudopotential approximation, but has to be included a priori in the calculation of the scattering K-matrix. To this end, the complex NIST close-coupling codes need to be modified to include the light shift in the molecular interaction potentials. What complicates this even more, is the fact that the light shift potentials are not well known for molecular states, since the detuning at close range is different from the separated atom case.

So far, we have only considered collisions between ^{133}Cs atoms due to the large scattering lengths present. Other atomic species such as other alkali or earth alkali atoms, might offer distinct advantages. The discussed scattering model and the trap-induced resonance should provide the method and motivation for further studies along these lines.

Appendices

Appendix A

Alternate derivation of "Busch" solutions

A.1 Derivation

A.1.1 Hamiltonian and ansatz

Here, we will present an alternative way of deriving the higher partial wave "Busch" solution presented in Section 3.2. We will follow the derivation of the eigenvalues and solutions as shown by Busch *et al.* in Ref. [64] for $l = 0$. Consider the δ-shell pseudopotential for higher partial waves Eq. (2.78) in harmonic oscillator length units of $r_0 = \sqrt{\hbar/(\mu\omega)}$ and energy units of $\hbar\omega$

$$v_{\text{shell}}^{(l)}(r) = \lim_{s\to 0} \frac{1}{2} \frac{[(2l+1)!!]}{[(2l)!!]} a_l^{2l+1} \frac{\delta(r-s)}{s^{l+2}} \frac{\partial^{2l+1}}{\partial r^{2l+1}} r^{l+1} \,. \tag{A.1}$$

The total Hamiltonian in scaled unit is given by Eq. (3.15),

$$\hat{H} = \hat{H}_{\text{osc}} + \sum_l v_{\text{shell}}^{(l)}(r) \,, \tag{A.2}$$

where

$$\hat{H}_{\rm osc} = \frac{\hat{\mathbf{p}}_r^2}{2} + \frac{1}{2}\mathbf{r}^2 \tag{A.3}$$

in scaled units. Following Ref. [64], we make the following ansatz

$$\psi(r) = \sum_{n,l,m} c_{nl}\phi_{nl}(r)Y_l^m\,, \tag{A.4}$$

where ϕ_{nl} are the harmonic oscillator eigenfunctions with $H_{\rm osc}\phi_{nl} = E_{nl}\phi_{nl}$. We insert this ansatz into Eq. (A.2) and obtain

$$\begin{aligned}\sum_{n,l,m} & c_{nl}(E_{nl}-E)\phi_{nl}(r)Y_l^m \\ & + \lim_{s\to 0}\sum_l \frac{1}{2}\frac{[(2l+1)!!]}{[(2l)!!]}a_l^{2l+1}\frac{\delta(r-s)}{s^{l+2}}\frac{\partial^{2l+1}}{\partial r^{2l+1}}r^{l+1}\sum_{n',l',m'} c_{n'l'}\phi_{n'l'}(r)Y_{l'}^{m'} = 0\,.\end{aligned} \tag{A.5}$$

Projecting this equation onto $\phi_{nl}^* Y_l^m$, we get separate eigenvalue equations for each l. The angular part of the integration is only nonzero for $m = m' = 0$,

$$\int \sin\theta d\theta \int d\phi\, Y_l^{m*}(\theta,\phi)Y_{l'}^{m'}(\theta,\phi) = \delta_{ll'}\delta_{m,m'}\delta_{m,0}. \tag{A.6}$$

Integrating the radial part and later taking the limit $s \to 0$, gives

$$\begin{aligned}\lim_{s\to 0}\int r^2 dr \frac{\phi_{nl}^*}{s^l}\frac{\delta(r-s)}{s^2}\frac{\partial^{2l+1}}{\partial r^{2l+1}}r^{l+1}\sum_{n'} c_{n'l}\phi_{n'l}(r) & \\ = \lim_{s\to 0}\left[\frac{\phi_{nl}^*}{s^l}\right]_{r=s}\left[\frac{\partial^{2l+1}}{\partial r^{2l+1}}r^{l+1}\sum_{n'} c_{n'l}\phi_{n'l}(r)\right]_{r=s}\,. &\end{aligned} \tag{A.7}$$

In summary, we arrive at the following eigenvalue equation for each l. Note that by doing the integration in r first, we followed the prescribed order of integration and limit as described in Section 2.4.

$$\lim_{s\to 0}\left\{c_{nl}(E_{nl}-E) + \frac{1}{2}\frac{[(2l+1)!!]}{[(2l)!!]}a_l^{2l+1}\left[\frac{\phi_{nl}^*}{s^l}\right]_{r=s}\left[\frac{\partial^{2l+1}}{\partial r^{2l+1}}r^{l+1}\sum_{n'} c_{n'l}\phi_{n'l}(r)\right]_{r=s}\right\} = 0\,.$$

(A.8)

The equation for $l = 0$ is solved analytically in [64]. Analogously to [64], the coefficients c_{nl} have to take the form,

$$c_{nl} = \frac{A}{E_{nl} - E} \left(\frac{\phi^*_{nl}(s)}{s^l} \right) . \tag{A.9}$$

Inserting this into Eq. (A.8) and dividing by $A \left(\frac{\phi^*_{nl}(s)}{s^l} \right)$, we get

$$\lim_{s \to 0} \left\{ \frac{1}{2} \frac{[(2l+1)!!]}{[(2l)!!]} \left[\frac{\partial^{2l+1}}{\partial r^{2l+1}} r^{l+1} \sum_n \frac{\left(\frac{\phi^*_{nl}(s)}{s^l} \right) \phi_{nl}(r)}{E_{nl} - E} \right]_{r=s} \right\} = -\frac{1}{a_l^{2l+1}} . \tag{A.10}$$

A.1.2 Harmonic oscillator solutions

The problem is reduced to solving this implicit equation for E. We insert the well-known harmonic oscillator solutions

$$\phi_{nl}(r) = \sqrt{\frac{2\Gamma(n+1)}{\Gamma(n+l+3/2)}} r^l e^{-\frac{r^2}{2}} L_n^{l+1/2}(r^2) \tag{A.11}$$

with

$$\begin{aligned}
\left[\frac{\phi^*_{nl}(s)}{s^l} \right]_{s \ll 1} &= \sqrt{\frac{2\Gamma(n+1)}{\Gamma(n+l+3/2)}} \left(1 - \frac{s^2}{2} \right) \left(L_n^{l+1/2}(s=0) + \left(L_n^{l+1/2} \right)'(s=0) s^2 \right) \\
&= \sqrt{\frac{2\Gamma(n+1)}{\Gamma(n+l+3/2)}} \left(1 - \frac{s^2}{2} \right) \\
&\quad \times \left(\frac{\Gamma(n+l+3/2)}{\Gamma(n+1)\Gamma(l+3/2)} + \frac{n\Gamma(n+l+3/2)}{\Gamma(n+1)\Gamma(l+5/2)} s^2 \right) \\
&= \frac{\sqrt{2}}{\Gamma(l+3/2)} \sqrt{\frac{\Gamma(n+l+3/2)}{\Gamma(n+1)}} + O(s^2) .
\end{aligned} \tag{A.12}$$

For very small $s << 1$, we only use the zeroth order term in the expansion and we get the eigenvalue equation

$$\lim_{s\to 0}\left\{\frac{1}{2}\frac{(l+1)[(2l-1)!!]}{[(2l)!!]}\left[\frac{\partial^{2l+1}}{\partial r^{2l+1}}r^{l+1}\sum_n \frac{\frac{2}{\Gamma(l+3/2)}r^l e^{-\frac{r^2}{2}}L_n^{l+1/2}(r^2)}{E_{nl}-E}\right]_{r=s}\right\}$$
$$=\lim_{s\to 0}\left\{\frac{1}{2}\frac{(l+1)[(2l-1)!!]}{[(2l)!!]}\frac{1}{\Gamma(l+3/2)}\left[\frac{\partial^{2l+1}}{\partial r^{2l+1}}r^{2l+1}e^{-\frac{r^2}{2}}\sum_n \frac{L_n^{l+1/2}(r^2)}{n-\nu_l}\right]_{r=s}\right\}$$
$$=-\frac{1}{a_l^{2l+1}}\,, \quad \text{(A.13)}$$

where the energy eigenvalues have been replaced by $E_{nl}=(2n+l+3/2)$ and $E=(2\nu_l+l+3/2)$.

A.1.3 Summation

We need to evaluate the sum (for simplicity we drop the index l here)

$$\sum_{n=0}^{\infty}\frac{L_n^{l+1/2}(r^2)}{n-\nu}\,. \quad \text{(A.14)}$$

The integral representation, which was used in [64],

$$\frac{1}{n-\nu}=\int_0^\infty \frac{dy}{(1+y)^2}\left(\frac{y}{1+y}\right)^{n-\nu-1}\,, \quad \text{(A.15)}$$

shifts the n-dependence of the sum from the denominator to the exponent. We further use the generating functions of the general Laguerre polynomials (see Arfken p.725, Eq. (13.42) [80]),

$$\sum_{n=0}^{\infty}L_n^k(x)z^n=\frac{e^{-xz/(1-z)}}{(1-z)^{k+1}}\,. \quad \text{(A.16)}$$

We can now evaluate the summation

$$\sum_{n=0}^{\infty}\frac{L_n^{l+1/2}(r^2)}{n-\nu}=\sum_{n=0}^{\infty}\int_0^\infty \frac{dy}{(1+y)^2}\left(\frac{y}{1+y}\right)^{-\nu-1}L_n^{l+1/2}(r^2)\left(\frac{y}{1+y}\right)^n \quad \text{(A.17)}$$

by identifying $x = r^2$, $z = \left(\frac{y}{1+y}\right)$, $y = \left(\frac{z}{1-z}\right)$, $(1-z) = (1+y)^{-1}$, and $k = l + 1/2$. We are left with the integral equation

$$\begin{aligned}\sum_{n=0}^{\infty} \frac{L_n^{l+1/2}(r^2)}{n-\nu} &= \int_0^{\infty} \frac{dy}{(1+y)^2} \left(\frac{y}{1+y}\right)^{-\nu-1} \frac{e^{-yr^2}}{(1+y)^{-l-3/2}} \\ &= \int_0^{\infty} dy\, e^{-yr^2} y^{-\nu-1} (1+y)^{\nu+l+1/2}\,. \end{aligned} \tag{A.18}$$

Comparing this to the integral representation of the Kummer U-functions (see Arfken p.754, Eq. (13.141) [80]),

$$U(a,b,x) = \frac{1}{\Gamma(a)} \int_0^{\infty} dt\, e^{-tx} t^{a-1} (1+t)^{b-a-1}\,, \tag{A.19}$$

we identify $t = y$, $a = -\nu$, $b = l + 3/2$, and $x = r^2$. In summary, we can write

$$\sum_{n=0}^{\infty} \frac{L_n^{l+1/2}(r^2)}{n-\nu} = \Gamma(-\nu) U(-v, l+3/2, r^2)\,. \tag{A.20}$$

A.1.4 Eigenvalue equation

Using Eq. (A.20), the new eigenvalue equation is

$$\begin{aligned}\lim_{s\to 0} \left\{ \frac{1}{2} \frac{[(2l+1)!!]}{[(2l)!!]} \frac{1}{\Gamma(l+3/2)} \left[\frac{\partial^{2l+1}}{\partial r^{2l+1}} r^{2l+1} e^{-\frac{r^2}{2}} \Gamma(-\nu) U(-v, l+3/2, r^2) \right]_{r=s} \right\} \\ = -\frac{1}{a_l^{2l+1}}\,. \end{aligned} \tag{A.21}$$

Before we take the derivative in the eigenvalue equation, it is helpful to find the behavior of the U-function around the origin. To this end, we use the representation of the U-functions in terms of the Kummer M-functions (see Abramowitz and Stegun

p.504, Eq. (13.1.3) [59]),

$$\begin{aligned} U(-\nu, l+3/2, r^2) &= \frac{\pi}{\sin(\pi(l+3/2))}\left[\frac{M(-\nu, l+3/2, r^2)}{\Gamma(-\nu-l-1/2)\Gamma(l+3/2)}\right. \\ &\quad \left. - \left(r^2\right)^{1-l-3/2} \frac{M(-\nu-l-1/2, -l+1/2, r^2)}{\Gamma(-\nu)\Gamma(-l+1/2)}\right] \\ &= (-1)^{l+1}\pi\left[\frac{M(-\nu, l+3/2, r^2)}{\Gamma(-\nu-l-1/2)\Gamma(l+3/2)}\right. \\ &\quad \left. - \frac{1}{r^{2l+1}}\frac{M(-\nu-l-1/2, -l+1/2, r^2)}{\Gamma(-\nu)\Gamma(-l+1/2)}\right]. \end{aligned} \tag{A.22}$$

Inserting this into the eigenvalue equation Eq. (A.21), we have to evaluate the following derivatives:

$$\begin{aligned} &\left[\frac{\partial^{2l+1}}{\partial r^{2l+1}} r^{2l+1} e^{-\frac{r^2}{2}} M(-\nu, l+3/2, r^2)\right]_{r=s} \\ &= \left[\frac{\partial^{2l+1}}{\partial r^{2l+1}} r^{2l+1}\left(1 - \frac{r^2}{2} + \frac{r^4}{8} - ...\right)\left(1 + \frac{-\nu}{l+3/2} r^2 + \frac{1}{2!}\frac{(-\nu)_2}{(l+3/2)_2} r^4 + ...\right)\right]_{r=s} \\ &= (2l+1)! \end{aligned} \tag{A.23}$$

and

$$\begin{aligned} &\left[\frac{\partial^{2l+1}}{\partial r^{2l+1}} e^{-\frac{r^2}{2}} M(-\nu-l-1/2, -l+1/2, r^2)\right]_{r=s} \\ &= \left[\frac{\partial^{2l+1}}{\partial r^{2l+1}} e^{-\frac{r^2}{2}}\left(1 + \frac{-\nu-l-1/2}{-l+1/2} r^2 + \frac{1}{2!}\frac{(-\nu-l-1/2)_2}{(-l+1/2)_2} r^4 + ...\right)\right]_{r=s} \\ &= 0\,, \end{aligned} \tag{A.24}$$

where we have used the Taylor-series expansion of the M-functions (see Abramowitz and Stegun p.504, Eq. 13.1.2 [59]). $(a)_n = a(a+1)...(a+n-1)$ is the Pochhammer symbol. For each equation, we need to examine the Taylor-series expansion of the product of functions before taking the derivative. Both, the M-functions and the exponential, have a series-expansion in even powers of r. After taking the derivative of order $(2l+1)$ of the product of functions and after taking the $r \to 0$ limit , only

the coefficient of the r^{2l+1}-element remains with factor of $(2l+1)!$. In Eq. (A.23), only the first element that is equal to one remains, because of the r^{2l+1} prefactor. In Eq. (A.24), the product of functions has an expansion in even orders of r, so that there is no element of odd order $(2l+1)$. After taking the limit $r \to s$ and then $s \to 0$, Eq. (A.24) is equal to zero.

In summary, we have the eigenvalue equation

$$\frac{\pi}{2}\frac{(-1)^l[(2l+1)!!]^2}{(\Gamma(l+3/2))^2}\frac{\Gamma(-\nu)}{\Gamma(-\nu-l-1/2)} = \frac{1}{a_l^{2l+1}}\,. \tag{A.25}$$

This is the general eigenvalue equation for the l-partial wave interaction derived in Section 3.2. The eigenenergy is contained in $\nu = E/2 - l/2 - 3/4$. For $l = 0$ this reduces to the known eigenvalue equation

$$2\frac{\Gamma(-\nu)}{\Gamma(-\nu-1/2)} = \frac{1}{a} \tag{A.26}$$

since $\Gamma(3/2) = \sqrt{\pi}/2$. Here, $a \equiv a_{l=0}$.

A.1.5 Eigenfunctions

The radial l-wave eigenfunctions are given by

$$\begin{aligned}
\psi_l(r) &= \sum_{n=0}^{\infty} c_{nl}\phi_{nl}(r)\,, \\
&= \sum_{n=0}^{\infty} \frac{A}{E_{nl}-E}\left[\frac{\phi^*_{nl}(s)}{s^l}\right]_{s\to 0}\phi_{nl}(r)\,, \\
&= \frac{A}{\Gamma(l+3/2)} r^l e^{-\frac{r^2}{2}} \sum_{n=0}^{\infty} \frac{L_n^{l+1/2}(r^2)}{n-\nu}\,, \\
&= \frac{A}{\Gamma(l+3/2)} r^l e^{-\frac{r^2}{2}} \Gamma(-\nu) U(-v, l+3/2, r^2)\,,
\end{aligned} \tag{A.27}$$

where A is found by normalizing the eigenfunctions. These eigenfunctions reduce to the correct harmonic oscillator solutions in the case of zero-interaction and $\nu = n$

with an integer n. Note that these solutions are equivalent to the outside solutions to the δ-shell potential in Eq. (3.20). For $l \ll 0$ these solutions diverge as $r^{-(l+1)}$ and are not normalizable. Only the solutions for finite shell radius can be correctly normalized when the inside wave function is included.

A.2 Normalization of the $l = 0$ eigenfunctions

The radial $l = 0$ eigenfunctions can always be normalized, even in the limit of $s \to 0$.

$$\begin{aligned}
I &= \int_0^\infty r^2 \psi(r)^2_{l=0} dr = A^2 \sum_{n=0,n'=0}^{\infty} \int_0^\infty r^2 \frac{\phi_n(0)^2 \phi_n(r)^2}{(E-E_n)^2} dr \,, \\
&= A^2 \sum_{n=0}^{\infty} \frac{\phi_n(0)^2}{(E-E_n)^2} \text{ (by orthonormality)} \,, \\
&= A^2 \sum_{n=0}^{\infty} \frac{2\Gamma(n+1)}{\Gamma(n+3/2)} \frac{\left(L_n^{1/2}(0) + O(s^2)\right)^2}{2^2(\nu-n)^2} \,, \\
&= \frac{A^2}{4} \sum_{n=0}^{\infty} \frac{2\Gamma(n+1)}{\Gamma(n+3/2)} \frac{\frac{2\Gamma(n+3/2)}{\sqrt{\pi}\Gamma(n+1)} L_n^{1/2}(0)}{(\nu-n)^2} \,, \\
&= \frac{A^2}{\sqrt{\pi}} \sum_{n=0}^{\infty} \frac{L_n^{1/2}(0)}{(\nu-n)^2} \,, \\
&= \frac{A^2}{\sqrt{\pi}} \left[-\frac{\partial}{\partial \nu} \sum_{n=0}^{\infty} \frac{L_n^{1/2}(0)}{(\nu-n)} \right] \,, \\
&= \frac{A^2}{\sqrt{\pi}} \left[-\frac{\partial}{\partial \nu} \left(-\sqrt{\pi} \frac{2\Gamma(-\nu)}{\Gamma(-\nu-1/2)} \right) \right] \,, \\
&= A^2 \frac{\partial}{\partial \nu} \left(\frac{2\Gamma(-\nu)}{\Gamma(-\nu-1/2)} \right) \,,
\end{aligned} \tag{A.28}$$

where we used

$$L_n^{1/2}(0) = \frac{2\Gamma(n+3/2)}{\sqrt{\pi}\Gamma(n+1)} \tag{A.29}$$

and

$$\sum_{n=0}^{\infty} \frac{L_n^{1/2}(r^2)}{n-\nu} = \Gamma(-\nu)U(-v, 3/2, r^2) = -\sqrt{\pi}\frac{2\Gamma(-\nu)}{\Gamma(-\nu-1/2)} - \frac{-\sqrt{\pi}}{r}\,. \tag{A.30}$$

Note that the diverging $1/r$ part of the hypergeometric U-function does not depend on ν. When the partial derivative with respect to ν is evaluated, the diverging term vanishes. The normalization constant A is

$$A^2 = \frac{1}{\frac{\partial}{\partial\nu}\left(\frac{2\Gamma(-\nu)}{\Gamma(-\nu-1/2)}\right)}\,, \tag{A.31}$$

or in terms of the s-wave scattering length a

$$\begin{aligned} A^2 &= \frac{1}{\frac{\partial}{\partial\nu}\left(\frac{1}{a}\right)}\,, \\ A^2 &= -\frac{a^2}{\frac{\partial a}{\partial\nu}}\,. \end{aligned} \tag{A.32}$$

We can rewrite Eq. (A.31) by rewriting the $l = 0$ eigenvalue equation,

$$\begin{aligned} \frac{1}{a} &= \frac{2\Gamma(-\nu)}{\Gamma(-\nu-1/2)}\,, \\ &= \frac{2\frac{\pi}{\sin\pi\nu}\frac{1}{\Gamma(\nu+1)}}{\frac{\pi}{\sin\pi(\nu+1/2)}\frac{1}{\Gamma(\nu+3/2)}}\,, \\ &= 2\frac{1}{\tan\pi\nu}\frac{\Gamma(\nu+3/2)}{\Gamma(\nu+1)}\,. \end{aligned} \tag{A.33}$$

The derivative is evaluated to be

$$\begin{aligned}
\frac{\partial a}{\partial \nu} &= \frac{\partial}{\partial \nu}\left[\frac{1}{2}\tan(\pi\nu)\frac{\Gamma(\nu+1)}{\Gamma(\nu+3/2)}\right], \\
&= \frac{\pi}{2}\sec(\pi\nu)^2\frac{\Gamma(\nu+1)}{\Gamma(\nu+3/2)} \\
&\quad +\frac{1}{2}\tan(\pi\nu)\frac{\Gamma(\nu+1)'\Gamma(\nu+3/2)-\Gamma(\nu+1)\Gamma(\nu+3/2)'}{\Gamma(\nu+3/2)^2}, \\
&= \pi a_0\frac{\sec(\pi\nu)^2}{\tan(\pi\nu)} + a_0\left(\frac{\Gamma(\nu+1)'}{\Gamma(\nu+1)} - \frac{\Gamma(\nu+3/2)'}{\Gamma(\nu+3/2)}\right), \\
&= a_0\left(\frac{\pi}{\sin(\pi\nu)\cos(\pi\nu)} + \frac{\Gamma(\nu+1)'}{\Gamma(\nu+1)} - \frac{\Gamma(\nu+3/2)'}{\Gamma(\nu+3/2)}\right), \\
&= a_0\left(\frac{2\pi}{\sin(2\pi\nu)} + \Phi(\nu+1) - \Phi(\nu+3/2)\right), \qquad \text{(A.34)}
\end{aligned}$$

where $\Phi(x) = \Gamma(x)'/\Gamma(x)$ is the digamma function. The normalization constant A is then

$$A^2 = \frac{-a}{\frac{2\pi}{\sin(2\pi\nu)} + \Phi(\nu+1) - \Phi(\nu+3/2)}. \qquad \text{(A.35)}$$

Note, this normalization is only possible for the $l = 0$ eigenfunctions. The $l > 0$ eigenfunctions are not normalizable due to the strongly diverging r^{-l} behavior around the origin as we will see in the next section.

A.3 Normalization of the l eigenfunctions

The radial l eigenfunctions are not normalizable in the limit of the shell radius s approaching zero since the solutions diverge as $r^{-(l+1)}$ around the origin for zero shell radius ($s \to 0$). We can attempt the normalization in a manner analogous to

the $l = 0$ case.

$$\begin{aligned}
I &= \int_0^\infty r^2\psi(r)^2_{l=0}dr = A^2\sum_{n=0,n'=0}^{\infty}\int_0^\infty r^2\frac{\left(\frac{\phi_n(s)}{s^l}\right)^2\phi_n(r)^2}{(E-E_n)^2}dr\,,\\
&= A^2\sum_{n=0}^{\infty}\frac{\left(\frac{\phi_n(s)}{s^l}\right)^2}{(E-E_n)^2}\text{ (by orthonormality)}\,,\\
&= A^2\sum_{n=0}^{\infty}\frac{2\Gamma(n+1)}{\Gamma(n+l+3/2)}\frac{\left(L_n^{l+1/2}(s=0)+O(s^2)\right)^2}{2^2(\nu-n)^2}\,,\\
&= \frac{A^2}{4}\sum_{n=0}^{\infty}\frac{2\Gamma(n+1)}{\Gamma(n+l+3/2)}\frac{\frac{\Gamma(n+l+3/2)}{\Gamma(n+1)\Gamma(l+3/2)}L_n^{l+1/2}(0)}{(\nu-n)^2}+O(s^2)\,,\\
&= \frac{A^2}{2\Gamma(l+3/2)}\sum_{n=0}^{\infty}\frac{L_n^{l+1/2}(0)}{(\nu-n)^2}\,,\\
&= \frac{A^2}{2\Gamma(l+3/2)}\left[-\frac{\partial}{\partial\nu}\sum_{n=0}^{\infty}\frac{L_n^{l+1/2}(0)}{(\nu-n)}\right]\,,\\
&= \frac{A^2}{2\Gamma(l+3/2)}\left[-\frac{\partial}{\partial\nu}\left(\Gamma(-\nu)U(-\nu,l+3/2,0)\right)\right]\,,\\
&= \frac{A^2}{2\Gamma(l+3/2)}\Bigg[-\frac{\partial}{\partial\nu}\Bigg(\frac{(-1)^{l+1}\pi\Gamma(-\nu)}{\Gamma(l+3/2)\Gamma(-\nu-l-1/2)}+\frac{(-1)^{l+1}\pi}{\Gamma(-l+1/2)}\frac{1}{s^{2l+1}}\\
&\quad+\frac{(-1)^{l+1}\pi(2\nu+2l+1)}{2\Gamma(-l+3/2)}\frac{1}{s^{2l-1}}+O\left(\frac{1}{s^{2l-3}}\right)\Bigg)\Bigg]\,, \qquad \text{(A.36)}
\end{aligned}$$

where we used

$$L_n^{l+1/2}(0) = \frac{\Gamma(n+l+3/2)}{\Gamma(l+3/2)\Gamma(n+1)} \qquad \text{(A.37)}$$

and

$$\begin{aligned}
\sum_{n=0}^{\infty}\frac{L_n^{l+1/2}(r^2)}{n-\nu} &= \Gamma(-\nu)U(-v,l+3/2,r^2)\,,\\
&= \frac{(-1)^{l+1}\pi\Gamma(-\nu)}{\Gamma(l+3/2)\Gamma(-\nu-l-1/2)}+\frac{(-1)^{l+1}\pi}{\Gamma(-l-1/2)}\frac{1}{r^{2l+1}}\\
&\quad+\frac{(-1)^{l+1}\pi(2\nu+2l+1)}{2\Gamma(-l+3/2)}\frac{1}{s^{2l-1}}+O\left(\frac{1}{r^{2l-3}}\right)\,. \qquad \text{(A.38)}
\end{aligned}$$

Note in the case of $l > 0$, the diverging $r^{-(2l+1)}$ part of the hypergeometric U-function does not depend on ν, however the second term in the expansion that diverges as $r^{-(2l-1)}$ does depend on ν. This is consistent with our expectation that the radial functions are not normalizable for $l > 0$.

Appendix B

Appendix: Matrix elements in the "Busch" basis

B.1 Separation of center of mass and relative coordinate motion

The Hamiltonian for two atoms of identical mass $m_1 = m_2 = m$ in identical anisotropic separated traps interacting via $\hat{V}_{\rm int}(r)$ is

$$\hat{H} = \frac{\hat{\mathbf{p}}_1^2}{2m} + \frac{\hat{\mathbf{p}}_2^2}{2m} + \hat{V}(\mathbf{r}_1) + \hat{V}(\mathbf{r}_2) + \hat{V}_{\rm int}(\mathbf{r}_2 - \mathbf{r}_1)\,. \tag{B.1}$$

The total mass M and the reduced mass μ are

$$\begin{aligned} M &= m_1 + m_2 = 2m\,, \\ \mu &= \frac{m_1 m_2}{m_1 + m_2} = \frac{m}{2}\,. \end{aligned} \tag{B.2}$$

The relative (RC) and center of mass (CM) coordinates are defined as

$$\begin{aligned} \mathbf{R} &= \frac{m_1\mathbf{r}_1 + m_2\mathbf{r}_2}{M} = \frac{\mathbf{r}_1 + \mathbf{r}_2}{2}\,, \\ \mathbf{r} &= \mathbf{r}_2 - \mathbf{r}_1\,, \end{aligned} \tag{B.3}$$

and

$$\begin{aligned} \mathbf{r}_1 &= \mathbf{R} - \frac{m_2}{M}\mathbf{r} = \mathbf{R} - \frac{1}{2}\mathbf{r}\,, \\ \mathbf{r}_2 &= \mathbf{R} + \frac{m_1}{M}\mathbf{r} = \mathbf{R} + \frac{1}{2}\mathbf{r}\,. \end{aligned} \tag{B.4}$$

For simplicity, we assume the anisotropy and the separation in the z direction. We further assume that the atoms are well-localized near potential minima. We can then approximate the trapping potential by harmonic potentials $\hat{V}_{\rm trap} = m_i\omega^2(\mathbf{r}_i \pm \Delta z\mathbf{e}_z)^2/2$. Because of the quadratic form of both, the kinetic energy term and the potential term, we can transform this Hamiltonian to the center of mass (CM) frame with CM and relative coordinates as follows. The potential term in Cartesian coordinates in the harmonic approximation is

$$\begin{aligned} \hat{V} = \frac{1}{2}m\omega_\perp^2\left(x_1^2 + y_1^2\right) + \frac{1}{2}m\omega_z^2\left(z_1 + \frac{\Delta z}{2}\right)^2 \\ + \frac{1}{2}m\omega_\perp^2\left(x_2^2 + y_2^2\right) + \frac{1}{2}m\omega_z^2\left(z_2 - \frac{\Delta z}{2}\right)^2 + \hat{V}_{\rm int}(\mathbf{r}_2 - \mathbf{r}_1)\,. \end{aligned} \tag{B.5}$$

With $x_1 = X - x/2$ and $x_2 = X + x/2$ we have

$$x_1^2 + x_2^2 = X^2 - xX + \frac{x^2}{4} + X^2 + xX + \frac{x^2}{4} = 2X^2 + \frac{x^2}{2} \tag{B.6}$$

and analogous for $y_1^2 + y_2^2$. For $z_{1,2}$ we have

$$\begin{aligned} \left(z_1 + \frac{\Delta z}{2}\right)^2 + \left(z_2^2 - \frac{\Delta z}{2}\right)^2 &= z_1 + z_1\Delta z + \frac{\Delta z^2}{4} + z_2^2 - z_2\Delta z + \frac{\Delta z^2}{4}\,, \\ &= 2Z^2 + \frac{z^2}{2} - z\Delta z + \frac{\Delta z^2}{2}\,, \\ &= 2Z^2 + \frac{(z - \Delta z)^2}{2}\,. \end{aligned} \tag{B.7}$$

In summary, we obtain separate Hamiltonians for the CM and RC motion

$$\begin{aligned}\hat{H}_{CM} &= \frac{p_R^2}{2M} + \frac{1}{2}M\omega_\perp^2\left(X^2+Y^2\right) + \frac{1}{2}M\omega_z^2 Z^2\,,\\ \hat{H}_{rel} &= \frac{p_r^2}{2\mu} + \frac{1}{2}\mu\omega_\perp^2\left(x^2+y^2\right) + \frac{1}{2}\mu\omega_z^2\left(z-\Delta z\right)^2 + V_{\rm int}(r)\,. \end{aligned} \tag{B.8}$$

The CM part has the trivial anisotropic trap solutions. The relative coordinate part is an anisotropic trap centered at Δz and the interaction potential at the origin.

B.2 Relative coordinate Hamiltonian

We can write the RC Hamiltonian as

$$\begin{aligned}\hat{H}_{rel} &= \frac{\hat{\mathbf{p}}_r^2}{2\mu} + \frac{1}{2}\mu\omega_\perp^2\left(x^2+y^2\right) + \frac{1}{2}\mu\omega_z^2\left(z-\Delta z\right)^2 + \hat{V}_{\rm int}(r)\,,\\ &= \frac{\hat{\mathbf{p}}_r^2}{2\mu} + \frac{1}{2}\mu\omega_\perp^2 r^2 + \frac{1}{2}\mu\left(\omega_z^2-\omega_\perp^2\right)z^2 - \mu\omega_z^2 z\Delta z + \frac{1}{2}\mu\omega_z^2\Delta z^2 + \hat{V}_{\rm int}(r)\,. \end{aligned} \tag{B.9}$$

Using the spherical harmonics

$$Y_{10} = \sqrt{\frac{3}{4\pi}}\cos\theta\,, \tag{B.10}$$

$$Y_{20} = \sqrt{\frac{5}{16\pi}}\left(3\cos\theta^2-1\right)\,, \tag{B.11}$$

and $z = r\cos\theta$, we can rewrite this as

$$\begin{aligned}\hat{H}_{rel} &= \frac{\hat{\mathbf{p}}_r^2}{2\mu} + \frac{1}{2}\mu r^2\left(\omega_\perp^2 + \left(\omega_z^2 - \omega_\perp^2\right)\frac{\sqrt{\frac{16\pi}{5}}Y_{20} + 1}{3}\right) \\ &\quad -\mu\omega_z^2\Delta z r\sqrt{\frac{4\pi}{3}}Y_{10} + \frac{1}{2}\mu\omega_z^2\Delta z^2 + \hat{V}_{\rm int}(r)\,, \\ &= \frac{\hat{\mathbf{p}}_r^2}{2\mu} + \frac{1}{2}\mu\omega^2 r^2\left(1 - \Lambda\sqrt{\frac{16\pi}{5}}Y_{20}\right) - \mu\omega_z^2\Delta z r\sqrt{\frac{4\pi}{3}}Y_{10} + \frac{1}{2}\mu\omega_z^2\Delta z^2 + \hat{V}_{\rm int}(r)\,.\end{aligned} \tag{B.12}$$

Here, the mean frequency ω is

$$\omega = \left(\frac{2}{3}\omega_\perp^2 + \frac{1}{3}\omega_z^2\right)\,. \tag{B.13}$$

The parameter Λ measures the anisotropy of the trap according to

$$\Lambda = \frac{\omega_z^2 - \omega_\perp^2}{3\omega} = \frac{\omega_z^2 - \omega_\perp^2}{2\omega_\perp^2 + \omega_z^2}\,. \tag{B.14}$$

We can write the momentum operator $\hat{\mathbf{p}}_r$ in spherical coordinates with

$$\frac{\hat{\mathbf{p}}_r^2}{2\mu} = -\frac{\hbar^2}{2\mu}\frac{1}{r}\frac{\partial^2}{\partial r^2}r + \frac{\hbar^2 l(l+1)}{2\mu r^2}\,. \tag{B.15}$$

B.2.1 Hamiltonian in the "Busch" basis

We represent the relative coordinate Hamiltonian for arbitrary Λ and Δz in the basis corresponding to the solutions with $\Delta z = 0$ and a *fixed* scattering length a. This basis set, derived by Busch *et al.* [64], consists of 3D-harmonic-oscillator-like solutions and has been discussed in detail in Chapter 3. We only consider s-wave interactions with an s-wave pseudopotential. Therefore, we only need to consider the irregular radial waves for $l = 0$, which includes the pseudopotential bound state at negative energy. The $l \geq 1$ wave functions are the regular 3D-harmonic oscillator wave functions,

since the pseudopotential affects only s-wave solutions. The first three terms of the Hamiltonian plus the interaction potential are diagonal in this basis

$$\langle\psi_{\nu',l'}| - \frac{\hbar^2}{2\mu}\frac{1}{r}\frac{\partial^2}{\partial r^2}r + \frac{\hbar^2 l(l+1)}{2\mu r^2} + \frac{1}{2}\mu\omega^2 r^2 + \hat{V}_{\rm int}(r)\,|\psi_{\nu,l}\rangle = E_{\nu l}\delta_{\nu'\nu}\delta_{l'l} \tag{B.16}$$

with

$$E_{\nu l} = \hbar\omega\left(2\nu + l + \frac{3}{2}\right). \tag{B.17}$$

The other important terms are the Λ anisotropic term and the Δz separation term. The first one couples partial waves with $l - l' = 0, \pm 2$, the second, dipolar term couples partial waves with $l - l' = 0, \pm 1$. The term with Δz^2 only adds a constant energy.

Regular $l > 0$ anisotropic matrix elements

We evaluate the matrix elements of the anisotropic potential term in the basis of partial waves, isotropic harmonic oscillator functions, and the irregular s-wave oscillator eigenfunctions. The angle-dependent term of the Hamiltonian is evaluated using

$$\begin{aligned} I_{ll'} &= \sqrt{\frac{4\pi}{5}}\int_0^{\pi}\int_0^{2\pi}\sin\theta d\theta d\phi\, Y^*_{l'0}(\theta,\phi)Y_{20}(\theta,\phi)Y_{l0}(\theta,\phi)\,, \\ &= \sqrt{\frac{2l+1}{2l'+1}}\,\langle l'0|20;l0\rangle^2\,. \end{aligned} \tag{B.18}$$

Evaluating the Clebsch-Gordan coefficient $\langle l'0|20;l0\rangle$, we get the quadrupole selection rules,

$$I_{ll} = \frac{l(l+1)}{(2l-1)(2l+3)}\,, \tag{B.19}$$

$$I_{l,l+2} = I_{l+2,l} = \frac{3(l+1)(l+2)}{2(2l+3)\sqrt{(2l+1)(2l+5)}}\,, \tag{B.20}$$

while all other angular matrix elements are zero.

For computing the regular $l > 0$ radial matrix element $\langle n'l'|\, r^2\, |nl\rangle$ we use the n- and l-ladder operators given in [24] as

$$\hat{b}^{\pm}_{nl} = \pm r\frac{\partial}{\partial r} \pm \frac{1}{2} - r^2 + 2n + l + \frac{1}{2}\,, \tag{B.21}$$

$$\hat{\mathcal{L}}^{+}_{l} = \frac{\partial}{\partial r} + r - \frac{l}{r}\,. \tag{B.22}$$

The ladder operators can be derived by applying the type C factorization method described in Ref. [97] to the radial Schrödinger Equation. Acting the ladder operators on normalized wave functions, yields [24]

$$\hat{b}^{-}_{nl}\,|nl\rangle = \sqrt{2n(2n+2l+1)}\,|n-1,l\rangle\ , \tag{B.23}$$

$$\hat{b}^{+}_{nl}\,|n-1,l\rangle = \sqrt{2n(2n+2l+1)}\,|nl\rangle\ , \tag{B.24}$$

$$\hat{\mathcal{L}}^{+}_{l}\,|nl\rangle = -2\sqrt{n}\,|n-1,l+1\rangle\ . \tag{B.25}$$

Evaluating $\left(\hat{b}^{+}_{nl} + \hat{b}^{-}_{nl}\right)/2$ using Eq. (B.21), we can write r^2 in terms of the ladder operators

$$r^2 = 2n + l + \frac{3}{2} - \frac{1}{2}\hat{b}^{+}_{n+1,l} - \frac{1}{2}\hat{b}^{-}_{n,l}\,. \tag{B.26}$$

Using orthonormality, we can now easily compute the regular $l = l' > 0$ matrix elements

$$\langle nl|\, r^2\, |nl\rangle = 2n + l + \frac{3}{2}\,, \tag{B.27}$$

$$\langle n+1,l|\, r^2\, |nl\rangle = -\frac{1}{2}\sqrt{2(n+1)(2n+2l+3)}\,, \tag{B.28}$$

$$\langle nl|\, r^2\, |n+1,l\rangle = -\frac{1}{2}\sqrt{2(n+1)(2n+2l+3)}\,. \tag{B.29}$$

The radial operator couples only n to n and $n+1$ wave functions while all other matrix elements vanish.

Appendix B. Appendix: Matrix elements in the "Busch" basis

For $l' = l \pm 2$, we can rewrite the matrix elements first using the l-ladder operator (B.22) and Eq. (B.25)

$$\langle nl|\, r^2\, |n', l+2\rangle = \frac{\langle nl|\, r^2 \hat{\mathcal{L}}^+_{l+1}\hat{\mathcal{L}}^+_l\, |n'+2, l\rangle}{4\sqrt{(n'+1)(n'+2)}}\,. \tag{B.30}$$

We can express the l-ladder operator (B.22) conveniently in terms of any n-ladder operator $\hat{b}^-_{n''l''}$ (B.21) via

$$r\hat{\mathcal{L}}^+_l = -\hat{b}^-_{n''l''} + 2n'' + l'' - l\,. \tag{B.31}$$

We further need the commutator

$$\left[r, \hat{\mathcal{L}}^+_l\right] = r\frac{d}{dr} - \frac{d}{dr}r = r\frac{d}{dr} - r\frac{d}{dr} - 1 = -1\,. \tag{B.32}$$

Using this, we can rewrite

$$\begin{aligned}
r^2\hat{\mathcal{L}}^+_{l+1}\hat{\mathcal{L}}^+_l &= r\left(\left[r, \hat{\mathcal{L}}^+_{l+1}\right] + \hat{\mathcal{L}}^+_{l+1}r\right)\hat{\mathcal{L}}^+_l\,, \\
&= \left(-1 + r\hat{\mathcal{L}}^+_{l+1}\right) r\hat{\mathcal{L}}^+_l\,, \\
&= \left(-1 - \hat{b}^-_{n''l''} + 2n'' + l'' - l - 1\right)\left(-\hat{b}^-_{n'''l'''} + 2n''' + l''' - l\right)\,, \\
&= \left(-\hat{b}^-_{n''l''} + 2n'' + l'' - l - 2\right)\left(-\hat{b}^-_{n'''l'''} + 2n''' + l''' - l\right)\,.
\end{aligned} \tag{B.33}$$

We can arbitrarily choose $n'' = n' + 1$, $n''' = n' + 2$, and $l''' = l'' = l$ so that

$$\begin{aligned}
r^2\hat{\mathcal{L}}^+_{l+1}\hat{\mathcal{L}}^+_l &= \left(-\hat{b}^-_{n'+1} + 2(n'+1) - 2\right)\left(-\hat{b}^-_{n'+2} + 2(n'+2)\right)\,, \\
&= \left(-\hat{b}^-_{n'+1} + 2n'\right)\left(-\hat{b}^-_{n'+2} + 2(n'+2)\right)\,, \\
&= \hat{b}^-_{n'+1}\hat{b}^-_{n'+2} - 2(n'+2)\hat{b}^-_{n'+1} - 2n'\hat{b}^-_{n'+2} + 4n'(n'+2)\,, \\
&= \hat{b}^-_{n'+1}\hat{b}^-_{n'+2} - 2(n'+2)(\hat{b}^-_{n'+2} - 2) - 2n'\hat{b}^-_{n'+2} + 4n'(n'+2)\,, \\
&= \hat{b}^-_{n'+1}\hat{b}^-_{n'+2} - 4(n'+1)(\hat{b}^-_{n'+2} - 2) + 4(n'+1)(n'+2)\,.
\end{aligned} \tag{B.34}$$

For convenience, we drop the same index l for the b operators. Here, we used the identity $\hat{b}^-_{n'+1} = (\hat{b}^-_{n'+2} - 2)$. We can now express the matrix element as

$$\begin{aligned}\langle nl|\, r^2 \hat{\mathcal{L}}^+_{l+1}\hat{\mathcal{L}}^+_l \,|n'+2,l\rangle &= \langle nl|\, \hat{b}^-_{n'+1}\hat{b}^-_{n'+2} \,|n'+2,l\rangle \ , \\ &\quad - \langle nl|\, 4(n'+1)(\hat{b}^-_{n'+2} - 2) \,|n'+2,l\rangle \ , \\ &\quad + \langle nl|\, 4(n'+1)(n'+2) \,|n'+2,l\rangle \ . \end{aligned} \tag{B.35}$$

The non-vanishing matrix elements can then be obtained after some more straightforward algebra

$$\langle nl|\, r^2 \,|n,l+2\rangle = \frac{1}{2}\sqrt{(2n+2l+3)(2n+2l+5)}\,, \tag{B.36}$$

$$\langle n+1,l|\, r^2 \,|n,l+2\rangle = -\sqrt{2(n+1)(2n+2l+5)}\,, \tag{B.37}$$

$$\langle n+2,l|\, r^2 \,|n,l+2\rangle = \sqrt{(n+1)(n+2)}\,. \tag{B.38}$$

Irregular $l = 0$ anisotropic matrix elements

For the special case of $l = 0$, we do not need the matrix elements $\langle \nu,0|\, r^2 \,|\nu,0\rangle$ since the angular part of the integration $I_{l=0,l=0}$ vanishes. Only the matrix elements $\langle n,2|\, r^2 \,|\nu,0\rangle$ have to evaluated. To this end, we use the expansion of the irregular solutions in terms of the regular harmonic wave functions $|nl\rangle$ (see Appendix A and Ref. [64])

$$\begin{aligned}\langle n,2|\, r^2 \,|\nu,0\rangle &= \sum_{k=0}^{\infty} c_k \langle n,2|\, r^2 \,|k,0\rangle \ , \\ &= c_n \langle n,2|\, r^2 \,|n,0\rangle + c_{n+1} \langle n,2|\, r^2 \,|n+1,0\rangle + c_{n+2} \langle n,2|\, r^2 \,|n+2,0\rangle \ , \end{aligned} \tag{B.39}$$

where

$$c_k = A\frac{\psi_n(0)}{E_n - E} = A\frac{\psi_n(0)}{2\hbar\omega(n-\nu)} \tag{B.40}$$

and

$$\psi_n(0) = \eta_{n0} L_n^{1/2}(0) = \left(\frac{2}{\sqrt{\pi}}\right)^{\frac{1}{2}} \sqrt{L_n^{1/2}(0)} = \frac{2}{\sqrt{\pi}} \sqrt{\frac{2\Gamma(n+3/2)}{n!}}\,. \tag{B.41}$$

The normalization constant A has been determined in Section A.2. Inserting the regular matrix elements, we get

$$\langle n, 2|\, r^2\, |\nu, 0\rangle = \frac{A}{\hbar\omega} \sqrt{\frac{2\Gamma(n+\frac{7}{2})}{\pi\Gamma(n+1)}} \left(\frac{1}{n-\nu} - \frac{2}{n+1-\nu} + \frac{1}{n+2-\nu}\right)\,. \tag{B.42}$$

Regular $l > 0$ separation matrix elements

We evaluate the matrix elements of the separation potential term analogously to the isotropic case. In the case of separated traps, the off-diagonal matrix element are due to the $r\cos\theta = \sqrt{4\pi/3} r Y_{10}$ term. As a spherical tensor of rank one, this term couples partial waves with $l' = l$ and $l' = l \pm 1$. Because of the cylindrical symmetry of the problem, we are only interested in matrix element between states with magnetic quantum number $m = 0$. For $m = 0$, the $l' = l$ matrix elements are zero. In detail, we can evaluate the angle-dependent term of the Hamiltonian

$$\begin{aligned} I_{ll'} &= \sqrt{\frac{4\pi}{3}} \int_0^\pi \int_0^{2\pi} \sin\theta d\theta d\phi\, Y^*_{l'0}(\theta,\phi) Y_{10}(\theta,\phi) Y_{l0}(\theta,\phi)\,, \\ &= \sqrt{\frac{2l+1}{2l'+1}}\, \langle l'0|10;l0\rangle^2\,. \end{aligned} \tag{B.43}$$

Evaluating the Clebsch-Gordan coefficient $\langle l'0|10;l0\rangle$ we get the dipole selection rules

$$I_{ll} = 0\,, \tag{B.44}$$

$$I_{l,l+1} = I_{l+1,l} = \frac{(l+1)}{\sqrt{(2l+1)(2l+3)}}\,, \tag{B.45}$$

while all other angular matrix elements are zero.

Appendix B. Appendix: Matrix elements in the "Busch" basis

We further have to compute the regular $l > 0$ radial matrix element $\langle nl|\, r\, |n'l+1\rangle$, which can be done using n- and l-ladder operators in Eq. (B.21) and (B.22). As a reminder, the operators are

$$\hat{b}^{\pm}_{nl} = \pm r\frac{\partial}{\partial r} \pm \frac{1}{2} - r^2 + 2n + l + \frac{1}{2}\,, \tag{B.46}$$

$$\hat{\mathcal{L}}^{+}_{l} = \frac{\partial}{\partial r} + r - \frac{l}{r} \tag{B.47}$$

with

$$\hat{b}^{-}_{nl}\,|nl\rangle = \sqrt{2n(2n+2l+1)}\,|n-1,l\rangle\ , \tag{B.48}$$

$$\hat{b}^{+}_{nl}\,|n-1,l\rangle = \sqrt{2n(2n+2l+1)}\,|nl\rangle\ , \tag{B.49}$$

$$\hat{\mathcal{L}}^{+}_{l}\,|nl\rangle = -2\sqrt{n}\,|n-1,l+1\rangle\ . \tag{B.50}$$

For $l' = l \pm 1$, we can rewrite the matrix elements first using the l-ladder operator (B.47) and Eq. (B.50)

$$\langle nl|\, r\,|n', l+1\rangle = \frac{\langle nl|\, r\hat{\mathcal{L}}^{+}_{l}\,|n'+1,l\rangle}{-2\sqrt{n'+1}}\,. \tag{B.51}$$

We can express the l-ladder operator (B.47) conveniently in terms of any n-ladder operator $\hat{b}^{-}_{n''l''}$ (B.46) via

$$r\hat{\mathcal{L}}^{+}_{l} = -\hat{b}^{-}_{n''l''} + 2n'' + l'' - l\,. \tag{B.52}$$

Choosing $n'' = n'+1$, $l'' = l$ and inserting this representation into the matrix element, we get

$$\begin{aligned}\langle nl|\, r\hat{\mathcal{L}}^{+}_{l}\,|n'+1,l\rangle &= \langle nl| - \hat{b}^{-}_{n'+1,l} + 2n + 2\,|n'+1,l\rangle\ ,\\ &= \langle nl| - \hat{b}^{-}_{n'+1,l}\,|n'+1,l\rangle\ ,\\ &\quad + \langle nl|\, 2n+2\,|n'+1,l\rangle\ .\end{aligned} \tag{B.53}$$

The nonvanishing matrix elements can then be easily obtained after some more algebra,

$$\begin{aligned} \langle n,l|r\cos\theta|n,l+1\rangle &= (l+1)\sqrt{\frac{(n+l+3/2)}{(2l+1)(2l+3)}}\,, \\ \langle n,l|r\cos\theta|n-1,l+1\rangle &= -(l+1)\sqrt{\frac{n}{(2l+1)(2l+3)}}\,. \end{aligned} \tag{B.54}$$

Irregular $l=0$ separation matrix elements

For the irregular $l=0$ solutions only the matrix elements $\langle n,1|\,r\cos\theta\,|\nu,0\rangle$ have to evaluated. To this end, we use again the expansion of the irregular solutions in terms of the regular harmonic wave functions $|nl\rangle$ (see Appendix A and Ref. [64]),

$$\begin{aligned} \langle n,1|\,r\cos\theta\,|\nu,0\rangle &= \sum_{k=0}^{\infty} c_k\,\langle n,2|\,r^2\,|k,0\rangle\ , \\ &= c_n\,\langle n,1|\,r\,|n,0\rangle + c_{n+1}\,\langle n,1|\,r\,|n+1,0\rangle\ , \end{aligned} \tag{B.55}$$

where

$$c_k = A\frac{\psi_n(0)}{E_n-E} = A\frac{\psi_n(0)}{2\hbar\omega(n-\nu)} \tag{B.56}$$

and

$$\psi_n(0) = \eta_{n0}L_n^{1/2}(0) = \left(\frac{2}{\sqrt{\pi}}\right)^{\frac{1}{2}}\sqrt{L_n^{1/2}(0)} = \frac{2}{\sqrt{\pi}}\sqrt{\frac{2\Gamma(n+3/2)}{n!}}\,. \tag{B.57}$$

Inserting the regular matrix elements, we obtain

$$\langle n,1|\,r\cos\theta\,|\nu,0\rangle = \frac{A}{\hbar\omega}\sqrt{\frac{2\Gamma(n+\frac{5}{2})}{\pi\Gamma(n+1)}}\left(\frac{1}{n-\nu}-\frac{1}{n+1-\nu}\right)\,. \tag{B.58}$$

Appendix C

Numerical calculation of energy spectra for interacting atoms

C.1 Separated traps with δ interactions

In Section 4.2 the problem of two interacting atoms in separated traps was reduced to solving the Schrödinger equation for the relative coordinate Hamiltonian,

$$\hat{H}_{\rm rel} = -\frac{\hbar^2}{2\mu}\frac{1}{r}\frac{\partial^2}{\partial r^2}r - \frac{\hbar^2 l(l+1)}{2\mu r^2} + \frac{1}{2}\mu\omega^2 r^2 - \mu\omega^2\Delta z r\cos\theta + \frac{1}{2}\mu\omega^2\Delta z^2 + \frac{2\pi\hbar^2}{\mu}a_{\rm eff}(E_K)\delta(\mathbf{r})\frac{\partial}{\partial r}r\,. \quad \text{(C.1)}$$

We have shown in Section 4.2.3 and Appendix B that, if we represent the Hamiltonian for arbitrary Δz in the basis corresponding to the solutions with $\Delta z = 0$ and scattering length a, the resulting Hamiltonian matrix is tri-diagonal. The diagonal elements are given by

$$E_{\nu l} = \hbar\omega\left(2\nu + l + \frac{3}{2}\right)\,. \quad \text{(C.2)}$$

For $l = 0$, these matrix elements can be found by numerically solving the implicit equation, Eq. (3.11), for ν. The $l \leq 1$ elements are the standard 3D harmonic oscillator eigenvalues with integer $\nu = n$. The off-diagonal elements due to the $r\cos\theta$ term in $\hat{H}_{\rm rel}$ are given by Eq. (4.11) and (4.12) as

$$\begin{aligned} \langle n, l|r\cos\theta|n, l+1\rangle &= (l+1)\sqrt{\frac{(n+l+3/2)}{(2l+1)(2l+3)}}, \\ \langle n, l|r\cos\theta|n-1, l+1\rangle &= -(l+1)\sqrt{\frac{n}{(2l+1)(2l+3)}} \end{aligned} \tag{C.3}$$

for $l \leq 1$; and

$$\langle n, 1|\, r\cos\theta\,|\nu, 0\rangle = a_\nu\sqrt{\frac{2\Gamma(n+\frac{5}{2})}{\pi\Gamma(n+1)}}\left(\frac{1}{n-\nu} - \frac{1}{n+1-\nu}\right) \tag{C.4}$$

for the special case involving the irregular $l = 0$ functions.

As a result, the Hamiltonian matrix is tri-diagonal in l and n. The matrix is diagonalized for each trap separation Δz using a sparse-matrix diagonalization algorithm implemented in Matlab, which allows us to determine the lowest energy eigenvalues. The main program "separd_trap_delta.m" calculates a list of matrix elements, assembles the corresponding sparse matrix and calculates the lowest eigenvalues of the sparse matrix. The subroutine "nusolve.m", which uses "diffatan2a.m" and "diffacota2.m", provides an accurate and stable routine for calculating the "Busch" eigenvalues for the $l = 0$ diagonal elements. "scriptA.m", which uses "digamma.m" and "psin.m", fixes the normalizations of the $l = 0$ wave functions. The main code further includes a loop over both the scattering length and the trap separation. The calculated energy spectra (energy vs. trap separation for a list of scattering lengths) provide a template for the calculation of self-consistent energy spectra. The self-consistent calculation of the energy spectra is implemented in the main program "energydep_spectrum.m" which is presented in Section C.3.

C.1.1 Main program

separd_trap_delta.m

```
%-----------------------------------------------------------------------
% Main Program: separd_trap_delta.m
%-----------------------------------------------------------------------
%
% Created by ERIC E. BOLDA and RENE STOCK
% NIST, Gaithersburg and UNM, Albuquerque
%
% original code by ERIC E. BOLDA:   May, 2002
%
% significantly modified by RENE STOCK:  June - October, 2002
%
% last modified: April, 2005
%
% This is the main program for determining the eigenenergies of
% two atoms interacting through an s-wave pseudopotential in
% SEPARATED ISOTROPIC harmonic traps. The Hamiltonian
% is expressed in the spherical hypergeometric "Busch-basis"
% for l=0 and the regular spherical Laguerre harmonic oscillator
% basis for l>0. The resulting tri-diagonal matrix is then
% diagonalized using the Matlab sparse matrix routine for finding
% the lowest matrix eigenvalues.
%
% The code includes a loop over both the scattering length and the
% trap separation. The calculated energy spectra (energy vs. trap
% separation for a list of scattering lengths) provides a template
```

```
% for the calculation of the self-consistent energy spectra using an
% energy-dependent scattering length, calculated for the realistic
% interaction.
%
% Note: This code only calculates m=0 levels, since only m=0
% levels are affected by the delta interaction.
%
% Note about scaling: In the main diagonalization routine
% energies are scaled to E = hbar omega,
% lengths are scaled to r0 = sqrt(hbar/(mu*omega)).
%-----------------------------------------------------------------

% include the following m-function subroutines
% scriptA.m with diffacota2.m, diffatan2a.m.
% nusolve.m with digamma.m, psin.m.
% gammaratio.m.

clear all;

calctime=cputime;       % calculation time for whole code

%=================================================================
% parameters
%=================================================================

%-----------------------------------------------------------------
% trap separation list
dzlist = 0:0.025:5;
```

```
dzlen = length(dzlist)

%-------------------------------------------------------------------
% scattering length list
a0list0 = 0.05:0.05:2; a0list1 = 2.5:0.5:10; a0list2 = 20:10:100;
a0list=-[a0list0 a0list1 a0list2];
a0len = length(a0list)

%-------------------------------------------------------------------
% max. partial wave (actual number of allowed VALUES is Ll+1)
Ll = 180;
% max. radial wave (actual number of allowed VALUES is Nn+1)
Nn = 180;
% max. number of eigenvalues to compute for each a0, dz
max_eig = 8;

%-------------------------------------------------------------------
% allocate memory for matrix elements lists
numeig = zeros(dzlen, a0len, max_eig);
sqerreig = zeros(dzlen, a0len, max_eig);
lenzlist=Ll*(3*Nn+2)+ Nn*(Nn+1) + 1;
nzlist=zeros(5,lenzlist);

%===================================================================
% outer loop over trap separation given in dzlist
%===================================================================

k = 0;
```

```
for dz = dzlist
    k = k+1;
    col = 0;

    %================================================================
    % sparse matrix elements
    %================================================================

    % nzlist: create lists of non-zero elements in the form
    % [l; lp; n; np; element].
    %
    % The matrix is symmetric: We need to calculate only off-diagonal
    % elements on one side of the diagonal and symmetrize later.
    %
    % n_nu is the Busch solution index, which is the "analog" of n,
    % such that nu(n_nu+1) -> n, when a0 -> 0-.

    % The following calculation of matrix elements is separated into
    % two parts, since only the l=0 matrix elements depend on the
    % scattering length:
    %
    % 1) regular l>=1 matrix elements  (outside a0-loop)
    % 2) irregular l=0 matrix elements  (inside a0-loop)

    %----------------------------------------------------------------
    % regular matrix elements for l>=1
    %----------------------------------------------------------------
```

```
% Notation: We use j instead of l in the following:
%
% Note: the vectors jn and nj are of the form with n and j:
% nj=(1_1 ... 1_j ... 1_Ll 2_1 ... 2_Ll ...
% n_1 ... n_j ... n_Ll ... Nn_1 ... Nn_Ll).
%
% Example: Nn=1, Ll=3
%
% jlist = (1 2 3)
% nlist = (0 1)
%
% nj = (0 1 0 1 0 1)
% jn = (1 1 2 2 3 3)
%
% E = 2"n" + "j" + 3/2 = 2.*nj + jn + 3/2
% E = (1 3 2 4 3 5) + 3/2
% simply replace n -> nj and j -> jn in equations

%-----------------------------------------------------------------
% diagonal matrix elements (l>=1): SHO solutions

% < n j | n j >
col = (Nn+1)*(Ll); % col: counter for matrix element list
jlist=1:1:Ll;
nlist=0:1:Nn;
jn=reshape((jlist'*ones(1,length(nlist)))',1,...
   length(nlist)*length(jlist));
```

```
nj=reshape(nlist'*ones(1,length(jlist)),1,...
   length(nlist)*length(jlist));
nzlist(1,1:col)=jn;
nzlist(2,1:col)=jn;
nzlist(3,1:col)=nj;
nzlist(4,1:col)=nj;
nzlist(5,1:col)=(2*nj + jn + 3/2) + 1/2*dz^2;
col = (Nn+1)*(Ll);

%-----------------------------------------------------------------
% off-diagonal matrix elements (l>=1) due to separation

% < n j | n j-1 >
colbefore = col;
col = (Nn+1)*(Ll-1) + colbefore;
jlist=2:1:Ll;
%nlist=0:1:Nn; % not necessary (same definition as before)
jn=reshape((jlist'*ones(1,length(nlist)))',1,...
   length(nlist)*length(jlist));
nj=reshape(nlist'*ones(1,length(jlist)),1,...
   length(nlist)*length(jlist));
nzlist(1,colbefore+1:col)=jn;
nzlist(2,colbefore+1:col)=jn-1;
nzlist(3,colbefore+1:col)=nj;
nzlist(4,colbefore+1:col)=nj;
nzlist(5,colbefore+1:col)=-dz*jn.*sqrt((2*nj+2*jn+1)./...
   (2*(2*jn-1).*(2*jn+1)));
```

```
% < n j | n+1 j-1 >
colbefore = col;
col = Nn*(Ll-1) + colbefore;
%jlist=2:1:Ll; % not necessary (same definition as before)
nlist=0:1:Nn-1;
jn=reshape((jlist'*ones(1,length(nlist)))',1,...
   length(nlist)*length(jlist));
nj=reshape(nlist'*ones(1,length(jlist)),1,...
   length(nlist)*length(jlist));
nzlist(1,colbefore+1:col)=jn;
nzlist(2,colbefore+1:col)=jn-1;
nzlist(3,colbefore+1:col)=nj;
nzlist(4,colbefore+1:col)=nj+1;
nzlist(5,colbefore+1:col)=dz*jn.*sqrt((nj+1)./...
   ((2*jn-1).*(2*jn+1)));

mark_col = col; % value for starting each nzlist in loop below



%=================================================================
% inner loop over scattering length
%=================================================================

kk = 0;
for a0 = a0list
    a0
    kk = kk + 1;
```

```
%-------------------------------------------------------------
% irregular matrix elements for l=0
%-------------------------------------------------------------

% calculate lowest (Nn+1) eigenvalues with n_nu=0:Nn
nu = nusolve(Nn+1, a0);
% normalization coefficient for wave functions
scrA = scriptA(nu, a0);
% counter for nzlist
col = mark_col;

% matrix elements involving l = 0, pseudopotential solutions

for n_nu = 0:Nn
  col = col+1;
  % diagonal elements
  nzlist(:,col) = ...
     [0; 0; n_nu; n_nu; 2*nu(n_nu+1) + 3/2+1/2*dz^2];
  % off-diagonal
  for n = 0:Nn
    col = col+1;
    if (n<150)
      nzlist(:,col) = [0; 1; n_nu; n; ...
         sqrt(2/(3*pi))*sign(a0)*dz*scrA(n_nu+1)* ...
         sqrt(gamma(n+5/2)/gamma(n+1)).* ...
         (1/(n-nu(n_nu+1))-1/(n+1-nu(n_nu+1)))];
    else
      nzlist(:,col) = [0; 1; n_nu; n; ...
```

```
            sqrt(2/(3*pi))*sign(a0)*dz*scrA(n_nu+1)* ...
            sqrt(gammaratio(n,5/2,1)).* ...
            (1/(n-nu(n_nu+1))-1/(n+1-nu(n_nu+1)))];
        end % if
      end % n
    end % n_nu

    %------------------------------------------------------------
    % construction of sparse matrix
    %------------------------------------------------------------

    % convert lists to numerical index notation
    nz_len =length(nzlist)
    rowS = nzlist(3,:)*(Ll+1) + nzlist(1,:) + 1;
    colS = nzlist(4,:)*(Ll+1) + nzlist(2,:) + 1;
    elS  = nzlist(5,:);

    % sparse matrix construction from list
    S = sparse(rowS,colS,elS);
    % symmetrize (not all off-diagonal elements were calculated)
    S = S + S' - diag(diag(S));

    %------------------------------------------------------------
    % numerical diagonalization
    %------------------------------------------------------------

    opts.tol = 1E-6;
    try
```

```
        [V, E, flag] = eigs(S, max_eig, 'sa', opts);
        catch % in case of numerical errors during symmetrization
        thisw=error
        S = (S+S')/2;
        [V, E, flag] = eigs(S, max_eig, 'sa', opts);
        end

        numeig(k,kk,:) = diag(E)';

        % calculation of errorbars
        % disp('the squared errors in the eigenvalues are')
        sqerreig(k,kk,:) = sum((S*V)'*(S*V))-diag(E^2)';

        % save inside loop in case of catastrophy
        save(['energy_N',num2str(Nn),'_l',num2str(Ll)], ...
             'Ll','Nn', 'dzlist', 'a0list', 'numeig', 'sqerreig')

end % a0 loop

%=====================================================================
% outer loop over trap separation: end of loop
%=====================================================================

end % dz loop

%=====================================================================
% final saving of data
%=====================================================================
```

```
save(['energy_complete',num2str(Nn),'_l',num2str(Ll)], ...
'Ll','Nn', 'dzlist', 'a0list', 'numeig', 'sqerreig')

calctime=cputime-calctime           % calculation time output
```

C.1.2 Subroutines

nusolve.m

```
function nu = nusolve(nmax, a0)

% This function defines an accurate function to solve for eigenvalues
% of nu for atoms in an isotropic harmonic trap with pseudopotential
% interaction. In this case, nmax is the number of solutions,
% including the bound state, which exists only for positive a.

% To get all the states, classify searches for zeros:
%
%       |   a > 0           |   a < 0           |
%       |   (bound state) & |   (no bound state)|
%-------+-------------------+-------------------+
%       |                   |                   |
% |a|>1 | use cot fn. in    |   use cot fn. in  |
%       | [0,1],[1,2],..    |   [-1,0],[0,1],.. |
%       |                   |                   |
%-------+-------------------+-------------------+
%       |                   |                   |
% |a|<1 | use tan fn. in    |   use tan fn. in  |
%       | [-1/2, 1/2],..    |   [-1/2, 1/2],..  |
%-------+-------------------+-------------------+
fzopts = optimset('fzero');
eps = 1E-08;
boundst = 0; % number of bound states; can only be 0 or 1
if a0>0
```

```
   boundst = 1;
   % find bound state
   if abs(a0) < 1
      nu(1) = fzero(@diffatan2a, [-2/a0^2 -0.5-eps], fzopts, a0);
   else
      nu(1) = fzero(@diffacota2, [-1 -0.5/a0^2], fzopts, a0);
   end
end
for n = 1:1:nmax-boundst
    % Use this as first guess to MATLAB's zero finder
    % Avoid going outside the interval n-1/2: n+1/2
    % by using 1/a instead when |a| > 1.
    if abs(a0) < 1
       nu(n+boundst) = ...
          fzero(@diffatan2a, [n-3/2+eps n-1/2-eps], fzopts, a0);
    else
       nu(n+boundst) = ...
          fzero(@diffacota2, [n-2+boundst+eps n-1+boundst-eps], ...
          fzopts, a0);
    end
end
```

diffatan2a.m

```
function y = diffatan2a(nu,a0)

% This function is needed for the subroutine nusolve.m.

i_asy = find(nu <-160); % use negative asymptotic form
i_neg = find((-160 <= nu) & (nu < 0.5));
i_pos = find((165 >= nu) &( nu >= 0.5));
i_big = find(nu > 165); % use positive asymptotic form

nu_asy = nu(i_asy);
nu_neg = nu(i_neg);
nu_pos = nu(i_pos);
nu_big = nu(i_big);

y(i_asy) = atan(1./sqrt(-nu_asy).*(1 - 3./(8*nu_asy) + ...
   75./(384*nu_asy.^2)))- atan(2*a0);
y(i_neg) = atan(gamma(-nu_neg-1/2)./gamma(-nu_neg)) - atan(2*a0);
y(i_pos) = atan(tan(pi*nu_pos).*...
    gamma(nu_pos + 1)./gamma(nu_pos + 3/2)) - atan(2*a0);
y(i_big) = atan(nu_big.^(-1/2).*(1 - 3./(8*nu_big) + ...
   75./(384*nu_big.^2)).*tan(pi*nu_big)) - atan(2*a0);

% cf. M. Abramowitz and I. A. Stegun, "Handbook of mathematical
% functions", Dover, New York (1972): p. 257, equation 6.1.47
```

diffacota2.m

```
function y = diffacota2(nu,a0)

% This function is needed for the subroutine nusolve.m.

i_neg = find(nu < -0.5);
i_pos = find((165 >=nu) & (nu >= -0.5));

i_big = find(nu > 165); % start asymptotic region (gamma(172) = NaN)

nu_neg = nu(i_neg);
nu_pos = nu(i_pos);
nu_big = nu(i_big);

y(i_pos) = atan(1./tan(pi*nu_pos).*gamma(nu_pos+3/2)./...
   gamma(nu_pos + 1))- atan(1/(2*a0));
y(i_neg) = atan(gamma(-nu_neg)./gamma(-nu_neg-1/2)) - atan(1/(2*a0));
y(i_big) = atan(sqrt(nu_big).*(1 + 3./(8*nu_big) - ...
   21./(384*nu_big.^2))./tan(pi*nu_big)) - atan(1/(2*a0));

% cf. M. Abramowitz and I. A. Stegun, "Handbook of mathematical
% functions", Dover, New York (1972): p. 257, equation 6.1.47
```

scriptA.m

```
function A = scriptA(nu,a0)

% This function calculates the normalization coefficient of the
% spherical hypergeometric "Busch-basis" l=0 wave functions.

i_neg = find(nu < 0);
i_pos = find(nu >= 0);

if ~isempty(i_pos)
   Psi1 = digamma(nu(i_pos)+1);
   Psi3_2 = digamma(nu(i_pos) + 1.5);
   A(i_pos) = sqrt(a0./((pi./(sin(pi.*nu(i_pos)).* ...
      cos(pi.*nu(i_pos)))) + Psi1 - Psi3_2));
end
if ~isempty(i_neg)
   Psin = digamma(-nu(i_neg));
   Psinm1_2 = digamma(-nu(i_neg) - 0.5);
   A(i_neg) = sqrt(a0./(Psin - Psinm1_2));
end
```

gammaratio.m

```
function f = gammaratio(z, a, b);

% This function computes the ratio gamma(nu+a)/gamma(nu+b) for large
% values of z using the asymptotic expansion 6.1.47 of
% Abramowitz & Stegun and further terms (cf. Olver Asymptotics and
% Special functions).
% nu may be a matrix but a & b are numbers. The expansion is good
% when z >> |a|,|b|. The error scales as a-b.
% Error < 10^-8 for a = 1.5, b = 0, z = 100.

d = a-b;

f = z.^d.*(1 + d.*(a+b-1)/2./z + d*(d - 1)*(2+a*(-7+3*a) - ...
    5*b+6*a*b+3*b^2)/ 24./z.^2 + ...
    d*(d-1)*(d-2)*(a+b-1)*(a^2 + (-1+b)*b+a*(-3+2*b))/48./z.^3);
```

digamma.m

```
function dg = digamma(x)

% This function evaluates the digamma function for
% positive and negative arguments.

indxn=find(x<0);
indxp=find(x>=0);
if ~isempty(indxn)
dgn = psin(x(indxn));
dgp = psi(x(indxp));
dg = [dgn dgp];
else
dg = psi(x);
end
```

psin.m

```
function pn = psin(x)

% This function evaluates the "psi" function (digamma function)
% for negative arguments.

pn = psi(1-x) + pi*cot(pi*(1-x));
```

C.2 Separated and anisotropic traps with δ interactions

Following Section 4.6, the relative coordinate Hamiltonian in the anisotropic case is given by

$$\hat{H}_{\rm rel} = \frac{\hat{\mathbf{p}}_r^2}{2\mu} + \frac{1}{2}\mu\omega^2 r^2\left(1 - \Lambda\sqrt{\frac{16\pi}{5}}Y_{20}\right) - \mu\omega_z^2\Delta z r\sqrt{\frac{4\pi}{3}}Y_{10} + \frac{1}{2}\mu\omega_z^2\Delta z^2 + \frac{2\pi\hbar^2}{\mu}a_{\rm eff}(E_K)\delta(\mathbf{r})\frac{\partial}{\partial r}r\,. \quad \text{(C.5)}$$

Here, the "mean" frequency ω is defined by

$$\omega^2 = \left(\frac{2}{3}\omega_\perp^2 + \frac{1}{3}\omega_z^2\right), \quad \text{(C.6)}$$

and the anisotropy parameter Λ is

$$\Lambda = \frac{\omega_z^2 - \omega_\perp^2}{3\omega^2} = \frac{\omega_z^2 - \omega_\perp^2}{2\omega_\perp^2 + \omega_z^2}\,. \quad \text{(C.7)}$$

We represent the relative coordinate Hamiltonian in the same spherical basis as in the isotropic case. As before, the Δz separation term couples partial waves with $l - l' = 0, \pm 1$. The Λ anisotropic term couples partial waves with $l - l' = 0, \pm 2$. The additional matrix elements due to the anisotropy are given by Eq. (4.24) and (4.27) as

$$\langle nl|\, r^2\, |n, l+2\rangle = \frac{1}{2}\sqrt{(2n+2l+3)(2n+2l+5)}\,, \quad \text{(C.8)}$$

$$\langle n+1, l|\, r^2\, |n, l+2\rangle = -\sqrt{2(n+1)(2n+2l+5)}\,, \quad \text{(C.9)}$$

$$\langle n+2, l|\, r^2\, |n, l+2\rangle = \sqrt{(n+1)(n+2)} \quad \text{(C.10)}$$

for $l \leq 1$; and

$$\langle n, 2|\, r^2\, |\nu, 0\rangle = a_\nu\sqrt{\frac{\partial\nu_n}{\partial a}}\sqrt{\frac{2\Gamma(n+\frac{7}{2})}{\pi\Gamma(n+1)}}\left(\frac{1}{n-\nu_n} - \frac{2}{n+1-\nu_n} + \frac{1}{n+2-\nu_n}\right) \quad \text{(C.11)}$$

for the special case involving the irregular $l = 0$ functions. The main program "separd_aniso_trap_delta.m" constructs the resulting sparse Hamiltonian matrix, which is then diagonalized for each trap separation Δz using the same routines as in the isotropic case.

C.2.1 Main program

separd_aniso_trap_delta.m

```
%-----------------------------------------------------------------------
% Main Program: separd_aniso_trap_delta.m
%-----------------------------------------------------------------------
%
% Created by ERIC E. BOLDA and RENE STOCK
% NIST, Gaithersburg and UNM, Albuquerque
%
% based on codes by ERIC E. BOLDA:   May, 2002
%
% created by RENE STOCK:  August, 2003
%
% last modified: April, 2005
%
% This is the main program for determining the eigenenergies of
% two atoms interacting through an s-wave pseudopotential in
% SEPARATED ISOTROPIC harmonic traps. The Hamiltonian
% is expressed in the spherical hypergeometric "Busch-basis"
% for l=0 and the regular spherical Laguerre harmonic oscillator
% basis for l>0. The resulting tri-diagonal matrix is then
```

```
% diagonalized using the Matlab sparse matrix routine for finding
% the lowest matrix eigenvalues.
%
% The code includes a loop over both the scattering length and the
% trap separation. The calculated energy spectra (energy vs. trap
% separation for a list of scattering lengths) provides a template
% for the calculation of the self-consistent energy spectra using an
% energy-dependent scattering length, calculated for the realistic
% interaction.
%
% Note: This code only calculates m=0 levels, since only m=0
% levels are affected by the delta interaction.
%
% Note about scaling: In the main diagonalization routine
% energies are scaled to E = hbar omega,
% lengths are scaled to r0 = sqrt(hbar/(mu*omega)).
%
% In the anisotropic case omega means the mean trap frequency omega
% as defined below. Note that even the trap separation and scattering
% length are scaled to r0 defined by the mean trap frequency omega.
%-----------------------------------------------------------------------

% include the following m-function subroutines
% scriptA.m with diffacota2.m, diffatan2a.m.
% nusolve.m with digamma.m, psin.m.
% gammaratio.m.

clear all;
```

```
calctime=cputime;       % calculation time for whole code

%=====================================================================
% parameters
%=====================================================================

%---------------------------------------------------------------------
% trap separation list
dzlist = 0:0.025:5;                  % measured in r_0
dzlen = length(dzlist)

%---------------------------------------------------------------------
% scattering length list
a0list0 = 0.05:0.05:2; a0list1 = 2.5:0.5:10; a0list2 = 20:10:100;
a0list=-[a0list0 a0list1 a0list2];  % measured in r_0
a0len = length(a0list)

%---------------------------------------------------------------------
% trap anisotropy:
% trap frequencies of atoms in the same well
omega_perp = 1;
omega_z_list = 4;
omlen = length(omega_z_list)

%---------------------------------------------------------------------
% max. partial wave (actual number of allowed VALUES is Ll+1)
Ll = 300;
```

```
% max. radial wave (actual number of allowed VALUES is Nn+1)
Nn = 100;
% max. number of eigenvalues to compute for each a0, dz
max_eig = 8;

%-------------------------------------------------------------------
% allocate memory for matrix elements lists
numeig = zeros(dzlen, a0len, omlen, max_eig);
sqerreig = zeros(dzlen, a0len, omlen, max_eig);
lenzlist=Ll*(7*Nn+2)+ Nn*(2*Nn-3) + 2;
nzlist=zeros(5,lenzlist);

%===================================================================
% outer loop over anisotropy given by omega_z_list
%===================================================================

kkk=0;

for omega_z = omega_z_list
    omega_z
    kkk = kkk+1;

% aspect ratio = omega_z/omega_perp
A = omega_z /omega_perp;
% coefficient of potential anisotropy
C = (A^2 -1) /(A^2 +2);
% actual trap frequencies are related to C
omega = omega_perp/sqrt(1-C);
```

```
%=====================================================================
% middle loop over trap separation given in dzlist
%=====================================================================

k = 0;

for dz = dzlist
    dz
    k = k+1;
    col = 0;

    %=================================================================
    % sparse matrix elements
    %=================================================================

    % nzlist: create lists of non-zero elements in the form
    % [l; lp; n; np; element].
    %
    % The matrix is symmetric: We need to calculate only off-diagonal
    % elements on one side of the diagonal and symmetrize later.
    %
    % n_nu is the Busch solution index, which is the "analog" of n,
    % such that nu(n_nu+1) -> n, when a0 -> 0-.

    % The following calculation of matrix elements is separated into
    % two parts, since only the l=0 matrix elements depend on the
    % scattering length:
```

```
%
% 1) regular l>=1 matrix elements  (outside a0-loop)
% 2) irregular l=0 matrix elements  (inside a0-loop)

%-----------------------------------------------------------------
% regular matrix elements for l>=1
%-----------------------------------------------------------------

% Notation: We use j instead of l in the following:
%
% Note: the vectors jn and nj are of the form with n and j:
% nj=(1_1 ... 1_j ... 1_Ll 2_1 ... 2_Ll ...
% n_1 ... n_j ... n_Ll ... Nn_1 ... Nn_Ll).
%
% Example: Nn=1, Ll=3
%
% jlist = (1 2 3)
% nlist = (0 1)
%
% nj = (0 1 0 1 0 1)
% jn = (1 1 2 2 3 3)
%
% E = 2"n" + "j" + 3/2 = 2.*nj + jn + 3/2
% E = (1 3 2 4 3 5) + 3/2
% simply replace n -> nj and j -> jn in equations

%-----------------------------------------------------------------
% diagonal matrix elements (l>=1): SHO solutions
```

```
% < n j | n j >
col = (Nn+1)*(Ll); % col: counter for matrix element list
jlist=1:1:Ll;
nlist=0:1:Nn;
jn=reshape((jlist'*ones(1,length(nlist)))',1, ...
   length(nlist)*length(jlist));
nj=reshape(nlist'*ones(1,length(jlist)),1, ...
   length(nlist)*length(jlist));
nzlist(1,1:col)=jn;
nzlist(2,1:col)=jn;
nzlist(3,1:col)=nj;
nzlist(4,1:col)=nj;
nzlist(5,1:col)=(2*nj + jn + 3/2) +  C*jn.*(jn+1)./ ...
   ((2*jn-1).*(2*jn+3)).*(2*nj+jn+3/2) + ...
   1/2*(omega_z/omega)^2*dz^2;
col = (Nn+1)*(Ll);

%-----------------------------------------------------------------
% off-diagonal matrix elements (l>=1) due to anisotropy

% < n j | n-1 j >
colbefore = col;
col = Nn*Ll + colbefore;
%jlist=1:1:Ll; % not necessary (same definition as before)
nlist=1:1:Nn;
jn=reshape((jlist'*ones(1,length(nlist)))',1, ...
   length(nlist)*length(jlist));
```

```
nj=reshape(nlist'*ones(1,length(jlist)),1, ...
   length(nlist)*length(jlist));
nzlist(1,colbefore+1:col)=jn;
nzlist(2,colbefore+1:col)=jn;
nzlist(3,colbefore+1:col)=nj;
nzlist(4,colbefore+1:col)=nj-1;
nzlist(5,colbefore+1:col)=- C*jn.*(jn+1)./ ...
   ((2*jn-1).*(2*jn+3)).* sqrt(nj.*(nj+jn+1/2));

% < n j | n j-2 >
colbefore = col;
col = (Nn+1)*(Ll-2) + colbefore;
jlist=3:1:Ll;
nlist=0:1:Nn;
jn=reshape((jlist'*ones(1,length(nlist)))',1, ...
   length(nlist)*length(jlist));
nj=reshape(nlist'*ones(1,length(jlist)),1, ...
   length(nlist)*length(jlist));
nzlist(1,colbefore+1:col)=jn;
nzlist(2,colbefore+1:col)=jn-2;
nzlist(3,colbefore+1:col)=nj;
nzlist(4,colbefore+1:col)=nj;
nzlist(5,colbefore+1:col)=C*3*jn.*(jn-1)./ ...
   (2*(2*jn-1).*sqrt((2*jn-3).*(2*jn+1))).* ...
   1/2.*sqrt((2*nj+2.*jn-1).*(2*nj+2*jn+1));

% < n j | n+1 j-2 >
colbefore = col;
```

```
col = (Nn)*(Ll-2) + colbefore;
%jlist=3:1:Ll; % not necessary (same definition as before)
nlist=0:1:Nn-1;
jn=reshape((jlist'*ones(1,length(nlist)))',1, ...
   length(nlist)*length(jlist));
nj=reshape(nlist'*ones(1,length(jlist)),1, ...
   length(nlist)*length(jlist));
nzlist(1,colbefore+1:col)=jn;
nzlist(2,colbefore+1:col)=jn-2;
nzlist(3,colbefore+1:col)=nj;
nzlist(4,colbefore+1:col)=nj+1;
nzlist(5,colbefore+1:col)=- C*3*jn.*(jn-1)./(2*(2*jn-1).* ...
   sqrt((2*jn-3).*(2*jn+1))).* ...
   sqrt(2*(nj+1).*(2*nj+2*jn+1));

% < n j | n+2 j-2 >
colbefore = col;
col = (Nn-1)*(Ll-2) + colbefore;
%jlist=3:1:Ll; % not necessary (same definition as before)
nlist=0:1:Nn-2;
jn=reshape((jlist'*ones(1,length(nlist)))',1, ...
   length(nlist)*length(jlist));
nj=reshape(nlist'*ones(1,length(jlist)),1, ...
   length(nlist)*length(jlist));
nzlist(1,colbefore+1:col)=jn;
nzlist(2,colbefore+1:col)=jn-2;
nzlist(3,colbefore+1:col)=nj;
nzlist(4,colbefore+1:col)=nj+2;
```

```
nzlist(5,colbefore+1:col)=C*3*jn.*(jn-1)./(2*(2*jn-1).* ...
   sqrt((2*jn-3).*(2*jn+1))).*sqrt((nj+1).*(nj+2));

%-----------------------------------------------------------------
% off-diagonal matrix elements (l>=1) due to separation

% < n j | n j-1 >
colbefore = col;
col = (Nn+1)*(Ll-1) + colbefore;
jlist=2:1:Ll;
nlist=0:1:Nn;
jn=reshape((jlist'*ones(1,length(nlist)))',1, ...
   length(nlist)*length(jlist));
nj=reshape(nlist'*ones(1,length(jlist)),1, ...
   length(nlist)*length(jlist));
nzlist(1,colbefore+1:col)=jn;
nzlist(2,colbefore+1:col)=jn-1;
nzlist(3,colbefore+1:col)=nj;
nzlist(4,colbefore+1:col)=nj;
nzlist(5,colbefore+1:col)=-(omega_z/omega)^2*dz*jn.* ...
   sqrt((2*nj+2*jn+1)./(2*(2*jn-1).*(2*jn+1)));

% < n j | n+1 j-1 >
colbefore = col;
col = Nn*(Ll-1) + colbefore;
%jlist=2:1:Ll; % not necessary (same definition as before)
nlist=0:1:Nn-1;
jn=reshape((jlist'*ones(1,length(nlist)))',1, ...
```

```
   length(nlist)*length(jlist));
nj=reshape(nlist'*ones(1,length(jlist)),1, ...
   length(nlist)*length(jlist));
nzlist(1,colbefore+1:col)=jn;
nzlist(2,colbefore+1:col)=jn-1;
nzlist(3,colbefore+1:col)=nj;
nzlist(4,colbefore+1:col)=nj+1;
nzlist(5,colbefore+1:col)=(omega_z/omega)^2*dz*jn.* ...
   sqrt((nj+1)./((2*jn-1).*(2*jn+1)));

mark_col = col; % value for starting each nzlist in loop below


%================================================================
% inner loop over scattering length
%================================================================

kk = 0;
for a0 = a0list
    a0
    kk = kk + 1;

    %---------------------------------------------------------
    % irregular matrix elements for l=0
    %---------------------------------------------------------

    % calculate lowest (Nn+1) eigenvalues with n_nu=0:Nn
    nu = nusolve(Nn+1, a0);
```

```
% normalization coefficient for wave functions
scrA = scriptA(nu, a0);
% counter for nzlist
col = mark_col;

% matrix elements involving l = 0, pseudopotential solutions
for n_nu = 0:Nn
  col = col+1;
  % diagonal elements
  nzlist(:,col) = [0; 0; n_nu; n_nu; ...
     2*nu(n_nu+1) + 3/2 + 1/2*(omega_z/omega)^2*dz^2];
  % off-diagonal elements due to separation
  for n = 0:Nn
    col = col+1;
    if (n<150)
      nzlist(:,col) = [0; 1; n_nu; n; ...
         sqrt(2/(3*pi))*sign(a0)*(omega_z/omega)^2*dz* ...
         scrA(n_nu+1)* sqrt(gamma(n+5/2)/gamma(n+1)).* ...
         (1/(n-nu(n_nu+1))-1/(n+1-nu(n_nu+1)))];
    else
      nzlist(:,col) = [0; 1; n_nu; n; ...
         sqrt(2/(3*pi))*sign(a0)*(omega_z/omega)^2*dz* ...
         scrA(n_nu+1)* sqrt(gammaratio(n,5/2,1)).* ...
         (1/(n-nu(n_nu+1))-1/(n+1-nu(n_nu+1)))];
    end % if
  end % n
  % off-diagonal elements due to anisotropy
  % matrixelements=10
```

```
  for n = 0:Nn
    col = col+1;
    if (n<150)
      nzlist(:,col) = [0; 2; n_nu; n; ...
         -sqrt(2/(5*pi))* sign(a0)*C*scrA(n_nu+1)* ...
         sqrt(gamma(n+7/2)/gamma(n+1))*(1/(n-nu(n_nu+1)) ...
         -2/(n+1-nu(n_nu+1))+ 1/(n+2-nu(n_nu+1)))];
    else
      nzlist(:,col) = [0; 2; n_nu; n; ...
         -sqrt(2/(5*pi))* sign(a0)*C*scrA(n_nu+1)* ...
         sqrt(gammaratio(n,7/2,1))*(1/(n-nu(n_nu+1))  ...
         - 2/(n+1-nu(n_nu+1))+ 1/(n+2-nu(n_nu+1)))];
    end %if
  end % n
end % n_nu

%-------------------------------------------------------------
% construction of sparse matrix
%-------------------------------------------------------------

% convert lists to numerical index notation
nz_len =length(nzlist);
rowS = nzlist(3,:)*(Ll+1) + nzlist(1,:) + 1;
colS = nzlist(4,:)*(Ll+1) + nzlist(2,:) + 1;
elS  = nzlist(5,:);

% sparse matrix construction
S = sparse(rowS,colS,elS);
```

```
        % symmetrize (not all off-diagonal elements were calculated)
        S = S + S' - diag(diag(S));
        S = (S+S')/2;

        %------------------------------------------------------------
        % numerical diagonalization
        %------------------------------------------------------------

        opts.tol = 1E-6;
        opts.disp = 0;
        try
        [V, E, flag] = eigs(S, max_eig, 'sa', opts);
        catch % in case of numerical errors during symmetrization
        thisw=error
        S = (S+S')/2;
        [V, E, flag] = eigs(S, max_eig, 'sa', opts);
        end

        numeig(k,kk,kkk,:) = diag(E)';

        % calculation of errorbars
        % disp('the squared errors in the eigenvalues are')
        sqerreig(k,kk,kkk,:) = sum((S*V)'*(S*V))-diag(E^2)';

        % save inside loop in case of catastrophy
save(['energy_aniso_N',num2str(Nn),'_L',num2str(Ll)], ...
             'Ll','Nn','omega_perp','omega_z_list','dzlist', ...
             'a0list','numeig','sqerreig')
```

```
end % a0 loop

%=====================================================================
% middle loop over trap separation: end of loop
%=====================================================================

end % dz loop

%=====================================================================
% outer loop over anisotropy: end of loop
%=====================================================================

end % omega_z loop


%=====================================================================
% final saving of data
%=====================================================================

save(['energy_aniso_complete_N',num2str(Nn),'_L',num2str(Ll)], ...
      'Ll','Nn','omega_perp','omega_z_list','dzlist','a0list', ...
      'numeig','sqerreig')

calctime=cputime-calctime           % calculation time output
```

C.2.2 Subroutines

"separd_aniso_trap_delta.m" uses the subroutines listed in Section C.1.2.

C.3 Self-consistent calculation of energy spectra

The main programs discussed in Section C.1 and C.2 provide a template, $E(a)$, for the calculation of the self-consistent energy spectra. The following program, "energydep_spectrum.m", uses this template and the energy-dependent scattering length, $a(E)$, that has been calculated for the channel of interest using the multichannel close coupling codes described in Appendix D. The self-consistent eigenvalues are then calculated at each separation, Δz, by finding the intersections of the two curves $a(E)$ and $E(a)$.

C.3.1 Main program

energydep_spectrum.m

```
%-----------------------------------------------------------------------
%
% Created by RENE STOCK: December, 2002
%
% last modified: April, 2005
%
% This code calculates the self-consistent energy spectrum using the
% energy-dependent scattering length calculated for Cs and the
% eigenspectra (energy vs. trap separation) template that has been
% calculated for a range of scattering lengths in the program
% "separd_trap_delta"

% The scattering length and energy as calculated from the NIST close
% coupling codes are scaled in Bohr radii and muK, and need to be
```

```
% converted to harmonic oscillator units. The scattering length is
% loaded into the main program and scaled in the subroutine
% "edependenta.m". Then, at each separation, the intersections of the
% two curves a(E) and E(a), which determine the self-consistent
% eigenvalues, are found.
%
%-----------------------------------------------------------------------

% include the following m-function subroutine: edependenta.m.

clear

calctime=cputime;

%-----------------------------------------------------------------------
% general parameters
%-----------------------------------------------------------------------

% energy scales: recoil energy ER, temp. units in muK
% muK to ER conversion; hbar omega to ER
en_muK=1;
a_bohr=1;
en_ER=0.09915*en_muK;
nm=1./(5.29177249*10^(-2));

% optical lattice parameters (in harmonic approximation)
eta=0.25;                   % Lamb-Dicke parameter
en_osc=en_ER./(eta.^2);     % harmonic oscillator frequency in ER
```

```
z0=eta./(2*pi./(852*nm));   % harmonic oscillator width

% energyscales for scattering length calculation
enscale = en_osc;           % harmonic oscillator frequency
z0scale = z0.*2;            % characteristic length scale

% max. number of eigenvalues to compute for each a0, dz
max_eig = 2;

%-----------------------------------------------------------------------
% precalculated energy spectra for scattering lengths/separation
%-----------------------------------------------------------------------

load energy_dz=0_5_a=0_100.mat         % load data file
[aminmat,aminindex] = min(a0list);     % lowest a calculated
[amaxmat,amaxindex] = max(a0list);     % largest a calculated

%-----------------------------------------------------------------------
% loop over trap separation dz
%-----------------------------------------------------------------------

% shorten dzlist since we are only interested in dz<3
dz3=find(dzlist==3);
dzlist=dzlist(1:dz3);
% allocate memory
eigen=zeros(length(dzlist),max_eig);

% loop
```

```
for dzindex=1:length(dzlist)

    dz=dzlist(dzindex)

    %-------------------------------------------------------------
    % loop over number of eigenvalues to be calculated
    %-------------------------------------------------------------

    for k=1:max_eig         % number of energy eigenvalues calculated

        %-------------------------------------------------------------
        % scattering length evaluated for energy around eigenvalues

        % set de
        de=0.0001;
        % set emin
        if dz<2.5
           emin=floor(min(numeig(dzindex,:,k))/de)*de-2*de;
           if emin<-1
              emin=-1;
           else
           end
        else
           % emin for larger dz should be bigger than one
           emin=floor(min(numeig(dzindex,:,k))/de)*de-2*de;
           if emin<1
              emin=1;
           else
```

```
   end
end
% set emax
emax=ceil(max(numeig(dzindex,:,k))/de)*de+10*de;
energy=emin:de:emax;

% scattering length calculation for 133Cs
a = edependenta(energy-(dz^2)/2,enscale,z0scale);

%-------------------------------------------------------------
% interpolation of scattering length calculation

% a vector
da=0.0001;
amin=min(ceil(min(a)/da)*da);
amax=floor(max(a)/da)*da;
if amax > amaxmat
   error_atoobig=amax
   amax = amaxmat;
else
end
avec=amin:da:amax;

% interpolate energy spectra
edata=interp1(a0list,numeig(dzindex,:,k),avec,'linear');
% interpolate energy dep scattering length
escatt=interp1(a,energy,avec);
```

```
        %-------------------------------------------------------------
        % find root of escatt-edata == 0

        equation=escatt-edata;
        le=length(equation);
        % multiply each value by adjacent value: this multiplication
        % is only negative around zero!
        eq=equation(1:le-1).*equation(2:le);
        eqdiff=abs(equation(1:le-1)-equation(2:le));
        % condition for zero's without singularities
        j=find(eq<0 & eqdiff< max(equation));
        % root of equation (interpolated)
        aroot=-(avec(j+1)-avec(j))./(equation(j+1)-equation(j)).*...
              equation(j) + avec(j);

        % selfconsistent eigenvalue
        eigenval(k)=interp1(avec,edata,aroot,'linear');

    end % k

    eigen(dzindex,1:k)=eigenval;

end % dzindex

%-----------------------------------------------------------------------
% save and plot
%-----------------------------------------------------------------------
```

```
save(['eigenspectrum_Cs133_eta',num2str(eta),],'dzlist', 'eigen')

plot(dzlist,eigen(:,1),'b',dzlist,eigen(:,2),'b','Linewidth',2)
set(gca,'FontSize',24)
axis([0 3 -0.1 2.6])
```

C.3.2 Subroutines

edependenta.m

```
function a = edependenta(e,enscale,z0scale)

% This function loads the realistic energy-dependent scattering
% length for the scattering channel in question, which has been
% calculated using the NIST close-coupling code. The scattering
% length and energy as calculated from the codes are scaled in
% Bohr radii and muK, and need to be converted to harmonic
% oscillator units as given by the scales "enscale" and "z0scale."
% The energy vector "e" gives the energies for which the
% scattering length has to be calculated (via interpolation).

% load scattering length
load scattlength_all
% convert scattering length and energy to harmonic oscillator units
ascatt=a0./z0scale;
en=energy./enscale;
% interpolate scattering length for energies in question
a=interp1(en,ascatt,e,'linear');
```

Appendix D

Numerical calculation of ^{133}Cs scattering properties

D.1 Close-coupling codes

The Mies-Julienne-Sando (NIST) close-coupling code has been introduced in Section 5.2.1. The code solves the close-coupled set of Eqs. (5.8) for realistic ^{133}Cs interaction potentials in the presence of a magnetic field. The realistic interatomic interaction potential can be constructed using a different choice of basis set, as presented in Sections 5.1.1 and 5.2.1. The wave function is then propagated from the left starting point to the right end point using either a Numerov [86, 87] or a Gordon propagation algorithm [88, 89]. At the long-range right stopping point, r_{final}, the scattering boundary conditions are determined for both open and closed channels in the form of the logarithmic derivative matrix. The code allows the option of calculating the scattering K-matrix and the S-matrix for open channels only, the scattering cross section, and scattering length. The NIST close-coupling code is written in a combination of Fortran 77 and Fortran 90, and is controlled by various input

"cards". A more detailed description of the codes can be found in the documentation "couple_doc.html", which accompanies the codes.

As demonstrated in Section 5.2, for a detailed modeling of the atomic interaction in the context of the pseudopotential method, we need to obtain both the open-channel as well as the closed-channel part of the scattering K-matrix. Since the close-coupling code includes only open channels in the calculation of the K-matrix, we need to extend the calculation of the K-matrix to include closed channels. This calculation is broken down into two parts: We use the NIST Fortran code to construct the interaction potential, propagate the wave functions for all channels using the renormalized Numerov method, and calculate the logarithmic derivative matrix for all channels. A small modification of the codes allows us to save the logarithmic derivative matrix to the file "logderivative_cc.dat", which is used in a subsequent Matlab program. The Matlab code extends the calculation of the K-matrix to closed channels and allows us to calculate the numerical analytic continuation of the scattering length to negative energies for the channel of interest.

In the following, we will first discuss the input file, which controls the NIST Fortran codes, and the shell script that is necessary to run the Fortran codes for multiple energies. We will then discuss the extension of the K-matrix to closed channels and its implementation in the Matlab code "kmat.m".

D.1.1 Close-coupling codes: Input file

The NIST Fortran codes were compiled on an Apple Power Mac Dual G5 2.5 GHz processor using the Absoft 9.0 Fortran compiler for Mac OS X. The compiled main program, "Cs_magn.e", is run in a UNIX terminal via "Cs_magn.e < input.txt > out.txt". The file "input.txt" includes different cards that call the different subroutines of the main program. The different parameters and calculation results are saved

to the file "out.txt". Here, we will discuss the cards and initialization values that are important for our calculation of the scattering properties. A detailed discussion of the different cards and input parameters can be found in the code description "couple_doc.html".

Input card: OUT(IOFLAG(I),I=1,35)

The input card OUT is used to control the print output to the file "out.txt". Some flags for $I = 1, 35$ are operative in both the Gordon and Numerov sections of the code. In these cases, a value of 1 turns on print in the Gordon sections only, a value of 2 turns on print in the Numerov sections only, and a value of 3 turns on print in both Gordon and Numerov sections. The example input file below uses the following output options: IOFLAG (5) results in printout of the channel opening and closing information, as well as the output of the logarithmic derivative matrix at r_{final}. IOFLAG (6) and IOFLAG (7) control the output of the K-matrix and S-matrix. IOFLAG (19) turns on the modified part of the close-coupling codes. If IOFLAG (19) ≤ 1, then the scattering energy, logarithmic derivative matrix, and other important parameters are saved to the files "energy_cc.dat", "logderivative_cc.dat" and "parameters_cc.dat", respectively. IOFLAG (20) and IOFLAG (25) control the output of the potential matrix and the output of scattering properties for diagnostic purposes.

Input card: REP NREP

The flag NREP selects the basis used to represent the output K, S, and T matrices. If NREP = 0 (default), the channel state basis $\{\psi_\gamma\}$ of the ordered diagonalized representation is selected. If NREP = 1, the $\{\psi_\alpha\}$ basis, in which the potential matrix is constructed, is selected. If NREP = 2, a user defined basis is chosen, which

in our case is the Hund's case (m) basis [85], defined by the two-atom uncoupled basis states dressed by the magnetic field.

Input card: ROT FJMIN FJMAX FJSTEP

This card reads the range of the total projection angular momentum quantum number m_{total} to loop over, namely from FJ = FJMIN to FJMAX by steps of FJSTEP. In the case of the $|ap\rangle$ channel, the "in" channel projection quantum number is FJMIN = FJMAX = 7.

Input card: POT ...

This card causes the subroutine POT to be called with the following input parameters. The card sets the range of partial waves included in the calculation, e.g. from $l = 0$ (LMIN0=0) to $l = 4$ (LMAX0=4). LDRESS=.TRUE. chooses the two-atom uncoupled dressed state basis. IDENT=.TRUE. is chosen for identical atoms. BFIELD=0.0 selects the magnetic field strength in units of Gauss. chA_zero='a', chB_zero='p', ezero=0.0d0 choses the zero of energy to be the energy of the $|ap\rangle$ channel. The remaining parameters include information for the definition of the Cs interaction potential.

Input card: NUMEROV RN1 RN2 DRN NDIM ISM KSRC BCN

This card reads the parameters used to control the renormalized Numerov propagation algorithm. The propagation is done from RN1 to RN2 in steps of DRN. The remaining parameters are set to their standard values, as chosen by the NIST group. Note: The starting boundary condition for the propagated renormalized Numerov RN matrix is independent of representation and is taken to be RN = BCN $\times$ UNIT.

The calculation results are completely insensitive to the magnitude of BCN, since a different boundary condition only changes the normalization of the wave functions.

Input card: ER E ...

This card causes a close-coupling calculation to be carried out at energy E using the renormalized Numerov algorithm and the propagation parameters set by the NUMEROV card.

Input card: END

The END card in the input deck causes the program to stop. This card is normally the last one, although it can be placed anywhere in the input stream. Cards after the END card are ignored.

Example file: input.txt

```
C Input file for NIST Cs_2 Magnetic Field Code
C Numerov propagation only
C
C   0 0 0 0 0 0 0 0 0 1 1 1 1 1 1 1 1 1 2 2 2 2 2 2
C   1 2 3 4 5 6 7 8 9 0 1 2 3 4 5 6 7 8 9 0 1 2 3 4 5
OUT 0 0 0 0 2 2 2 0 0 0 0 0 0 0 0 0 0 2 1 0 0 0 0 4
REP 2
ROT 7 7 1
PARITY 1
POT SSMAG
 &magnet
```

```
   LMIN0=0   LMAX0=4  LDRESS=.TRUE.  IDENT=.TRUE.  BFIELD=0.0
   chA_zero='a'  chB_zero='p'  ezero=0.0d0
 /
 &Dipolar
 A2NDORD_SO =  -5.8595500000000005E-002,
 B2NDORD_SO =   0.8299999999999999     ,
 R_2NDORD_SO =    10.00000000000000     ,
 SCALE_SPSP =    1.000000000000000
 /
 &ADJUST_POT
 SHIFT1 =   1.8916058999999999E-004,
 SHIFT3 =   2.9065349999999999E-005,
 C6 =    6859.278890000000     ,
 C8 =    860000.0000000000
 /
NUMEROV  3.0 1500 0.001 6 2 0 1.0E6
ER 0.10D0/3.1577325D11
C  1D0/3.1577325D11  is 1 muK
 &NML_XSCT_SS_B
   File_Label='2ndSO_max'
   File_DIR='.'
 /
END
```

D.1.2 Close-coupling codes: Shell script

The NIST close-coupling code can be run multiple times for a range of energies (or a range of r_{final} values) using a shell script via the UNIX-terminal command "sh run_codes.scrp". An example of a shell script, which runs the compiled main code ("Cs_magn.e") several times for different energies, is shown in the following. At each step, the command "sed" modifies the input file "input.txt" inserting a different value for the energy. If IOFLAG(19) is set in the input card OUT, the results of the calculation are appended each time to the logarithmic derivative and parameter files, which then can be used for further calculations.

Example file: run_codes.scrp

```
#! /bin/sh
i=1
while [ $i -lt 501 ]
do
   aa=‘echo " -0.01 * $i" | bc‘
   echo $aa
   sed "s/ER 0.10/ER $aa/" input.txt >input.temp
   Cs_magn.e <input.temp >temp.o
   i=‘echo "$i + 1" | bc‘
done
```

D.2 Numerical code for calculation of the closed-channel K-matrix and scattering length matrix

The K-matrix can be determined from the logarithmic derivative matrix $m_{\gamma',\gamma}(r_{\text{final}})$ following Eq. (5.54) via

$$K_{\gamma',\gamma} = \left[N_{\gamma'}(r_{\text{final}})m_{\gamma',\gamma}(r_{\text{final}}) - N'_{\gamma'}(r_{\text{final}})\right]^{-1}\left[J_{\gamma'}(r_{\text{final}})m_{\gamma',\gamma}(r_{\text{final}}) - J'_{\gamma'}(r_{\text{final}})\right] . \tag{D.1}$$

Here, $J'_{\gamma'}(r_{\text{final}})$ and $N'_{\gamma'}(r_{\text{final}})$ are the derivatives of the reduced spherical Bessel functions, $J_{\gamma'}$ and $N_{\gamma'}$, at $r = r_{\text{final}}$. As argued in Section 5.2, we need to extend the K-matrix to include closed channels, since the NIST code includes only open channels in the calculation of the K-matrix. This can be achieved by continuing the reduced spherical Bessel functions $J'_{\gamma'}(kr_{\text{final}})$ and $N'_{\gamma'}(kr_{\text{final}})$ to negative energies by using a purely imaginary wave vector, $k = i\kappa$, and allowing a complex argument of the Bessel functions. The K-matrix then defines the scattering length matrix that is appropriate for use in the generalized multichannel pseudopotential according to

$$a^{l'+l''+1}_{\gamma'',\gamma'} = K_{\gamma'',\gamma'}k^{-l'-1/2}_{\gamma'}k^{-l''-1/2}_{\gamma''}, \tag{D.2}$$

where k_γ are the channel state wave vectors.

The Matlab code, "kmat.m", uses the logarithmic derivative matrix, which is obtained from the close-coupling codes, and calculates the K-matrix according to Eq. (D.1). Furthermore, the code calculates the scattering length matrix element for the channel of interest using Eq. (D.2).

D.2.1 Main program

kmat.m

```
%-----------------------------------------------------------------------
% Main Program: kmat.m
%-----------------------------------------------------------------------
%
% Created by RENE STOCK, UNM: October, 2004
%
% last modified: April, 2005
%
% This is the main program for calculating the K-matrix and
% scattering length matrix for open and closed channels. The program
% uses the logarithmic derivative matrix calculated in the NIST
% close-coupling codes.
%
% The NIST close-coupling (CC) code propagates the multichannel
% wave function for a given scattering energy E using a Numerov
% method from an inner radius r_initial to a final radius r_final.
% At r_final, the code determines the logarithmic derivative matrix
% for the (asymptotic) wave functions for open and closed channels.
% The CC code has been modified to output the necessary data to
% the following files:
%
% energy_cc.dat:       List of scattering energies E, for which the
%                      CC calculation has been performed.
% logarithmic_cc.dat:  Logarithmic derivative matrix calculated at
%                      r_final for the list of scattering energies.
```

```
% parameters_cc.dat:   List of other important parameters
%                      (rfinal, l quantum numbers, energy E_gamma,
%                      k-vector k_gamma, Bessel function argument
%                      for each participating channel, additional
%                      values for test and diagnostics).
% kmatrix_cc.dat:      OPEN CHANNEL part of the K-matrix, calculated
%                      in the CC code.
%
% Note: This code calculates the K-matrix for open channels (similar
% to the CC code) and closed channels close to dissociation. Lower
% lying closed channels are ignored.
%
%-----------------------------------------------------------------------

% include the following m-function subroutines
% sphericalbesselj.m, sphericalbessely.m
% dsphericalbesselj.m, dsphericalbessely.m

clear

calctime=cputime;

%-----------------------------------------------------------------------
% NIST close-coupling code calculations
%-----------------------------------------------------------------------

% read the nist data from files
load energy_cc.dat
```

```
load logderivative_cc.dat;
load parameters_cc.dat;
load kmatrix_cc.dat;

% read energy list
energy=energy_cc(:,1)/0.3166829362525166D-11; % energy in muK
rf=energy_cc(:,2);   % list of rfinal
ntot=energy_cc(:,3); % number of participating channels at each E
a0=energy.*0;        % allocate memory for a0

% make sure ntot is the same for all energies
diff=ntot(1)*(ntot./ntot)-ntot;
if max(abs(diff))>0.5
   error='number of participating channels does not match'
else
end

% create index for parameter_cc.dat file
nindex=ntot;
for m=2:length(ntot)
    nindex(m)=nindex(m-1)+ntot(m);
end

%-----------------------------------------------------------------------
% loop over list of energies (or alternatively rf)
%-----------------------------------------------------------------------

% loop over energy or rf
```

```
% for n=1:length(rf)              % alternative loop over rfinal
for n=1:length(energy)

    %-----------------------------------------------------------------
    % load remaining NIST parameters

    parameters=parameters_cc((nindex(n)-ntot(n)+1):nindex(n),:);
    logderivative=logderivative_cc(n,:);
    kmatrix=kmatrix_cc(n,:);

    % contents of parameter file
    rfinal=parameters(:,1);       % list of rfinal values
    lvec=parameters(:,2);         % list of partial wave l values
    e0vec=parameters(:,3);        % energy of hyperfine states
    kvec=parameters(:,4);         % k-vector
    z=rfinal.*kvec;               % Bessel argument (z=kvec*rfinal)
    zalt=parameters(:,5);         % z calculated in NIST codes

    % logderivative file
    % The log-derivative matrix of size (ntot x tot) is arranged in
    % rows of length ntot^2 in the file logderivative_cc.dat. Each
    % row corresponds to E from the energy list. The following
    % command reshapes the rows back into matrix form
    logder=reshape(logderivative',ntot(n),ntot(n))';

    %-----------------------------------------------------------------
    % define open and closed channels
```

```
open=find(e0vec>0);
closed=find(e0vec<=0);

nopen=length(open);          % number of open channels
kvec(closed)=i*kvec(closed); % kvec is imag. for neg. energies
z(closed)=i*z(closed);       % z is imag. for neg. energies

%-------------------------------------------------------------
% construction of Besselvector at radius rfinal
%-------------------------------------------------------------

% allocate memory for reduced Bessel functions and derivatives
xjl=0.*z;
xyl=0.*z;
dxjl=0.*z;
dxyl=0.*z;

xjl(open)=z(open).*sphericalbesselj(lvec(open),z(open)) ...
          ./kvec(open);
xyl(open)=-z(open).*sphericalbessely(lvec(open),z(open)) ...
          ./kvec(open);
dxjl(open)=(sphericalbesselj(lvec(open),z(open)) ...
           .*(lvec(open)+1)-z(open) ...
           .*sphericalbesselj(lvec(open)+1,z(open)));
dxyl(open)=(-sphericalbessely(lvec(open),z(open)) ...
           .*(lvec(open)+1)+z(open) ...
           .*sphericalbessely(lvec(open)+1,z(open)));
```

```
xjl(closed)=z(closed) ...
            .*real(sphericalbesselj(lvec(closed),z(closed))) ...
            ./ kvec(closed);
xyl(closed)=-z(closed).*i ...
            .*imag(sphericalbessely(lvec(closed),z(closed))) ...
            ./kvec(closed);
dxjl(closed)=(real(sphericalbesselj(lvec(closed),z(closed))) ...
            .*(lvec(closed)+1)-z(closed).*i ...
            .*imag(sphericalbesselj(lvec(closed)+1,z(closed))));
dxyl(closed)=(-i ...
             .*imag(sphericalbessely(lvec(closed),z(closed)))...
             .*(lvec(closed)+1)+z(closed) ...
             .*real(sphericalbessely(lvec(closed)+1,z(closed))));

% codes breaks down for very low lying closed channels
% (xjl -> Inf)
reg=find(xjl<Inf);
logder=logder(reg,reg);
xjl=xjl(reg);
xyl=xyl(reg);
dxjl=dxjl(reg);
dxyl=dxyl(reg);
e0vec=e0vec(reg);

open=find(e0vec>0);
closed=find(e0vec<=0);

%-------------------------------------------------------------------
```

```
    % calculation of K-matrix
    %-------------------------------------------------------------

    dum1=(logder.*(ones(length(reg),1)*transpose(xjl)))-diag(dxjl);
    dum2=-(logder.*(ones(length(reg),1)*transpose(xyl)))+diag(dxyl);
    dum2=inv(dum2);

    % The multichannel K-matrix has four blocks
    % kopen, koc, kco, kclosed
    kmatrixcalc=dum2*dum1;
    kclosed=i*imag(kmatrixcalc(closed,closed));
    kopen=real(kmatrixcalc(open,open));
    koc=kmatrixcalc(open,max(open)+1:length(kmatrixcalc));
    kco=kmatrixcalc(max(open)+1:length(kmatrixcalc),open);
    kvecopen=kvec(open);
    kvecclosed=kvec(closed);

    % scattering length matrix element for channel of interest
    a0(n)=-kclosed(1,1)/kvecclosed(1);

end

[energy,I]=sort(energy);
a0=a0(I);

%-------------------------------------------------------------------
% Tests for open part of K-matrix: Compare to NIST code calculation
%-------------------------------------------------------------------
```

```
%test1=xjl-parameters(open,6);
%test2=xyl-parameters(open,7);
%test3=xjl-xjlalt;
%test4=xyl-xylalt;
%test5=xjlalt-parameters(open,6);
%test6=xylalt-parameters(open,7);
%test7=dxjl-parameters(open,8);
%test8=dxyl-parameters(open,9);
%kmatrix=reshape(kmatrix,nopen,nopen)';
%test9=(kmatrixcalc(open,open)./kmatrix)-1;

%-----------------------------------------------------------------------
% Plot and Save
%-----------------------------------------------------------------------

% plot(energy,a0,'r')
save('scattlength','a0','energy')

calctime=cputime-calctime
```

D.2.2 Subroutines

sphericalbesselj.m

```
function b = sphericalbesselj(nu,z)

% SPERICALBESSELJ(nu,z) spherical bessel function
% (of the first kind)
%
% nu bessel function index
% z (spatial) coordinate

b=sqrt(pi./(2*z)).*besselj(nu+1/2,z);
```

sphericalbessely.m

```
function b=sphericalbessely(nu,z)

% SPERICALBESSELY(nu,z) spherical bessel function
% (of the second kind)
%
% nu bessel function index
% z (spatial) coordinate

b=sqrt(pi./(2*z)).*bessely(nu+1/2,z);
```

dsphericalbesselj.m

```
function d = dsphericalbesselj(nu,z)

% DSPERICALBESSELJ(nu,z) first order derivative of the
% spherical bessel function SPHERICALBESSELJ with respect to z
%
% nu bessel function index
% z (spatial) coordinate

d=1/(2*nu+1)*(nu*sphericalbesselj(nu-1,z) ...
  - (nu+1)*sphericalbesselj(nu+1,z));
```

dsphericalbessely.m

```
function d = dsphericalbessely(nu,z)

% DSPERICALBESSELY(nu,z) first order derivative of the
% spherical bessel function SPHERICALBESSELY with respect to z
%
% nu bessel function index
% z (spatial) coordinate

d=1/(2*nu+1)*(nu*sphericalbessely(nu-1,z) ...
  - (nu+1)*sphericalbessely(nu+1,z));
```

References

[1] For a review see Nature Insight, Nature **416**, 205 (2002).

[2] I. H. Deutsch and P. S. Jessen, Phys. Rev. A **57**, 1972 (1998).

[3] N. Schlosser, G. Reymond, I. Protsenko, and P. Grangier, Nature **411**, 1024 (2001).

[4] R. Dumke, M. Volk, T. Müther, F. B. J. Buchkremer, G. Birkl, and W. Ertmer, Phys. Rev. Lett. **89**, 097903 (2002).

[5] R. Folman, P. Krüger, J. Schmiedmayer, J. Denschlag, and C. Henkel, Adv. At. Mol. Opt. Phys. **48**, 263 (2002).

[6] M. Greiner, O. Mandel, T. Esslinger, T. W. Hänsch, and I. Bloch, Nature **415**, 39 (2002).

[7] M. Greiner, O. Mandel, T. W. Hänsch, and I. Bloch, Nature **419**, 51 (2002).

[8] B. Paredes, A. Widera, V. Murg, O. Mandel, S. Fölling, I. Cirac, G. V. Shlyapnikov, T. W. Hänsch, and I. Bloch, Nature (London) **429**, 277 (2004).

[9] M. A. Nielsen and I. L. Chuang, *Quantum computation and information* (University Press, Cambridge, 2000).

[10] J. Grondalski, *Ph. D. Thesis, University of New Mexico* (University of New Mexico, Albuquerque, New Mexico, USA, 2001).

[11] E. A. Cornell and C. E. Wieman, Rev. Mod. Phys. **74**, 875 (2002).

[12] S. Inouye, M. R. Andrews, J. Stenger, H.-J. Miesner, D. M. Stamper-Kurn, and W. Ketterle, Nature **392**, 151 (1998).

[13] H. Feshbach, Annals of Physics **5**, 357 (1958).

[14] H. Feshbach, Annals of Physics **19**, 287 (1962).

[15] H. Feshbach, *Theoretical nuclear physics* (Wiley, New York, 1992).

[16] L. Tonks, Phys. Rev. **50**, 955 (1936).

[17] M. Girardeau, J. Math. Phys. (N. Y.) **1**, 516 (1960).

[18] M. Olshanii, Phys. Rev. Lett. **81**, 938 (1998).

[19] D. S. Petrov, G. V. Shlyapnikov, and J. T. M. Walraven, Phys. Rev. Lett. **85**, 3745 (2000).

[20] T. Bergeman, M. G. Moore, and M. Olshanii, Phys. Rev. Lett. **91**, 163201 (2003).

[21] M. D. Girardeau and M. Olshanii, Phys. Rev. A **70**, 023608 (2004).

[22] D. S. Petrov, M. Holzmann, and G. V. Shlyapnikov, Phys. Rev. Lett. **84**, 2551 (2000).

[23] D. S. Petrov and G. V. Shlyapnikov, Phys. Rev. A **64**, 012706 (2001).

[24] E. L. Bolda, E. Tiesinga, and P. S. Julienne, Phys. Rev. A **68**, 032702 (2003).

[25] B. Paredes, P. Fedichev, J. I. Cirac, and P. Zoller, Phys. Rev. Lett. **87**, 010402 (2001).

[26] H. T. C. Stoof and M. Bijlsma, Phys. Rev. E **47**, 939 (1993).

[27] D. Jaksch, C. Bruder, J. I. Cirac, C. W. Gardiner, and P. Zoller, Phys. Rev. Lett. **81**, 3108 (1998).

[28] D. Jaksch, H.-J. Briegel, J. I. Cirac, C. W. Gardiner, and P. Zoller, Phys. Rev. Lett. **82**, 1975 (1999).

[29] E. Charron, E. Tiesinga, F. Mies, and C. Williams, Phys. Rev. Lett. **88**, 077901 (2002).

[30] K. Eckert, J. Mompart, X. X. Yi, J. Schliemann, D. Bruß, G. Birkl, and M. Lewenstein, Phys. Rev. A **66**, 042317 (2002).

[31] G. K. Brennen, C. M. Caves, P. S. Jessen, and I. H. Deutsch, Phys. Rev. Lett. **82**, 1060 (1999).

[32] G. K. Brennen, I. H. Deutsch, and C. J. Williams, Phys. Rev. A **65**, 022313 (2002).

[33] G. K. Brennen, *Ph. D. Thesis, University of New Mexico* (University of New Mexico, Albuquerque, New Mexico, USA, 2001).

[34] J. L. Bohn and P. S. Julienne, Phys. Rev. A **56**, 1486 (1997).

[35] D. Jaksch, J. I. Cirac, P. Zoller, S. L. Rolston, R. Côté, and M. D. Lukin, Phys. Rev. Lett. **85**, 2208 (2000).

[36] S. E. Hamann, D. L. Haycock, G. Klose, P. H. Pax, I. H. Deutsch, and P. S. Jessen, Phys. Rev. Lett. **80**, 4149 (1998).

[37] M. T. DePue, C. McCormick, S. L. Winoto, S. Oliver, and D. S. Weiss, Phys. Rev. Lett. **82**, 2262 (1999).

[38] A. J. Kerman, V. Vuletic, C. Chin, and S. Chu, Phys. Rev. Lett. **84**, 439 (2000).

[39] O. Mandel, M. Greiner, A. Widera, T. Rom, T. W. Hänsch, and I. Bloch, Phys. Rev. Lett. **91**, 010407 (2003).

[40] O. Mandel, M. Greiner, A. Widera, T. Rom, T. W. Hänsch, and I. Bloch, Nature (London) **425**, 937 (2003).

[41] R. Scheunemann and F. S. Cataliotti and T. W. Hänsch and M. Weitz, Phys. Rev. A **62**, 051801 (2000).

[42] S. Peil, J. V. Porto, B. L. Tolra, J. M. Obrecht, B. E. King, M. Subbotin, S. L. Rolston, and W. D. Phillips, Phys. Rev. A **67**, 051603(R) (2003).

[43] P. Rabl, A. J. Daley, P. O. Fedichev, J. I. Cirac, and P. Zoller, Phys. Rev. A **91**, 110403 (2003).

[44] P. J. Leo, C. J. Williams, and P. S. Julienne, Phys. Rev. Lett. **85**, 2721 (2000).

[45] C. Chin, V. Vuletić, A. J. Kerman, S. Chu, E. Tiesinga, P. J. Leo, and C. J. Williams, Phys. Rev. A **70**, 032701 (2004).

[46] Paul S. Julienne in *Scattering*, edited by P. Sabatier and E. R. Pike, Academic Press, London 2001.

[47] J. Weiner, V. S. Bagnato, S. Zilio, and P. S. Julienne, Rev. Mod. Phys. **71**, 1 (1999).

[48] G. Herzberg, *Molecular spectra and molecular structure: I. Spectra of diatomic molecules* (van Nostrand, Princeton, New Jersey, 1950).

[49] B. H. Bransden and C. J. Joachain, *Physics of atoms and molecules* (Prentice Hall, England, 2003).

[50] G. F. Gribakin and V. V. Flambaum, Phys. Rev. A **48**, 546 (1993).

[51] J. R. Taylor, *Scattering theory* (John Wiley & Sons, New York, 1972).

[52] J. J. Sakurai, *Modern quantum mechanics* (Addison-Wesley, New York, 1994).

[53] E. Fermi, La Ricerca Scientifica, Serie II, Anno VII, **II**, 13 (1936).

[54] E. L. Bolda, E. Tiesinga, and P. S. Julienne, Phys. Rev. A **66**, 013403 (2002).

[55] D. Blume and C. H. Greene, Phys. Rev. A **65**, 043613 (2002).

[56] K. Huang and C. N. Yang, Phys. Rev. **105**, 767 (1957).

[57] K. Huang, *Statistical mechanics* (John Wiley & Sons, Inc., New York, 1963).

[58] R. Roth and H. Feldmeier, Phys. Rev. A **64**, 043603 (2001).

[59] M. Abramowitz and I. A. Stegun, *Handbook of mathematical functions* (Dover, New York, 1972).

[60] S. M. Blinder, Am. J. Phys. **71**, 819 (2003).

[61] R. Roth, *Ph. D. Thesis, Technische Universität Darmstadt* (Technische Universität Darmstadt, Darmstadt, 2000).

[62] A. Omont, J. Phys. (France) **38**, 1343 (1977).

[63] C. Wodkiewicz, Phys. Rev. A **43**, 68 (1991).

[64] T. Busch, B.-G. Englert, K. Rzążewski, and M. Wilkens, Found. Phys. **28**, 549 (1998).

[65] E. Tiesinga, C. J. Williams, F. H. Mies, and P. S. Julienne, Phys. Rev. A **61**, 063416 (2000).

[66] M. Block and M. Holthaus, Phys. Rev. A **65**, 052102 (2002).

[67] C. J. Williams, E. Tiesinga, P. S. Julienne, H. Wang, W. C. Stwalley, and P. L. Gould, Phys. Rev. A **60**, 4427 (1999).

[68] G. Peach, I. B. Whittingham, and T. J. Beams, Phys. Rev. A **70**, 032713 (2004).

[69] K. Kanjilal and D. Blume, Phys. Rev. A **70**, 042709 (2004).

[70] E. Merzbacher, *Quantum Mechanics* (John Wiley & Sons, Inc., New York, 1998).

[71] E. L. Hamilton, C. H. Greene, and H. R. Sadeghpour, J. Phys. B: At. Mol. Opt. Phys. **35**, L199 (2002).

[72] E. Jane, G. Vidal, W. Dür, P. Zoller, and J. I. Cirac, Quant. Inf. Comp **3**, 15 (2003).

[73] L.-M. Duan, E. Demler, and M. D. Lukin, Phys. Rev. Lett. **91**, 090402 (2003).

[74] F. H. Mies, E. Tiesinga, and P. S. Julienne, Phys. Rev. A **61**, 022721 (2000).

[75] D. Jaksch, V. Venturi, J. I. Cirac, C. J. Williams, and P. Zoller, Phys. Rev. Lett. **89**, 040402 (2002).

[76] P. O. Fedichev, M. J. Bijlsma, and P. Zoller, Phys. Rev. Lett. **92**, 080401 (2004).

[77] I. Rappert, *M.S. Thesis, University of New Mexico* (University of New Mexico, Albuquerque, New Mexico, USA, 2005).

[78] C. Chin, V. Vuletić, A. J. Kerman, S. Chu, E. Tiesinga, P. J. Leo, and C. J. Williams, Phys. Rev. A **85**, 2717 (2000).

[79] F. H. Mies, Molecular Physics **61**, 953 (1980).

[80] G. Arfken, *Mathematical methods for physicists* (Academic Press, Orlando, Florida, 1985).

[81] G. Santarelli, P. Laurent, P. Lemonde, A. Clairon, A. G. Mann, S. Chang, A. N. Luiten, and C. Salomon, Phys. Rev. Lett. **82**, 4619 (1999).

[82] J. Söding, D. Guéry-Odelin, P. Desbiolles, G. Ferrari, and J. Dalibard, Phys. Rev. Lett. **80**, 1869 (1998).

[83] A. J. Kerman *et al.*, C. R. Acad. Sci. Paris, t. 2, Série IV **2**, 633 (2001).

[84] T. Weber, J. Herbig, M. Mark, H.-C. Nägerl, and R. Grimm, Science **302**, 2101 (2003).

[85] A. Simoni, P. S. Julienne, E. Tiesinga, and C. J. Williams, Phys. Rev. A **66**, 063406 (2002).

[86] B. R. Johnson, J. Chem. Phys. **67**, 4086 (1977).

[87] B. R. Johnson, J. Chem. Phys. **69**, 4678 (1978).

[88] R. G. Gordon, J. Chem. Phys. **51**, 14 (1969).

[89] R. G. Gordon, Meth. Comput. Phys. **10**, 81 (1971).

[90] B. DeMarco, S. B. Papp, and D. S. Jin, Phys. Rev. Lett. **86**, 5409 (2001).

[91] H. T. C. Stoof, J. M. V. A. Koelman, and B. J. Verhaar, Phys. Rev. B **38**, 4688 (1988).

[92] F. H. Mies, C. J. Williams, P. S. Julienne, and M. Krauss, J. Res. Natl. Inst. Stand. Technol. **101**, 521 (1996).

[93] Z. Idziaszek and T. Calarco, quant-ph/0410163 (2004).

[94] T. D. Visser, P. S. Carney, and E. Wolf, Phys. Lett. A **249**, 243 (1998).

[95] M. Kerker, *The scattering of light, and other electromagnetic radiation* (Academic Press, New York, 1969).

[96] P. M. Morse and K. U. Ingard, *Theoretical acoustics* (McGraw-Hill, New York, 1968).

[97] L. Infeld and T. E. Hull, Rev. Mod. Phys. **23**, 21 (1951).